THE DEVELOPMENT OF A TRANSPARENT SOIL AND ITS APPLICATION IN IMAGING ROOT TRAJECTORIES AND ROOT-BACTERIA INTERACTIONS

A thesis submitted in partial fulfilment of the requirements of the University of Abertay Dundee for the award of PhD

by

Helen Downie

University of Abertay Dundee

February 2013

Declaration

I hereby declare that this thesis has been composed by myself and that it has not been accepted in any previous application for a degree. The work of which it is a record, is my own, unless otherwise stated. All verbatims have been distinguished by quotation marks and sources of information specifically acknowledged by means of references.

Helen Downie

Acknowledgements

My PhD was funded by a joint studentship from The James Hutton Institute (formerly The Scottish Crop Research Institute) and The University of Abertay Dundee. There are a number of people to whom I am indebted for their assistance during my studies. Firstly I would like to thank my supervisors for their guidance, advice and support and for their help in the preparation of this thesis. They are Professor Wilfred Otten, Dr Tracy Valentine and Dr Andrew Spiers and I would like to thank Dr Lionel Dupuy in particular for his unwavering enthusiasm. I would also like to thank my examiners Dr Jim Haseloff and Dr Philip Collier for their assistance in improving this thesis.

There were project students who worked with me at various points along the way, carrying out some valuable work which has helped me to get to this stage. They are Shafeeq Rhaman, Vicky Helbig and Audrey Derumier. Thanks also to Carol Kyle and Jason Owen for their technical help with milling and chemical analyses. Kath Wright was always patient and helpful with the confocal imaging and with fluorescent dye issues. Professor Yossef A. Elabd kindly gave us the protocol for making cationic Nafion. Ursula in the library has been very helpful by finding me references. I would also like to thank Katharine Preedy and Christine Hackett from BioSS for their statistics advice and Philip Smith for proof-reading my thesis.

There have been many people at The James Hutton Institute and at Abertay who have helped to make my time here memorable. Thanks to lab and office mates past and present and everyone in the D-block corridor. Special thanks to Stefanie, Miriam, Sonja, Marzipan, Veronica, Linda and Lea for always making me smile. I am eternally grateful to my parents, Anne and Ron and to my brother Tom for their love and support during the past years, as always. Thanks also to Mike, for being you.

Abstract

Biological processes that occur in the soil have important environmental implications. These processes include root growth and microbial interactions with roots and soil particles and they influence the efficiency of crop production and, in turn, global food security. The observation and imaging of these below-ground processes is difficult due to the opacity of soil and so this thesis presents a new artificial soil analogue that is transparent and therefore allows optical imaging. Transparent soil is a 3D matrix of chemically treated particles of the low refractive index fluoropolymer Nafion, water, plant nutrients and air and has water retention and ion exchange properties similar to natural soils. Before imaging, the transparent soil was saturated with a refractive index matched liquid for appropriate transparency. The substrate was used for 3D imaging of living root systems and high resolution imaging of living roots at a cellular level in relation to the fluorescent-labelled Nafion particles of the substrate.

Soil physical conditions influence the growth rate and direction of roots. The substrate compaction and particle size range was varied in transparent soil to quantify the effect of these conditions on 3D root trajectories of lettuce plants. Root systems of plants grown in different substrate conditions were imaged and the root lengths were measured along with the curvature and verticality at sequential points along the roots. There was a greater range of root curvatures in substrates with larger particle sizes and deviation from vertical increased with distance along the root. In substrates with different compactions, there was no effect of compaction on the root curvature or

verticality measurements, however the measurements were influenced by the distance along the root.

Soil microbes were also studied using the transparent soil system. *Pseudomonas fluorescens*, a plant growth promoting rhizobacteria, associates closely with plant roots and can act as a biocontrol agent by conveying pathogen resistance to the plant. For this reason, the interaction between lettuce roots and GFP labelled *P. fluorescens* was studied with the aim of quantifying colonisation patterns along the root and the abundance of bacteria in the substrate surrounding the roots. Transparent soil with two different particle size categories was used to investigate if the substrate particle size affected the colonisation of the roots. Imaging of living roots and bacteria was carried out at 3D sample points along the root and adjacent to the root and it was found that there was a greater abundance of bacteria on the roots than in the substrate. There was a consistent base level of bacterial fluorescence in imaging points that did not include roots, regardless of whether or not there was a plant in the sample and the distance from the root. Substrate particle size had no effect on root colonisation.

Contents

CHAPTER 1. GENERAL INTRODUCTION 1

1.1 Root growth and function 2

1.1.1 Lateral root formation 3

1.1.2 Root system architecture 4

1.2 Root–soil interactions 5

1.2.1 Influence of soil factors on root growth and RSA 7

1.3 Classical methods of studying roots 9

1.4 Application of imaging to root research 11

1.4.1 Imaging roots in soil 13

1.4.2 Optical imaging of roots 14

1.4.2.1 Growth environments suitable for light imaging 15

1.4.2.2 Common methods for studying roots using light imaging 16

1.4.2.3 Emerging techniques for optical imaging 20

1.4.3 Challenges for high throughput phenotyping 22

1.5 Aims 23

CHAPTER 2. APPLICATION OF REFRACTIVE INDEX MATCHING TO ENGINEER A SOIL-LIKE TRANSPARENT SUBSTRATE 25

2.1 Introduction 25

2.2 Materials for refractive index (RI) matching 28

2.2.1 Cryolite 28

2.2.2 Fluorinated ethylene propylene (FEP) 29

2.2.3 Nafion 33

2.3 RI matching liquids 35

2.4 Engineering particle size distribution 38

2.5 Controlling the properties of the solid/liquid interface 40

2.6 Ion exchange 41

2.7 Labelling 45

2.7.1 Visualising transparent soil particles 45

2.7.2 Imaging rhizosphere pH 49

2.8 Conclusion 50

CHAPTER 3. DEVELOPMENT OF A TRANSPARENT SOIL FOR IMAGING ROOTS 52

3.1 Introduction 52

3.2 Materials and methods 53

3.2.1 Construction of transparent soil 53

3.2.2 Refractive index matching 54

3.2.3 Characterising the properties of transparent soil 55

3.2.4 Plant culture 57

3.2.5 Plant growth comparison 58

3.2.6 3D imaging of roots in transparent soil 59

3.2.6.1 Construction of 3D slides 59

3.2.7 Data analysis 60

3.3 Results 62

3.3.1 Selection of materials 62

3.3.2 Transparent soil 65

3.3.3 Characterisation of transparent soil 67

3.3.4 Root growth in transparent soil 68

3.3.5 3D imaging of roots in transparent soil 74

3.4 Discussion 77

CHAPTER 4. MEASURING THE EFFECTS OF SUBSTRATE PHYSICAL FACTORS ON 3D ROOT GROWTH TRAJECTORIES 80

4.1 Introduction 80

4.1.1 Root tropisms 80

4.1.2 Endogenous trajectories 81

4.1.3 Substrate effects on root trajectories 82

4.1.4 Aims 84

4.2 Materials and methods 84

4.2.1 Seed preparation 84

4.2.2 Sample set up 85

4.2.2.1 Substrate compaction experiment 85

4.2.2.2 Substrate particle size experiment 86

4.2.3 Plant culture 88

4.2.4 Imaging 88

4.2.5 Image analysis 89

4.2.6 Data analysis 90

4.2.6.1 Statistical analysis 90

4.3 Results 93

4.3.1 The effect of substrate compaction on primary root trajectories 93

4.3.2 The effect of substrate texture on root growth trajectories 103

4.4 Discussion 113

4.4.1 The effect of substrate compaction on root trajectories 113

4.4.2 The effect of substrate texture on root trajectories 115

4.4.3 Future directions 116

4.4.3.1 Manipulating transparent soil for mimicking soil physical conditions 116

4.4.3.2 Image analysis and data analysis 117

4.4.4 Conclusions 118

CHAPTER 5. HIGH RESOLUTION 3D DISTRIBUTION OF LIVING *PSEUDOMONAS FLUORESCENS* ON AND AROUND LETTUCE (*LACTUCA SATIVA*) ROOTS 120

5.1 Introduction **120**

5.2 Materials and methods **123**

5.2.1 Bacterial culture 123

5.2.2 Plant preparation 123

5.2.3 Sample set up 124

5.2.4 Image acquisition 125

5.2.5 Biomass measurement 128

5.2.6 Image processing and analysis 128

5.2.6.1 Quantifying bacterial abundance 128

5.2.6.2 Correcting results for available area 130

5.2.6.3 Measuring the perimeter of Nafion particles 132

5.2.7 Image analysis software 133

5.2.8 Statistical analyses 133

5.3 Results **134**

5.3.1 Comparative analysis between XY positions 136

5.3.2 Analysis comparing X and Y directions 143

5.3.3 Relationship between particle perimeter length and bacterial abundance 146

5.3.4 Root colonisation pattern 148

5.4 Discussion **151**

5.4.1 A new system for imaging the interaction between *P. fluorescens* and lettuce roots 151

5.4.2 Influence of particle size on bacterial distribution along the roots 152

5.4.3 Spatial distribution of bacteria 152

5.4.4 Bacterial distribution along the roots 154

5.4.5 Conclusion 156

CHAPTER 6. SUMMARY AND CONCLUSIONS 158

6.1 Summary **158**

6.2 A new approach for soil microscopy **159**

CHAPTER 7. REFERENCES 164

APPENDIX 1 203

Research article: Transparent soil for imaging the rhizosphere 203

Abstract 204

Introduction 204

Results and Discussion 206

Making soils transparent using Refractive Index matching 206

Mimicking physical and chemical properties of soil 208

Root growth in transparent soil 209

Application of transparent soil to the study of root bacteria interactions 210

New opportunities for plant sciences 212

Materials and methods 213

Construction of transparent soil 213

Refractive index matching 214

Characterising properties of transparent soil 215

Plant culture 215

Analysis of plant growth in different substrates 216

Bacterial culture and experimental setup 217

3D optical imaging of soil biological processes 217

Data analysis 218

Acknowledgements 219

References 219

APPENDIX 2 226

Captions for videos on CD 226

Table of Figures

Figure 1.1. The electromagnetic (EM) spectrum. Imaging uses EM radiation in the range of infrared (10^{-5} m) to X-ray (10^{-10} m). This image is reproduced under a free documentation license (GNU). 12

Figure 2.1. Illustration of the use of RI matching for soil science. A) Soil sample saturated with water where the soil itself is opaque and therefore the laser beam cannot penetrate the sample. B) Transparent particles of the low refractive index fluoropolymer, Nafion in water. The laser beam can penetrate these transparent materials but because of the RI mismatch between the liquid and particles, the laser beam is scattered and imaging at depth is not possible. C) Nafion particles in a RI matching liquid. The laser beam penetrates the sample and the amount of scattering of the laser beam is greatly reduced by matching the RI of the liquid and particles. 26

Figure 2.2. Particles of the mineral cryolite – a candidate material for constructing a transparent, granular, RI matched substrate. Scale bar = 1 cm. 31

Figure 2.3. FEP - a candidate material for constructing a transparent substrate. A) Granulates of FEP in its unprocessed form. Scale bar = 1 cm. B) Root imaging was achieved in an FEP-based, saturated, RI matched substrate. Red arrow indicates the root. 31

Figure 2.4. Mean primary root lengths of Nicotiana benthamiana plants grown in Modified Strullu Romand (MSR) medium (Strullu & Romand, 1986) with and without FEP after 3, 7 and 10 days of growth. Error bars show standard error. 32

Figure 2.5. Nafion. A) Nafion pellets as supplied by Ion Power Inc. Scale bar = 1 cm. B) Chemical structure of Nafion. 33

Figure 2.6. Schematic diagram of the steps taken to produce cationic Nafion. DMP is added to precursor Nafion, which exchanges with the fluoride ions. KOH is then used to hydrolyse the Nafion, leaving an exchangeable hydroxide ion. Reproduced from Salerno et al. (2012) with permission from John Wiley and Sons. 44

Figure 2.7. CLSM images showing the interaction between red fluorescent dyes and FEP, etched FEP and Nafion particles. Binding was evident where there was a bright red region around the surface of the particle. Sulphorhodamine B, sulphorhodamine 101 and Rhodamine 6G bound to the Nafion particles, but in all other cases, the dye did not bind to the material. 46

Figure 2.8. FEP granulates (red) and pore spaces (green). Top view (A) and oblique view (B) of 3D reconstruction of confocal image stack. 48

Figure 3.1. A) Samples that were prepared for confocal imaging with transparent soil in 3D slides including Arabidopsis thaliana plants. B) Schematic diagram of 3D slides (not to scale). 61

Figure 3.2. Refractive index of Nafion. A) Optimal RI of nutrient solution for RI matching with Nafion using projected straight line images deformed by the substrate. Curve shows Gaussian non-linear regression (R^2

= 0.38). B) Refractive index of common transparent materials and Nafion. Error bar shows standard error. 63

Figure 3.3. Refractive indices of solutions used for RI matching with Nafion. A) Sorbitol solutions have RIs very similar to sucrose solutions. A linear regression is shown where R^2 = 0.99. B) The range of RIs that can be achieved using Percoll covers the value required for matching with Nafion. A linear regression is shown where R^2 = 0.99. 64

Figure 3.4. Samples of transparent soil. A) Fully saturated with RI matching solution. B) Large pores partially drained. C) Large pores fully drained. Scale bar = 2.5 cm. D) Latuca sativa plants growing in transparent soil and saturated with RI matched liquid for imaging making the roots visible (right)..... 66

Figure 3.5. Water retention in transparent soil, sand and vermiculite. Water retention in 3 different particle size categories of transparent soil was plotted along with water retention data for sand from Schroth et al. (1996) and vermiculite from Schmidt (2011). 67

Figure 3.6. Images of plants after excavation from soil, sand, phytagel and transparent soil (TS). Plants grown in soil and sand have short primary roots but numerous long lateral roots. Plants grown in phytagel have long primary roots and usually no lateral roots and plants grown in TS have long primary roots but more lateral roots than plants grown in phytagel. Scale bar = 1 cm. 70

Figure 3.7. Root and shoot dry weights of plants grown in soil, sand, phytagel and transparent soil (TS). Letters above the bars correspond to the results from the Fisher's protected LSD test. Error bars signify standard error..... 71

Figure 3.8. Mean primary root lengths and cumulative lateral root lengths of plants grown in soil, sand, phytagel and TS. Letters above the bars correspond to the results from the Fisher's protected LSD test. Error bars signify standard error..... 72

Figure 3.9. Mean number of lateral roots and primary root diameter in plants grown in soil, sand phytagel and TS. Letters above the bars correspond to the results from the Fisher's protected LSD tests. Error bars signify standard error. 73

Figure 3.10. OPT images of Nicotiana benthamiana roots in transparent soil. A) Projection image of roots and small air bubbles trapped in the substrate. B) Root (green) and air bubbles (blue) after application of the root tracking algorithm. Scale bars = 1 mm. 74

Figure 3.11. 3D volume renderings of confocal images of Arabidopsis thaliana roots (grey) in transparent soil with Nafion particles dyed with sulphorhodamine B (orange). A–C) Arabidopsis thaliana roots with plasma membrane localised expression of GFP in transparent soil at a range of scales where the scale bars represent 300 µm (A), 170 µm (B) and 40 µm (C). D) Root tip with nuclear RFP expression linked to auxin reporter (Federici et al., 2012). 76

Figure 4.1. Imaging process. A) Top view diagram of the plant sample, where 4 projection images were taken at 90° intervals by rotating the sample. B) Examples of 2 consecutive images of a root system. Only 2

out of 4 images were used because the image pairs were mirror images of one another. The images that were used were selected based on how clearly the roots appeared. 88
Figure 4.2. Representation of the method by which root length, curvature and verticality were measured along the roots. A) Root length was the length of the 3D trajectory representing the root (r), which was compared with the vector representing the Euclidean distance between the root extremities (v). B) Curvature was a measure of the change in direction of the root, where the blue sections (i) represent the angles measured along the root. The 2 vectors representing sections of the root, P_1 and P_2, occupy a 2D plane in 3D space and curvature (K) is calculated in this plane. C) Verticality was a measure of how far the root trajectory deviated from vertical. The green sections represent the angles that were measured. 92
Figure 4.3. Mean primary root lengths and distance between root extremities (vector) of lettuce plants grown in transparent soil with 3 different substrate compactions. Error bars represent standard error. ... 93
Figure 4.4. Ratio between the root length and the length of the distance between the root extremities. This was used as a global measure of root tortuosity of plants grown in transparent soil with 3 different levels of compaction. 94
Figure 4.5. Box plot showing the spread of data on root curvature in substrates with different compaction levels. The black line inside the box denotes the median and the white line denotes the mean. The data shown have been square root transformed. 95
Figure 4.6. Relationship between the log transformed curvature values of roots grown in transparent soil with 3 different densities (data from all roots have been pooled in this plot) and the fitted values from the REML variance component analysis. The red line shows the linear regression with 95% confidence limits (blue lines) where $p < 0.001$. 98
Figure 4.7. Linear mixed model from REML variance component analysis (curves) as applied to curvature data from each plant (data points) from the three substrate density treatments: high density (0.78 g cm^{-3}), low density (0.62 g cm^{-3}) and medium density (0.70 g cm^{-3}). The different symbols signify data from different individual plant samples. 99
Figure 4.8. Overall mean verticality in lettuce roots grown in transparent soil with different compaction levels. Error bars show standard error. 100
Figure 4.9. Linear mixed model from REML variance component analysis (lines) as applied to verticality data from each plant (data points) from the three substrate density treatments: high density (0.78 g cm^{-3}), low density (0.62 g cm^{-3}) and medium density (0.70 g cm^{-3}). The different symbols signify data from different individual plant samples. 102
Figure 4.10. Mean primary root lengths and distance between root extremities (vector) of lettuce plants grown in transparent soil with different particle size categories and phytagel with two different densities. Error bars represent standard error. 104

Figure 4.11. Root length : vector length ratio as a global measure of root tortuosity of plants grown in transparent soil with two different particle size compositions and in phytagel of two different densities. 105
Figure 4.12. Overall mean root curvature in substrates with different textures. The data shown has been square root transformed and the error bars represent standard error. The letters above the bars indicate the results from a Fisher's protected least significant difference test. 106
Figure 4.13. Relationship between the square root transformed curvature values of roots grown in transparent soil with four different textures (data from all roots has been pooled in this plot) and the fitted values from the REML variance component analysis. The red line shows the linear regression with 95% confidence limits (blue lines) where p < 0.001. 108
Figure 4.14. Linear mixed model from REML variance component analysis (lines) as applied to square root transformed curvature data from each plant (data points) from the four substrate texture treatments: medium particles, large particles, soft phytagel and hard phytagel. The different colours signify data from different individual plant samples. 109
Figure 4.15. Mean verticality in lettuce roots grown in transparent soil with different substrate textures. Error bars show standard error. The letters above the bars indicate the results from a Fisher's protected least significant difference test. 110
Figure 4.16. Linear mixed model from REML variance component analysis (lines) as applied to square root transformed curvature data from each plant (data points) from the four substrate texture treatments: medium particles, large particles, soft phytagel and hard phytagel. The different colours signify data from different individual plant samples. 112
Figure 5.1. Diagram representing spatial distribution of points where images were acquired. A) Distribution of points in X (horizontal) and Y (vertical) directions on samples with and without plants. The naming convention for the sampling positions is also shown (R1, A1, etc.). B) At each point shown in (A), 3 images were taken in the Z direction to a depth of 90 µm from the first image. 127
Figure 5.2. Image analysis steps taken in order to analyse and quantify bacterial GFP expression. A) Example of original confocal image from the GFP channel. Scale bar represents 200 µm. B) Magnification of image (A) (white window). Scale bar represents 40 µm. C) Image after despeckle filter has been applied. D) Binary thresholded image – fluorescent aggregates are shown in white. E) Areas where P. fluorescens were detected. Outlines of fluorescent bacterial aggregates are in yellow. F) Outline of units has been overlaid on the unprocessed original image. 129
Figure 5.3. Method for estimation of the volumes of the image where bacteria could not be detected. A) Original confocal image of Nafion particles stained with sulphorhodamine B. B) Transformed image after processing by thresholding, despeckling and application of a median filter. C) Inverted skeleton of the thresholded image. D) Selection of areas of the image occupied by Nafion particles. Here three shades of blue are used to represent the areas occupied by the particles. Scale bar represents 200 µm. 131

Figure 5.4. Examples of the confocal images taken at each position for one sample with a lettuce plant and small particles. Each image shows a merged image of the channels used. At positions R1, R2 and R3, calcofluor staining on the surface of the root is shown in light grey, GFP detection from P. fluorescens is shown in green and sulphorhodamine B staining of the Nafion particles is shown in red. At each of the other positions, there was no detection of calcofluor staining but again, the GFP detection from P. fluorescens is shown in green and sulphorhodamine B staining of the Nafion particles is shown in red... 135

Figure 5.5. Root and shoot dry weights of plants grown in small and large particle size categories. There was no significant difference in root or shoot dry weight between the treatments. n = 4 for each particle size category. Error bars signify standard error..... 136

Figure 5.6. Mean number of bacterial aggregates present in the images at each position in samples with plants and small particles, with no plants and small particles, with plants and large particles and with no plants and large particles. The data has been square root transformed and error bars show standard error. 137

Figure 5.7. Mean average size of bacterial aggregate present in the images at each position in samples with plants and small particles, with no plants and small particles, with plants and large particles and with no plants and large particles. Error bars show standard error..... 139

Figure 5.8. Mean area occupied by aggregates classed as bacterial fluorescence in the images at each position in samples with plants and small particles, with no plants and small particles, with plants and large particles and with no plants and large particles. Error bars show standard error. 141

Figure 5.9. Overall mean number of aggregates (square root transformed) at X positions (R, A and B) and Y positions (1, 2 and 3) where there were plants or no plants. Letters above the error bars show the results of a Fisher's protected least significant difference (LSD) tests on the data where there was a significant difference in the means. Lower and upper case letters signify different tests. Error bars signify standard error..... 143

Figure 5.10. Overall mean average size of aggregates at X positions (R, A and B) and Y positions (1, 2 and 3) where there were plants or no plants. Letters above the error bars show the results of a Fisher's protected LSD test on the data where there was a significant difference in the means. Lower and upper case letters signify different tests. Error bars signify standard error..... 145

Figure 5.11. Overall mean area of bacterial fluorescence at X positions (R, A and B) and Y positions (1, 2 and 3) where there are plants or no plants. Letters above the error bars show the results of a Fisher's protected LSD test on the data where there was a significant difference in the means. Error bars signify standard error..... 146

Figure 5.12. Scatter plot showing relationship between the number of bacterial aggregates recorded in an image and the total length of the perimeter of the Nafion particles in that image. The red line shows the

result of a linear regression where r^2 = 0.270. The data on aggregate number have been square root transformed. 147
Figure 5.13. Mean area occupied by bacterial fluorescence at positions along the root. Only images that included a root were considered. Error bars signify standard error. 149
Figure 5.14. Maximum projection images of high resolution scans of lettuce roots (grey) with GFP expressing P. fluorescens (green). A–B) The bacterial density is highest in the junctions between the epidermal cells of the root. C) Bacterial flocks are visible in the liquid surrounding the root. D) The root epidermal cells appear to be damaged, and there are bacteria occupying spaces below the surface of the root, perhaps where the epidermal cells have ruptured. Scale bar represents 50 µm. 150

Table of Tables

Table 2.1. Summary of properties of the materials that were considered for use in constructing transparent soil. ++ indicates very suitable, + indicates suitable and – indicates not suitable. The autoclaving procedure was 121 °C for 20 minutes at 2 bar. Transparency, water retention and the effect of autoclaving were all assessed visually. Manipulation of particle size was tested using methods described in section 2.4, page 38. Values for RI are quoted from the cited literature. *34*

Table 2.2. Summary of chemicals used for increasing the refractive index of the matching solution for transparent soil. ++ indicates very suitable, + indicates suitable and – indicates not suitable. The most suitable concentrations to be used were determined later based on the refractive index matching. The effect on plant growth was inferred from the chemistry of the substances and from literature on the effect of sorbitol on plant development (Bustos et al., 2008). Transparency and viscosity were assessed visually. *36*

Table 3.1. Dry bulk density of 10 cm^3 samples of Nafion with different particle size categories. Error margins are shown in standard error. *56*

Table 4.1. Details of the setup of transparent soil samples for comparing root growth at different compaction levels. *86*

Table 4.2. Details of the setup of transparent soil and phytagel samples for comparing root growth in substrates with different textures..... *87*

Table 4.3. Fixed effects from the REML component analysis on root curvature in roots grown in transparent soil with different compaction levels. "Sequence" is the distance along the root and n.d.f. = the number of degrees of freedom. The sequence^2 term was used to allow non-linear fitting. *97*

Table 4.4. Fixed effects from the REML component analysis on root verticality in plants grown in transparent soil with different compaction levels. "Sequence" is the distance along the root and n.d.f. = the number of degrees of freedom. The sequence^2 term was used to allow non-linear fitting...... *101*

Table 4.5. Fixed effects from the REML component analysis on root curvature in plants grown in transparent soil with different substrate textures. "Sequence" is the distance along the root and n.d.f. = the number of degrees of freedom. The sequence^2 term was used to allow non-linear fitting...... *107*

Table 4.6. Fixed effects from the REML component analysis on root verticality in plants grown in transparent soil with different substrate textures. "Sequence" is the distance along the root and n.d.f. = the number of degrees of freedom. The sequence^2 term was used to allow non-linear fitting...... *111*

Table 5.1. Summary of sample set up for experiment comparing bacterial distribution under different conditions. *124*

Table 5.2. Resulting p values from analysis of variance of the effect of particle size and presence of plant on the number of aggregates at each position. Presence of plant had a significant effect on number of aggregates at positions R1, R2 and R3. These p values are shown in red. *138*

Table 5.3. Resulting p values from analysis of variance of the effect of particle size and presence of plant on the average size of aggregates at each position. Presence of plant had a significant effect on number of aggregates at positions R1, R2 and R3. These p values are shown in red. *140*
Table 5.4. Resulting p values from analysis of variance of the effect of particle size and presence of plant on the % of the image classed as bacterial fluorescence at each position. Presence of plant had a significant effect on the number of aggregates at positions R1, R2 and R3. These p values are shown in red. *142*

List of abbreviations

CLSM	Confocal laser scanning microscopy
DMP	Dimethyl piperazine
DMSO	Dimethyl sulphoxide
FEP	Fluorinated ethylene propylene
GFP	Green fluorescent protein
ICP-MS	Inductively coupled plasma mass spectrometry
MSR	Modifiied Stullu Romand
OPT	Optical projection tomography
REML	Restricted maximum likelihood
RI	Refractive index
RFP	Red fluorescent protein
RSA	Root system architecture
wt	Weight
dpi	Dots per inch

Chapter 1. General Introduction

The agricultural revolution of the mid-20th Century greatly increased the yield of crops around the world. This was achieved through the breeding of heavy-cropping dwarf varieties of wheat and rice that were compatible with generous fertiliser application (Evans, 1998). Now, half a century on, the agriculture industry is facing more challenges than ever before. These include a decrease in the application of fertilisers because fewer resources will be available to produce them and because of the harmful environmental effects of the fertilisers from agricultural land (Rouse et al., 1999, Hart et al., 2004). In addition, many parts of the world are experiencing an increasing number of extreme weather events such as flooding (Manton, 2010) which can have direct impacts on agricultural productivity. An increasing world population, estimated to reach 15 billion by the end of the century under some projections from the United Nations (Anon., 2010), will have unprecedented food demands.

Plant nutrient use efficiency (NUE) is the percentage of nutrient input that is recovered as nutrient output (Sheldrick et al., 2002) and the global NUE of nitrogen, phosphorus and potassium has been estimated at 50%, 40% and 75% respectively (Tan et al., 2005). The roots of crop plants are responsible for the plant's uptake of resources from the soil (Waisel et al., 2002) and it is thought that plant's NUE is influenced by numerous root properties such as the architecture of the root system (Lynch, 2007) and also by rhizosphere processes such as the release of compounds in root exudates and the

association between roots and soil microorganisms (Rengel & Marschner, 2005). Manipulation of root phenotype for improving NUE and therefore crop production is one area that holds great potential for improving the efficiency of agriculture (Zhu et al., 2011). First, we need to gain a better understanding of the mechanisms that are involved in soil exploration and nutrient acquisition by roots.

1.1 Root growth and function

Root elongation is localised to meristematic regions, unlike in most animals where growth is diffuse with parts growing simultaneously. Russell (1977) described a conceptual model of the root apex which divided the apex into zones: meristematic, elongation and maturation or differentiation. This model was expanded to include the branching zone and the zone of moribund roots (Coleman et al., 1983).

As well as contributing to the root cap, cells from the meristem also go on to form all of the other root tissues. This process begins when the meristem moves forward. Cells divide and elongate, pushing the root tip through the soil in the zone of elongation. This zone is temporal and spatial because the same region of soil is occupied first by the meristem, then by the zone of elongation, the zone of differentiation and eventually the same cells in the same space will be mature, differentiated root tissue. During elongation, the cells expand and the differentiation process begins, where protoderm, provascular tissue and ground tissue form with cells that will become the epidermis, vascular tissue and cortex during maturation, respectively. In maturation, the cortex cells begin to transport minerals from the epidermis to the vascular tissue. Intercellular

spaces also appear which allow oxygen to diffuse through the root. A mature endodermis is also formed during this time. This provides a water tight sheath (the Casparian band) around the vascular tissue which is required for the processes of nutrient transport and transpiration to operate (Moore et al., 1998b).

1.1.1 Lateral root formation

Lateral roots are roots that initiate from another root, and so most of the mature root system consists of lateral roots. Therefore where and when they form are extremely important aspects in the formation of the root system. Lateral root initiation is a genetically regulated process in that the actual initiation will always happen in the same way, but the timing of initiation and the resulting lateral root density are very plastic depending on soil characteristics and other environmental factors. In angiosperms and gymnosperms, lateral roots develop from a small group of founder cells of the pericycle inside the parent root (McCully, 1975). Although these cells have left the apical meristem, where division usually occurs, they remain competent to divide (Dubrovsky et al., 2000, Beeckman et al., 2001). Once the founder cells are specified, they undergo cell divisions to give rise to the lateral root primordium, which then grows through the cortex of the parent root.

The development of lateral roots in *Arabidopsis* has been described in detail and divided into distinct stages based on anatomy and cell divisions (Malamy & Benfey, 1997). Once the primordium has reached the root surface, it emerges through the epidermis, and becomes a new meristem (De Smet et al., 2006). Overall, describing lateral roots by

measuring parameters such as their distribution along the parent root, branching angle and length provides a great deal of information about the root system and its responses to environmental conditions.

1.1.2 **Root system architecture**

The root system architecture (RSA) results from the branching pattern and trajectories of root apical meristems growing through the soil and has an influence on the survival and yield of the plant (Yang et al., 2012). Each root apical meristem executes individual growth actions such as expansion and initiation of new apical meristems, and the resulting root system is a complex network of interconnected roots (Dupuy et al., 2010b). The shape of the root system can be quantified by measuring variables such as root depth, volume and diameter (Hodge et al., 2009) and the topology of root architecture can be described using densities of graph structures (Fitter & Stickland, 1992, Dupuy et al., 2005). High throughput phenotyping of root system architecture is a promising new approach for selective breeding of plants with desirable rooting characteristics and new methods are needed for improving the reliability and throughput for root system imaging (De Dorlodot et al., 2005, Yazdanbakhsh & Fisahn, 2009, Trachsel et al., 2011, Zhu et al., 2011).

Roots are adapted to grow in soil, which is an extremely complex environment. It usually consists of a heterogeneous matrix of mineral fragments, organic matter particles, air-filled pore spaces and moisture and thus provides a spatially and temporally variable

supply of resources for plants (Park, 2001). Roots must interact effectively with the soil in order to exploit the resources and to securely anchor the plant.

1.2 Root–soil interactions

Soil conditions are highly variable depending on, for example, the soil structure, moisture content and compaction. Roots are able to respond to these variable factors. For example, the root cap is an important part of the root, which facilitates its passage through the soil along with its other functions in perceiving signals such as gravity, pressure and moisture (Barlow, 2002). Root cap cells produce mucilage which lubricates the root and promotes nutrient mobilisation for uptake. Along with mucilage to promote movement through the soil, border cells of the root cap are sloughed off at the edges, reducing friction experienced by the root (Iijima et al., 2000). There is a constant turnover of cells as division occurs in the meristem adding cells to the root cap.

Root hairs are tip-growing extensions that form from root epidermal cells. Their pattern of formation differs greatly between species (Datta et al., 2011). They greatly increase the root surface area (Smith et al., 1979) and have a strong influence on the rhizosphere by releasing organic compounds and interacting with microorganisms (Bertin et al., 2003). Root hairs can enter narrow soil pore spaces because of their very small diameters (e.g. 10 μm in *Arabidopsis* (Grierson & Schiefelbein, 2002)) and thus increase the effective diameter of the root. There is also developmental plasticity in the formation of root hairs. For example, root hair length is influenced by external phosphorus supply (Zhu et al., 2010).

The rhizosphere is the zone of soil surrounding the roots which is influenced by the plant (Waisel et al., 2002). The rhizosphere is distinct from the bulk soil for a number of reasons. The chemistry of the rhizosphere is strongly influenced by the plant, because it is a site of exchange, where mineral elements are taken up by roots, forming a nutrient depletion zone. Organic compounds are released by roots, which act as a food source for rhizosphere microorganisms (Badri & Vivanco, 2009). Roots can cause physical compaction of soil in the rhizosphere which can in turn affect the soil hydraulic conductivity (Aravena et al., 2011). In some soil types, there can be a higher water content in the rhizosphere soil than in the bulk soil despite water uptake by the roots, for example, due to hydraulic redistribution (Caldwell & Richards, 1989) and compaction (Aravena et al., 2011).

Rhizosphere microorganisms play very important roles in the soil ecosystem. They can enhance the availability of nutrients to the plant, for example rape plant roots form essential associations with soil bacteria which produce siderophores (compounds that enhance the availability of Fe) in order to acquire Fe from the soil (Rroco et al., 2003). Rhizosphere bacteria can also protect the plant from other bacterial and fungal pathogens (Dowling & O'Gara, 1994). Arbuscular mycorrhizal fungi associate with plants and many studies have concluded that the association between AM fungi and plant roots has a positive influence on the plant's nutrient acquisition (Koide, 1991, Hernando Posada et al., 2013), for example by increasing phosphorus supply to plants (Matsubara & Harada, 1996, Hernando Posada et al., 2013).

1.2.1 Influence of soil factors on root growth and RSA

Phenotypic plasticity is a fundamental characteristic of the modular growth of root systems. Individual roots have an enormous capacity for altering their growth in response to local environmental factors to effectively explore the soil (Hutchings & de Kroon, 1994). This capacity tends to be larger in roots than in other plant organs, such as shoots, and in other organisms, for example animals, where there is very little plasticity. These plastic responses in root growth serve the purpose of investing the plants' resources in the most profitable, efficient way. The parameters of RSA that are sensitive to alteration include root hair formation, primary root growth, root branching angle, lateral root formation and anatomy. Roots alter aspects of their growth in order to maximize the plant's performance by responding to the environment (Hodge, 2006).

An illustrative example of root plasticity is the proliferation of root growth in soil patches with a relatively higher nutrient content, a response first noted around 150 years ago (Nobbe, 1862). There have been many studies since then focusing on the changes in RSA induced by nutrient heterogeneity (Jackson et al., 1990, Hutchings & de Kroon, 1994, Hodge, 2004, Hodge, 2006). The plasticity of root growth in response to nutrient availability is usually considered as foraging and is appropriate in soils considering the inherently patchy distribution of nutrients that occurs (Robinson, 1994).

The proliferation of lateral roots within a nutrient rich patch is the most frequently studied local response to nutrients. The first detailed studies focused on lateral root responses to nitrate (Drew et al., 1973, Drew & Saker, 1975) and phosphate (Drew &

Saker, 1978). This was achieved by applying NO_3^- (nitrate), NH_4^+ (ammonium) and P_i (inorganic phosphate) to a segment of barley seminal roots and it was found that this stimulated lateral root proliferation. This proliferation consisted of an increase in the number of primary and secondary lateral roots and a faster elongation rate in the treated zone. The proliferation response in nitrate patches has also been investigated in Douglas fir (*Pseudotsuga menziesii*) where root proliferation in a N rich patch increased twofold when the rest of the root system was deprived of N (Friend et al., 1990). The direction of root growth is not only determined by nutrient availability, but in fact the soil physical conditions play an important role in shaping the root system.

Mechanical impedance to the root can occur in soil that is too hard due to compaction or soil drying and can limit root elongation (Taylor & Ratliff, 1969, Bengough & Mullins, 1990). Strong soils result in an increase in root diameter and a decrease in root elongation, which alleviates stresses at the root tip and decreases bending but limits plant development (Clark et al., 2003, Valentine et al., 2012). Certain root tip traits may be beneficial for growing through strong soil and root hairs could play an important role for anchorage when the root tip experiences mechanical impedance (Bengough et al., 2011). The overall effect of strong soils is that they can cause plants to have smaller, shallower root systems. In barley, high soil strength influenced seminal root elongation more than lateral elongation and in a split-root experiment with roots growing in compacted and loose soil simultaneously, there was a proliferation of root growth in the loose soil (Bingham & Bengough, 2003).

There is still much to learn about the implications of soil factors, such as compaction, on the growth and development of the whole plant (Tracy et al., 2011). A complete understanding of the reasons for yield reduction in crops grown at high soil strength would require a systems approach to link RSA phenotype, root cellular responses, root to shoot signalling and genetic processes (Whalley et al., 2006). The tools for studying these plant processes are becoming available, however the observation of plant roots in an environmentally relevant way has long been a problem for plant scientists.

1.3 Classical methods of studying roots

Because of the opacity of soil, roots are difficult to observe in their natural environment. There are some classical methods for observing roots which have sought to evade this problem. Whole plant excavation allows measurements of the entire root system, but provides little information about the root distribution and may cause damage to the plant, especially to fine roots (Weaver, 1926). The profile wall method (Schuurman & Goedewaagen, 1971) involves digging a trench into the soil surrounding the roots and using the vertical wall of the trench to observe root distribution. This enables only a section of the root system to be observed and it may be difficult to determine which plant the roots are connected to. In order to obtain more information about the position of roots, the pinboard method was developed (Schuurman & Goedewaagen, 1971), where a board with a grid made of metal pins is driven into a trench wall to hold the roots close to their original position while the surrounding soil is removed. This provided

more information on the root architecture *in situ* but the process of separating the roots from the soil could cause the roots to move and image analysis was difficult.

Another widely used method is coring where a sample of soil is taken using an auger (Polomski & Kuhn, 2002). Coring gives information about root length and weight in a small area but no insight into the overall architecture. In this case also, the roots must be separated from the soil. Despite these restrictions, coring can provide useful data and has recently been tested for its suitability in characterising root length density in maize (Buczko et al., 2009). To observe root distribution precisely, blocks of soil containing roots can be embedded with resin which fixes the soil particles and roots *in situ*. It is then possible to grind the surface of the block so that it can be imaged at a series of thin sections (Melhuish, 1968). This method has been built upon since its original inception, for example, through fixing samples with varnish in the field before removal and impregnation with resin to improve the precision of the technique (Mooney et al., 2006). Despite its advantage of accuracy, this process is extremely time consuming and requires the use of specialised equipment.

The techniques described above can be used to study the distribution of roots in soil but different approaches have been used to investigate changes in distribution over time, or growth. Rhizotrons can be used for this purpose. They can be subsoil structures consisting of transparent windows or transparent (usually Perspex) tubes, through which the roots can be viewed and their growth can be tracked over time (Rogers, 1933, Pierret et al., 2003, Faget et al., 2010). This method has provided useful information, for

example on the uptake of water from soil by wheat roots (Boyer et al., 2010), although there are restrictions. The nature of this observation method determines that to be able to see a root, it must be touching the viewing panel, which undoubtedly will affect the roots' growth and behaviour compared with unrestricted growth in soil. Recording and measuring roots often requires the production of images.

1.4 Application of imaging to root research

Imaging is the reproduction or visual representation of objects. An image represents an object in a way that can persist over time and can also be manipulated, measured and observed. Imaging utilises electromagnetic (EM) radiation from a range of wavelengths in the EM spectrum (Figure 1.1), usually ranging from infrared radiation with a wavelength of c. 10^{-5} m to X-rays with a wavelength of c. 10^{-10} m. The way in which the EM radiation is used in imaging varies with wavelength and with application. Imaging with visible light can be performed by capturing light that is reflected from objects, as in the very first cameras and modern CCD cameras. Fluorescence imaging can also be performed with light in the visible and ultraviolet spectra and involves the absorption of light by a material which subsequently emits light of a different, longer wavelength. X-rays can penetrate some materials more easily than light and so in X-ray imaging, the X-rays are projected through an object and are then detected from the opposite side of that object. An image is produced which maps the different levels of X-ray absorption across the object.

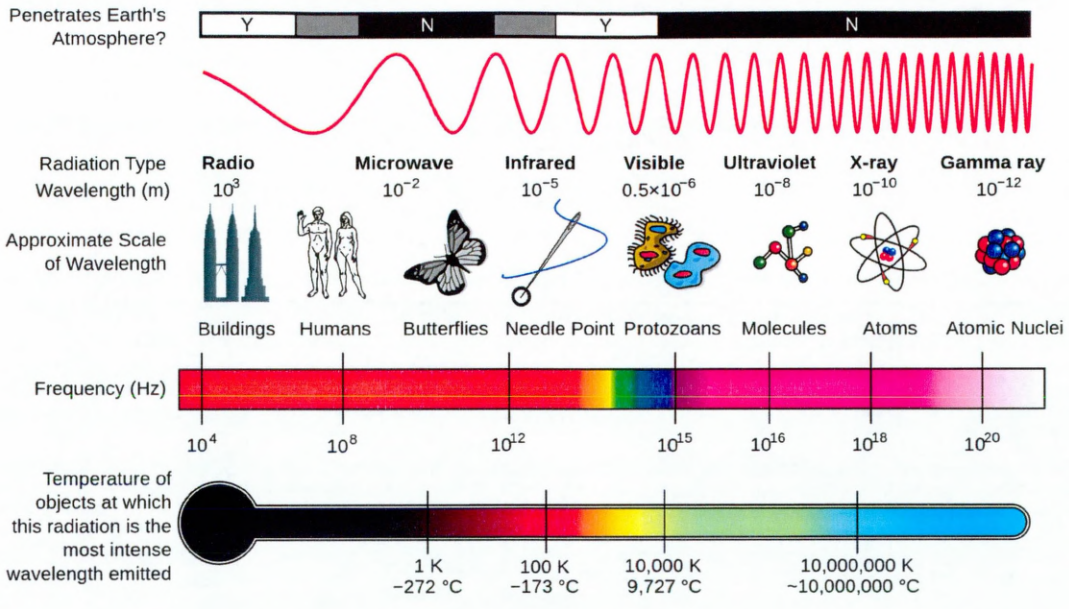

Figure 1.1. The electromagnetic (EM) spectrum. Imaging uses EM radiation in the range of infrared (10^{-5} m) to X-ray (10^{-10} m). This image is reproduced under a free documentation license (GNU).

Imaging has proved to be an important tool in root biology. On the large scale, imaging allows researchers to address questions about the structure and geometry of the root system (Wang et al., 2008) and individual roots and imaging at different time points allows the measurement of further parameters such as growth rate (Yazdanbakhsh & Fisahn, 2009). Live cell imaging and its associated genetic tools has provided information about signalling between root cells and the activity of various cell types, mostly through targeted expression of fluorescent proteins (Day & Davidson, 2009). The science of image analysis is also facilitating quantification of image data, and in fact there are tens

of software packages dedicated to analysing root system architecture (Lobet, 2012). Ultimately, being able to use imaging to find out where roots are and to localise events within their cells and in the rhizosphere in relation to the substrate structure will contribute to knowledge about their functionality and may be helpful in parameterizing root models.

1.4.1 Imaging roots in soil

X-ray micro-tomography (X-ray μCT) provides a useful, non-destructive tool for imaging roots in soil (Gregory et al., 2003, Heeraman et al., 1997, Watanabe et al., 1992). Recently, it has been demonstrated that this technique can be used in screening of crop plants for root traits (Gregory et al., 2009) and for imaging root system architecture at a series of time points (Tracy et al., 2012). One major limitation of X-ray μCT has been the image resolution. However, as the technology for the scanners has improved, the resolution has increased and it has been demonstrated that it is possible to acquire 3D images of the small roots of *Arabidopsis thaliana* plants in soil (Tracy et al., 2010, Dhondt et al., 2010). One of the main advantages of X-ray μCT is that it is possible to analyse soil structure in 3D as well (Young et al., 2001). Therefore, there is potential for this technique to be used for detailed analysis of the interaction between roots and soil particles, although the development of tools for this kind of analysis is extremely complex (Schmidt et al., 2012).

Another technique that can be used for analysis of roots in soil is Nuclear Magnetic Resonance (NMR) imaging, which has been used in studies of root systems in different

types of soil (Bottomley et al., 1993, Bottomley et al., 1986). The effectiveness of this technique varies with different soil types, soil water content and the amount of ferromagnetic particles in the soil (Rogers & Bottomley, 1987). It has proved to be a useful tool for studying water movement in plants (Scheenen et al., 2000) and in detailed investigations into plant metabolite production (Kockenberger, 2001).

Although there are new NMR and X-ray μCT scanners being developed to allow a greater image resolution (< 0.5 μm with X-ray scanners developed for materials research (Tracy et al., 2010)), there are physical limits to throughput and contrast with these methods and much higher resolutions can be achieved with optical techniques. The scanning process is time consuming and it is expensive to buy and run a scanner, therefore it is not yet suitable for high throughput screening of root traits and the technology is not available to all researchers. The data produced are always greyscale and so researchers rely on complex segmentation techniques (Zhou et al., 2006, Mairhofer et al., 2012) to discriminate the roots from the soil particles.

1.4.2 Optical imaging of roots

Light imaging covers a broad range of techniques where the uniting factor is that the information from the sample that is captured to create the image is in the form of light, ranging from ultraviolet to near infrared in the electromagnetic spectrum (Figure 1). Light interacts with matter in many different ways such as reflectance, absorption and fluorescence and it is these interactions that can be exploited in order to produce images in powerful ways. In many cases light imaging is suitable for studying biological

samples because it is possible to cover a huge range of scales, from satellite imaging covering thousands of kilometres per image, down to a few nanometres in resolution in 3D with 3D structured illumination microscopy (Gustafsson, 2005, Schermelleh et al., 2008). Acquisition is usually quick, facilitating imaging over time or studying large numbers of samples and numerous research groups have custom-built their own systems at relatively low cost to suit a particular application (Sharpe et al., 2002, Huisken et al., 2004, Santi et al., 2009, Clark et al., 2011). It is also possible to image a host of root and rhizosphere processes using light imaging, rather than simply the root structures themselves. However, light cannot penetrate the soil for imaging roots, and so various methods for growing roots in transparent systems have been developed to circumvent this problem.

1.4.2.1 *Growth environments suitable for light imaging*

Common methods for culturing plants for optical imaging of the roots involve using growing conditions which are usually homogenous physically and in water and nutrient distribution. These methods include hydroponics (Alloush, 2003) and aeroponics (Redjala et al., 2011). In hydroponics the root system is supplied with a plant nutrient solution which is usually circulated and aerated to provide oxygen and maintain the supply of nutrients to the roots. Aeroponics is similar to hydroponics, but the roots are misted with the nutrient solution. Such systems have been used to grow plants for studying, for example, cellular divisions in *Arabidopsis* roots (Sena et al., 2011), pH in maize root cortices (Kosegarten et al., 1999), and the root system architecture of rice

plants (De Dorlodot et al., 2005). Another approach is the pouch system where plant roots grow on the surface of moistened germination paper (Hund et al., 2009, Liao et al., 2001). Previous imaging studies on 3D root system architecture (RSA) have been conducted using plants grown in phytagel, which is similar to agar (Fang et al., 2009, Fang et al., 2011, Clark et al., 2011). Previous work has shown that agar and agarose behave very differently to soil with relation to soil strength and therefore great care should be taken when interpreting the results of experiments using different gel strengths to impose physical impedance on roots (Clark et al., 1999). The availability of suitable transparent growth substrates for root studies, particularly in situ and/or in 3D, has been a major limitation in the application of optical imaging to root research.

1.4.2.2 *Common methods for studying roots using light imaging*

1.4.2.2.1 Cameras and light microscopes

Information on root growth has been obtained using fairly simple imaging techniques, such as cameras and scanners. For example, time lapse video recording was used to image root growth in response to physical impedance (Gordon et al., 1992) and maize roots' response to tensile loading (Hamza et al., 2006). Root gravitropism has also been studied using video recording (Mullen et al., 2000, Brooks et al., 2010). Images from a relatively simple camera setup have also been reconstructed to produce 3D images at the root system scale in order to measure phenotypic root traits of rice genotypes (Clark et al., 2011). For detailed studies of the cells of root tissues, magnification is required and so microscopes are used and most modern light microscopes can be operated with

a CCD camera for capturing images. The light microscope has helped to provide great insight into the anatomy of roots, and has often been used to examine sections of roots with coloured stains (e.g. Zeier et al., 1999, Kubo & Hayashi, 2011). It has also been used to study living plants and for example, Beemster and Baskin (1998) analysed the relationship between root cell division and expansion. Arguably the most exceptional benefit of using light for imaging is the potential to detect luminescence, which is light emitted from material as an output from a reaction other than heat. This includes fluorescence, where light is emitted as the result of the absorption of photons and bioluminescence, where light is emitted via a chemical reaction (Daintith & Martin, 2005).

1.4.2.2.2 Fluorescence microscopy

To use fluorescence microscopy, the sample being studied must have some form of luminescent properties. The advantage of using fluorescence is that the fluorescent molecules (fluorophores) are excited by and emit light of different wavelengths. Therefore, with the use of filters, it is possible to image several fluorescent signals separately. Fluorescent dyes can be used to label particular anatomical features without the need for modification of the plant itself (Haseloff, 2003), such as neutral red which is taken up into the vacuoles of living plant cells (Dubrovsky et al., 2006). Alternatively, plants can be modified to express genetically encoded fluorescent proteins such as the green fluorescent protein from *Aequorea* (GFP) and its spectral variants, which have become indispensable tools in the life sciences as biological markers (Day & Davidson, 2009). It has allowed, for example, the production of plants with a range of spectral

variants of fluorescent proteins marking cell membranes and nuclei. This has enabled automated analysis of the dynamics of root cell shape during development (Federici et al., 2012) and new image analysis tools (Wuyts et al., 2011) to compute tissue growth in the root meristem.

Compound microscopes can be equipped with UV light illumination and excitation / emission filters so that a combination of light imaging and fluorescence imaging can be used. For example, Kubo and Hayashi (2011) related gene expression to root morphology of an *Arabidopsis* mutant and fluorescent probes were used to image Na^+ and K^+ in the cytosol of root hairs under salinity stress (Halperin & Lynch, 2003). However, confocal laser scanning microscopy (CLSM) has superseded fluorescence microscopy because of the various advantages that it offers. Confocal microscopes use laser illumination to excite fluorophores in the sample and a specified range of the emitted light is collected from the point of focus, and out-of-focus light is excluded by an aperture. The integration of the aperture, which blocks out of focus light, allows a sample to be scanned at different depths, or to be "optically sectioned", and by this means a 3D image can be acquired (Hepler & Gunning, 1998, Pawley, 2006). The latest confocal microscopes now allow subcellular resolution at more than 1 mm in depth and have up to 32 channel detectors.

CLSM has been used frequently in the field of root research. Bengough et al. (2010) used confocal imaging to collect data from roots growing in a granular media consisting of glass ballotini (spherical beads) and were able to track the movement of the root cells

over time. It has also been possible to image internal chemical processes which regulate the systemic functions of plants. The chemistry of the root apoplasm and cytosol is important for the regulation of nutrient uptake. Fluorescent probes injected into living plants have been used, for example, to measure spatial differences in apoplastic pH in relation to corn root gravitropism (Taylor et al., 1996) and Ca^{2+} (Monshausen et al., 2008). The CLSM system has been used to image spatial and temporal gene expression to gain insight into the function of potential regulators of root function. Brady et al. (2007) created a detailed spatiotemporal map of gene expression in the developing root using a combination of microarray analysis and image analysis, made possible by imaging plants with transcriptionally regulated GFP expression.

Another advantage of using fluorescent microscopy is the ability to discriminate between roots and microorganisms. This has provided great insight into the biology of the rhizosphere including the interaction between bacteria and roots. For example, the association between N fixing cyanobacteria and roots has been examined using confocal imaging of fluorescent stained roots and bioluminescent cyanobacteria (Ahmed et al., 2010) and the stages involved in the symbiotic process of root nodulation have also been observed in 3D (Haynes et al., 2004), although not in soil. The spatial colonisation of tomato roots by *Pseudomonas fluorescens* has been characterised from imaging studies (Gamalero et al., 2005, Humphris et al., 2005). Confocal imaging has also been used to examine the role of root hairs in initial root colonisation by rhizobia capable of biological fungal disease control (Prieto et al., 2011) and viral movements and interactions (Valentine et al., 2004).

Despite the advances made using these fluorescent imaging techniques, the systems have some limitations. Firstly, the commercial CLSM systems available are very costly and would be outwith the budget of many research groups. There are also physical limitations with these traditional fluorescent imaging techniques including poor axial resolution, quite a small potential imaging depth, so that an entire 3D root system could not be imaged and problems of image distortion that can be caused by spherical aberration. There is also the problem that during imaging, the whole depth of the sample is being illuminated even though only one thin section is being imaged, which can lead to photodamage of the sample due to prolonged exposure to intense laser light (Huisken, 2012).

1.4.2.3 *Emerging techniques for optical imaging*

Planar optode imaging has recently been applied to the study of rhizosphere pH (Blossfeld & Gansert, 2007, Blossfeld et al., 2010). The technique allows for detailed, dynamic 2D imaging of pH gradients with the plants growing in soil and the roots growing along a flat surface with a planar optode. By imaging roots at 15-minute intervals, daily variations in pH and overall acidification were revealed. The application of optodes is not limited to studying pH. For example, Blossfeld et al. (2011) carried out a combined study on the dynamics of rhizophere pH and soil oxygen, which has important implications in the survival of rhizosphere bacteria as the rhizosphere becomes hypoxic with root growth over time. The technique has also been used to study the depletion of ammonium around roots (Strömberg, 2008) and in bulk soil (Delin

& Strömberg, 2011). Because of the detailed quantification of rhizosphere processes made possible with this technique, it seems likely that this adaptable approach will become more popular and available to root researchers as an imaging tool.

Light sheet-based microscopy techniques are suitable for 3D fluorescent imaging of biological samples. The method involves a sheet of laser light which illuminates an optical section of the sample. An objective lens is positioned perpendicularly to the illumination plane which the illuminated section of the sample is focused on. 3D images are created by moving the sample through the illumination plane while a sequence of 2D images is captured (Huisken et al., 2004). This technique has advantages over CLSM because of an improvement in the axial resolution and also because the excitation light illuminates a much smaller section of the sample for each image, thus avoiding potential problems of photodamage to the sample. This is particularly important when imaging live specimens at multiple time points. Light sheet microscopy (LSM) has been applied to the study of plant roots. Sena et al. (2011) used light sheet fluorescence microscopy to image cell divisions and the nuclear dynamics of *Arabidopsis* roots grown in a small hydroponics system over a few days. *Arabidopsis* primary root tip growth and lateral root emergence have also been imaged using a light sheet based system (Maizel et al., 2011).

Recent advances in optical imaging allow imaging of large samples in 3D, up to several mm in size, and with high resolution. Optical projection tomography (OPT) was developed for imaging animal embryos and involves projecting light through the sample

and collecting transmission images while the sample is rotated through 360° (Sharpe et al., 2002). Fluorescence can also be captured by using a UV light source to illuminate the sample and emitted light can be captured as well as the transmission images. This has proved very useful for imaging embryo morphology and gene expression patterns simultaneously (Fisher et al., 2008, Fisher et al., 2011). OPT has been used to image plant shoots and roots (Lee et al., 2006) but the challenge remains to use this approach to image living plant roots over time.

There has been a recent development in microscope optics to allow imaging of large samples (up to 6 mm) but with subcellular resolution without the need to reconstruct the image from a series of tiles. The development is a giant lens, 0.5 meters in length, with 4× magnification, a N.A. of 0.47 and a large working distance of 3 mm. It has been called the mesolens (Amos et al., 2010, Saini, 2012). The aim is to integrate the mesolens into confocal laser scanning and light sheet microscopes for 3D imaging. The mesolens would be extremely useful for many kinds of biological samples and it would also be beneficial for imaging plant roots to gather information on the whole root and relate the morphology and growth to cellular processes with one image.

1.4.3 Challenges for high throughput phenotyping

Imaging can be used for plant high throughput phenotyping in crop breeding (Furbank, 2009). A large number of root systems can be imaged, information describing the root system architecture extracted and analysed and plants with beneficial traits can be selected in relation to the genomic information (De Dorlodot et al., 2005, Yazdanbakhsh

& Fisahn, 2009, Clark et al., 2011, Grift et al., 2011). High throughput, 3D imaging of roots in an environmentally relevant situation would provide useful information for the purpose of selective crop breeding. However this is currently an important challenge in the field of root biology because 3D imaging in soil is time consuming and therefore not currently suitable for high throughput studies and current growth systems for fast, optical imaging do not have the physical heterogeneity of a soil substrate. In order to aid the application of new optical imaging techniques to roots and soil biology, it would be beneficial to develop alternative growth substrates for plants and soil biota.

1.5 Aims

Because root structures have been evolving to function in naturally heterogeneous substrates for millions of years (Elick et al., 1998), it is only logical to try to incorporate the physical heterogeneity of soils into substrates for culturing plants for root studies. An optically transparent substrate which also incorporated soil-like physical heterogeneity would provide root researchers with more environmentally relevant alternatives to phytagel and hydroponics for imaging studies. The first aim of this thesis is to describe the development of a transparent soil: a transparent, heterogeneous substrate that can support the growth of soil biota and is compatible with many of the optical imaging techniques described in this Chapter. Secondly, the aim is to use the substrate to optically image roots in 3D, producing data suitable for image analysis. The third aim is to manipulate the physical properties of the transparent soil in order to replicate different soil conditions, grow plants in the substrates, image the root systems

and analyse the effect of substrate physical conditions on the root growth trajectories. The fourth aim is to use transparent soil to gain insight into the interactions between plant roots and their associated bacteria.

Chapter 2. Application of refractive index matching to engineer a soil-like transparent substrate

2.1 Introduction

Soil is a heterogeneous matrix of rock fragments, organic matter, water and air. It is this structure that is essential for hosting a vast array of soil organisms, and indirectly all other terrestrial life (Park, 2001). Although there are methods that enable imaging in natural soil in situ, ways of observing soil using light are limited. Light and optics as a medium for imaging biological samples can provide valuable information through the use of dyes and fluorescent proteins (Gurr, 1971, Day & Davidson, 2009). For this reason, it is beneficial to use a transparent substrate instead of soil so that the light used for imaging can penetrate the substrate. Previous studies have used gel-based substrates for growing plants and imaging the roots (Fang et al., 2009, Clark et al., 2011) but these substrates do not have any of the chemical and physical complexity of real soil. The objective of this study is to engineer a transparent heterogeneous substrate that can be used for imaging the roots of living plants and soil organisms in situ using the principle of refractive index (RI) matching.

Materials and techniques that can be applied to engineer a RI matched transparent granular substrate that could be used for imaging plants and soil organisms were investigated. At the boundary of two transparent materials with different refractive indices, the path of light is distorted through refraction (Figure 2.1, B). By matching the

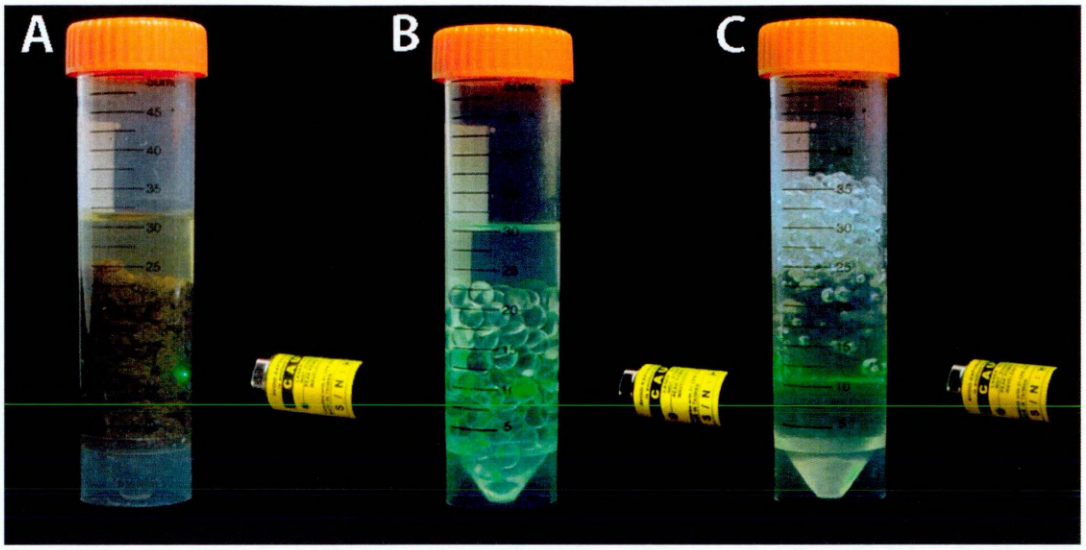

Figure 2.1. Illustration of the use of RI matching for soil science. A) Soil sample saturated with water where the soil itself is opaque and therefore the laser beam cannot penetrate the sample. B) Transparent particles of the low refractive index fluoropolymer, Nafion in water. The laser beam can penetrate these transparent materials but because of the RI mismatch between the liquid and particles, the laser beam is scattered and imaging at depth is not possible. C) Nafion particles in a RI matching liquid. The laser beam penetrates the sample and the amount of scattering of the laser beam is greatly reduced by matching the RI of the liquid and particles.

refractive index (RI) of a solid and a liquid, this effect is negated so that the boundaries between the materials become invisible. RI matching has proved a powerful approach in many areas of physical sciences, such as fluid dynamics (Budwig, 1994) and colloid sciences (de Villeneuve et al., 2005). In soil mechanics, amorphous silica particles have

been used with oil-based RI matching solutions (Mannheimer & Oswald, 1993) and have similar mechanical properties to clay (Iskander et al., 2002). This system has been used for investigating particle displacement in response to the application of mechanical forces. Recently, the technique of RI matching has been adapted for growing and imaging aquatic biofilms on particles of Nafion (Leis et al., 2005) where limited RI matching was achieved using water.

The aim of this Chapter is to develop a transparent, refractive index matched substrate with solid particles, water and plant nutrients. This will be done by searching for and testing solid transparent materials with low refractive indices and searching for suitable aqueous solutions to match the refractive index of the solid materials. Both materials are required to have chemical properties that have as little effect on the plants' physiology as possible. Manipulating the particle sizes of the solid material is one way to control the properties of the substrate and so methods of engineering this property will be tested. The interaction between the solid particles and fluorescent dyes is also of interest for the purpose of labelling the particles for detection during fluorescent imaging and so another aim of this Chapter is to explore the interaction between the solid transparent materials and a selection of fluorescent dyes. Overall, this Chapter compiles information on transparent materials that were considered and tested and describes a series of pilot experiments to test the suitability of different materials for use in constructing the transparent soil substrate.

2.2 Materials for refractive index (RI) matching

In the fields of geotechnical engineering, fluid dynamics and physics, RI matched soil-substitutes have been constructed using materials such as amorphous silica gels or powders (Lai et al., 1994, Iskander et al., 2002, Liu & Iskander, 2010, Iskander & Liu, 2010), quartz (Fontenot & Vigil, 2002, Ezzein & Bathurst, 2011) and glass (Mannheimer & Oswald, 1993, Marulanda et al., 2000). These materials have been suitable for physical studies of soil processes. However they are not suitable for biological studies because their RIs are significantly higher than water, meaning that aqueous solutions or organic liquids have to be used for matching. The aqueous solutions used in previous studies have included glycerine, zinc iodide and ammonium thiocyanate and the organic liquids have included kerosene, paraffin oil, turpentine and olive oil (Budwig, 1994). These liquids would be unsuitable for culturing plants and soil organisms. We searched the scientific literature and online materials databases for transparent materials with low RIs with a target value of $n \leq 1.34$ (RI of water: $n = 1.33$). The other properties that were considered in our search were transparency, suitability for sterilisation by autoclaving, water retention (how well water is retained in a matrix), suitability for manipulation of particle size, ion exchange capacity and cost. Three candidate materials are described below.

2.2.1 Cryolite

Cryolite (Na_3AlF_6) is a rare mineral with a white to transparent appearance (Figure 2.2) and a refractive index of 1.336 (Ralph & Chau, 1993-2012). Although cryolite's RI is very

close to that of water and is therefore suitable for RI matching, there are various practical issues which make it difficult to use. As it is a naturally occurring mineral, it is usually the case that there are impurities within the material which impede its transparency. It is also fragile and so small grains continually break off while it is being handled. Cryolite is also difficult to source because it has been located in very few mines globally, including in western Greenland and it is therefore very rare and costly. We were able to source the material only from ebay, UK.

2.2.2 Fluorinated ethylene propylene (FEP)

Given the lack of naturally occurring suitable materials, we turned our attention to transparent synthetic materials, and in particular fluoropolymers. Teflon FEP is a brand of fluorinated ethylene propylene that is produced by Dupont de Nemours® and was supplied by Dupont de Nemours®. Additionally, FEP is recycled industrially and we were also able to source low cost recycled FEP from Holscott Fluoroplastics Ltd., UK. It is often used as a non-stick hydrophobic coating but can be obtained in a non-processed form as granulates (Figure 2.3, A). It is reasonably transparent in small volumes and has a RI of 1.337 (DuPont, 1996). The hydrophobicity of FEP can be problematic for maintaining water availability for plants throughout the matrix, although chemical etching can be used to decrease the hydrophobicity (Acton Technologies, 2000 - 2008). It was possible to grow *Nicotiana benthamiana* (tobacco, from SCRI stocks) in a substrate composed of FEP granulates with added Modified Strullu Romand (MSR) nutrient medium (Strullu & Romand, 1986) medium in 3.5 ml plastic cuvettes (Fisher Scientific UK Ltd., Loughborough, UK). The seeds were surface sterilized by washing in 10% bleach

(Domestos, Unilever, UK) for 20 minutes followed by several sterile dH_2O washes. They were then transferred to the cuvettes on top of the substrate using a pair of fine forceps (Figure 2.3, B). Saturation of the substrate was necessary throughout the growth period to prevent the plants from drying out, due to the relatively large particle size (approx. 3 mm) and hydrophobic surface properties of the FEP. Ideally the substrate could be used at a variety of water contents therefore these properties were not ideal.

FEP was tested to assess whether it had any chemical effect on the growth of *Nicotiana benthamiana* plants. MSR medium was used for culturing tobacco seeds. FEP particles were incorporated into 7 g L^{-1} phytagel (Sigma, International) with MSR nutrient medium that was set in 9 cm petri dishes. Seeds were sown on the surface of the phytagel and the petri dishes were sealed with 50 mm parafilm (VWR, Pennsylvania, USA) and were placed vertically in the growth room so that the roots grew on the surface of the gel to negate any mechanical impedance caused by the particles. Controls were also set up using phytagel with no FEP. Plants were imaged and the root length was recorded after 3, 7 and 10 days. This was done by placing the petri dishes directly on a flatbed scanner and scanning at 300 dpi (Epson expression 1640 XL, Hemel Hempstead, UK) with a black background. Primary root lengths were measured from the resulting scans using the segmented line function from ImageJ software (National Institutes of Health, USA). 16 plants were subjected to each treatment. T-tests (performed in Sigmaplot 12.3, Systat Software Inc., London, UK) showed that there was no significant difference between the root lengths of plants grown with or without FEP at 3 days ($p = 0.809$), 7 days ($p = 0.511$) or 10 days ($p = 0.588$) (Figure 2.4).

Figure 2.2. Particles of the mineral cryolite – a candidate material for constructing a transparent, granular, RI matched substrate. Scale bar = 1 cm.

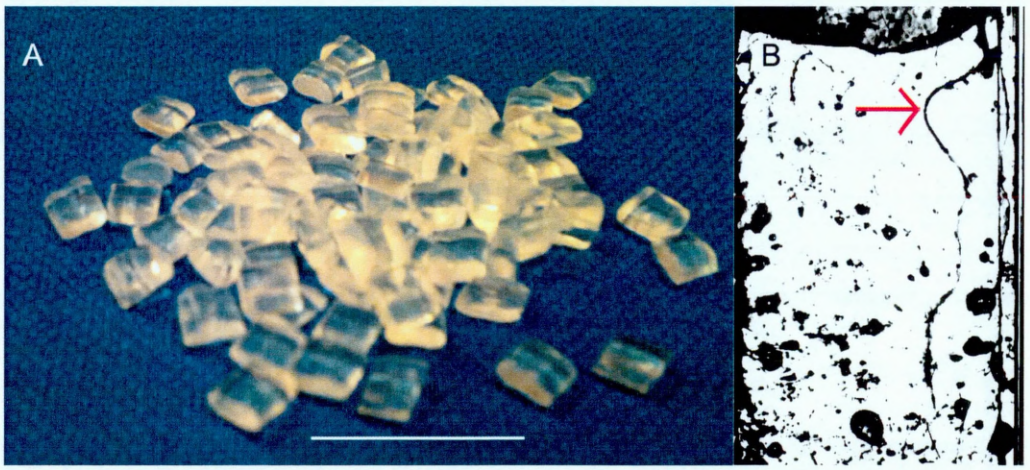

Figure 2.3. FEP - a candidate material for constructing a transparent substrate. A) Granulates of FEP in its unprocessed form. Scale bar = 1 cm. B) Root imaging was achieved in an FEP-based, saturated, RI matched substrate. Red arrow indicates the root.

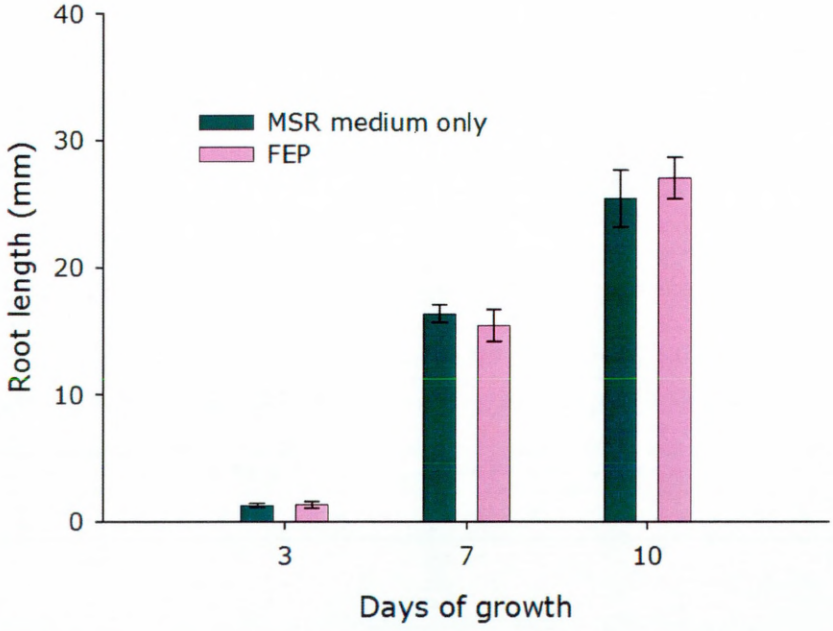

Figure 2.4. Mean primary root lengths of Nicotiana benthamiana *plants grown in Modified Strullu Romand (MSR) medium (Strullu & Romand, 1986) with and without FEP after 3, 7 and 10 days of growth. Error bars show standard error.*

2.2.3 **Nafion**

Nafion is a brand of perfluorosulfonic acid / tetrafluoroethylene (Teflon) copolymer that allows ion transport and therefore is commonly used in fuel cells in membrane form (e.g. Bi et al., 2008, Lu et al., 2012), although it is also available in pellet form from Ion Power Inc. (Figure 2.5, A). It has the chemical structure shown in Figure 2.5, B. The material has a low light attenuation, a refractive index of 1.34 (Leis et al., 2005) and is hydrophilic when hydrolysed, therefore providing water retention in a matrix of Nafion particles. Particles of Nafion have been used for growing and imaging aquatic biofilms (Leis et al., 2005) where limited RI matching was achieved using water. Given these properties and the fact that the material has been used in culturing live organisms, Nafion was a good candidate for a solid material to use in a transparent granular substrate for growing and imaging plants and soil organisms, despite its relatively high

A

B

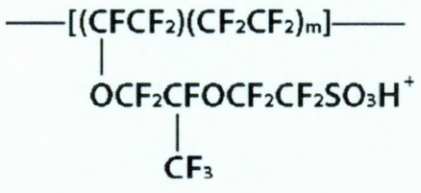

Figure 2.5. Nafion. A) Nafion pellets as supplied by Ion Power Inc. Scale bar = 1 cm. B) Chemical structure of Nafion.

cost (approx. $5 per gram, compared to approx. £5 per kg for FEP). Table 2.1 summarises the properties that were considered for cryolite, FEP and Nafion.

	Nafion	FEP	Cryolite
Transparency	++	+	-
Cost	-	++	-
Refractive index	1.34 (Leis et al., 2005)	1.34 (DuPont, 1996)	1.338 (Josephson & Flessa, 1972)
Sterilization by autoclaving	+	+	+
Water retention (how well water is retained in a matrix)	++	-	+
Suitability for manipulation of particle size	++	+	+
Ion exchange capacity	++	n/a	?

Table 2.1. Summary of properties of the materials that were considered for use in constructing transparent soil. ++ indicates very suitable, + indicates suitable and – indicates not suitable. The autoclaving procedure was 121 °C for 20 minutes at 2 bar. Transparency, water retention and the effect of autoclaving were all assessed visually. Manipulation of particle size was tested using methods described in section 2.4, page 38. Values for RI are quoted from the cited literature.

2.3 RI matching liquids

The RI matching liquids used in engineering studies (previously described in section 2.2, page 28) would not be suitable for growing and live imaging of plants. We did not find a suitable solid transparent material with a RI equal to that of water and so it was necessary to increase the RI of the solution used to saturate the pore spaces of the substrate so that it was equal to the RI of the solid material. The RI was increased by adding solutes to water-based plant nutrient solutions, which were either MSR medium (Strullu & Romand, 1986) or 2.2 g L^{-1} Murashige & Skoog Basal medium (Sigma), but the additive substance had to be considered carefully. The ideal substance should have little effect on the viscosity and light attenuation of the liquid and should not have an effect on the organisms cultured in the substrate. Various substances were considered based on their transparency, viscosity, effect on plant growth and cost and their properties are summarised in Table 2.2.

One of the substances considered was methyl cellulose, but this made the liquid too viscous and could not be sterilised by autoclaving without denaturisation. Sucrose was also considered as an additive. The relationship between sucrose solution and RI is well-described (Rosenbruch et al., 1974) and sucrose has been previously applied in RI matching (Budwig, 1994). However sucrose has been shown to invoke responses in the gene expression, development and growth of plants (Rook & Bevan, 2003). Sorbitol is an alcohol sugar and, like sucrose, is effective at increasing the refractive index of a solution. However, unlike sucrose it is a compatible solute (an organic compound that

does not interfere with enzyme function). Sorbitol solutions do however exert an osmotic stress on the plants, which has been found to decrease maize root elongation rates (Bustos et al., 2008).

Another option that was investigated was Percoll. Percoll is a commercially available transparent colloid suspension, normally used for density gradient centrifugation of cells and other particles. It is a silica solution with covalently linked silane and is impermeable to biological membranes. Although some light scattering occurs with Percoll because of

	Methyl cellulose	**Sorbitol**	**Percoll**
Effect on plant growth	+	-	++
Transparency	-	++	+
Cost	++	++	-
Viscosity	-	++	++

Table 2.2. Summary of chemicals used for increasing the refractive index of the matching solution for transparent soil. ++ indicates very suitable, + indicates suitable and – indicates not suitable. The most suitable concentrations to be used were determined later based on the refractive index matching. The effect on plant growth was inferred from the chemistry of the substances and from literature on the effect of sorbitol on plant development (Bustos et al., 2008). Transparency and viscosity were assessed visually.

the colloidal particles, it was deemed to be the most suitable RI matching liquid because of its impermeability to membranes and therefore would be suitable for imaging at multiple time points to reduce the stress on the plant. However, sorbitol was also used in some cases, especially where root imaging was carried out at only one time point, because it is much less expensive than Percoll. The properties of methyl cellulose, sorbitol and percoll are summarised in Table 2.2. It is worth noting that the concentration of the matching solution must be decided on through experimentation in combination with the solid material with which it is to match. One method for finding the best solute concentration for RI matching with a solid material is described in Section 3.2.2 (page 54).

In order to use transparent soil as a substrate for plant growth experiments, particles of the solid material could be added to a container with some water and plant nutrients to form a soil-like matrix of solid particles, air-filled pore spaces and liquid in the smaller pores. The process of saturating the pore spaces for refractive index matching of the transparent soil was performed using a 5 ml syringe and a 60 mm long hypodermic needle (BD Becton Dickinson UK Ltd., Oxford, UK). The needle was inserted from the surface of the substrate, as far from the plant as possible to the base of the tube where the RI matching liquid was slowly released. In cases where a lot of air bubbles were trapped in the transparent soil, gently tapping the sample on the bench helped to release them. Visual assessment revealed that trapping of air bubbles became more of an issue when small Nafion particle size categories were used (e.g. <500 µm, separated by sieving using a 500 µm mesh size sieve, Fisher Scientific UK Ltd., Loughborough, UK.)

and so another method for releasing air bubbles was investigated. Liquefaction, a process that occurs naturally in soil due to the application of certain forces (Sonmez, 2003), was also investigated as a means of releasing bubbles from the saturated substrate. This was tested using a lab orbital shaker (Stuart brand, Bibby Scientific Ltd., UK) at the highest frequency setting (1250 rpm). The results were that the bubbles were often released but the shaking also resulted in disturbance of the plant. For this reason, liquefaction was not used but as a technique it does have potential subject to some more development and testing and may be particularly useful for larger samples.

2.4 Engineering particle size distribution

Nafion particles were supplied as pellets with a diameter of 3–4 mm (Ion Power Inc.), but in order to control the particle size distribution to increase water retention, a number of techniques were investigated, mostly based on reducing the initial particle size by fracturing the material. The particle size range of sand (50–2000 μm (Jahn et al., 1990)) was used as a reasonable target particle size for the transparent soil. Although Nafion is rigid, the results of preliminary experiments to find a method for breaking up the pellets revealed that mechanical impact (using a hammer) of dry pellets at room temperature caused their deformation rather than breaking them up (i.e. they were squashed rather than shattered), due to the structure of the polymer. This was concluded after visual assessment. The results were similar when a standard ball mill (MM200, Retsch, Castleford, UK) was tested.

In general freezer milling involves a sample holding cylinder with a metal impactor which operates in a tank of liquid nitrogen. The effect of the liquid nitrogen is to cool the material, thus changing its mechanical properties making it more brittle. A freezer mill (6850, SPEX SamplePrep, UK) was effective for reducing the size of Nafion pellets into a range of particle sizes. Duration and frequency of milling could be controlled in order to manipulate the resulting particle sizes. The most effective procedure was found to involve a period of precooling a sample of 10–20 g for 2 minutes in the sample holder, in a polystyrene box with liquid N_2, milling at the highest frequency (10 arbitrary units) for a period of 2 minutes and then sieving through a series of sieves with mesh sizes 500, 850, 1250 and 1600 μm (Fisher Scientific UK Ltd.). Particles larger than 1600 μm were returned to the freezer mill. Once all of the particles were smaller than 1600 μm, the distribution of material in each of the size categories was visually assessed and there were usually more particles in the largest size categories. To even-out the distribution for subsequent experiments where equal volumes of the different particle size categories were required, some of the particles in the largest category were returned to the freezer mill.

Milling at room temperature or in liquid nitrogen was not sufficient to reduce the size of FEP particles. Some deformation occurred after using milling machines but the particles did not shatter. A Tesco BL09 350W Value Blender (Tesco, Dundee, UK) was also tested for breaking up the FEP particles but was not effective. These conclusions were drawn after visual assessment of the particles after hammering, milling or blending. The chemical structure of FEP is quite different from Nafion and it is possible that the

porosity of Nafion could make it more susceptible to breaking during freezer milling. Probably the best option for making FEP with customised particle sizes would be to commission production at the melt extrusion stage, although this was not carried out.

2.5 Controlling the properties of the solid/liquid interface

It is important to be able control the surface properties of the solid particles because the interaction with water has an effect on the overall water retention of the substrate. Water tension at the surface of particles is a significant contributing factor to soil water retention and therefore the availability of water to the roots. Since most polymers, such as FEP, are hydrophobic, the water retention of a particulate matrix of these materials would be poor. Hydrophilic particles of polymers such as Nafion however have a greater propensity to maintain a coating of water under non-saturated conditions, thus avoiding complete drying of the substrate. It was also desirable for the particles to be hydrophilic since the RI matching technique involves saturation of the substrate before imaging and it was thought that air bubbles were less likely to form and become trapped when the solid particles are hydrophilic.

A number of approaches were investigated for increasing the water retention of FEP. Hydrophilic coatings are available for use in the sailing industry. One such coating was tested by spray coating with an aerosol – hyspeedkote (Mailspeed Marine, UK), but was not effective because it did not adhere to the FEP particles. Hyspeedkote is orange in colour and so it was clear from visual assessment after spraying that the chemical was

not coating the FEP particles. Chemical etching is used for FEP to improve bonding with other materials. It involves submerging the FEP in the chemical etchant, FluoroEtch® (Acton Technologies, Pennsylvania, USA), which strips the fluorine from the carbon backbone of the FEP, replacing it with hydroxyl, carbonyl and carboxyl groups, changing its surface structure to allow bonding (Acton Technologies, 2000 - 2008). This process was tested on 2 pieces of FEP tubing, 5 cm length, 3 cm diameter (Holscott Fluoroplastics Ltd., UK) by submerging them in a beaker of undiluted FluoroEtch® (enough to submerge the tubes) for > 1 hour. It was found, from visual assessment of the contact angle between the etched and non-etched tubes and water (where an acute contact angle indicated high hydrophobicity and an obtuse contact angle indicated low hydrophobicity) to decrease the hydrophobicity of the material. The addition of surfactants to the liquid in the substrate was also tested as a means of reducing the number of trapped air bubbles after saturation. The number of bubbles was assessed visually and it was found that the addition of surfactants did not lead to a noticeable improvement.

Nafion is available in precursor and acid forms, which have different surface properties. They exchange ions in solution and this process is inextricably linked to physics of the solid / liquid interface.

2.6 Ion exchange

Ion exchange capacity is also an important property of soil, because it allows the adsorption of mineral ions to soil particles. These ions exchange with other ions in the

soil water, thus supplying nutrients for plant nutrition. It is therefore an important factor to control in an artificial system. Unlike FEP, Nafion has ion exchange capabilities and if directly combined with any plant nutrient solution to create a substrate, the protons of the Nafion's sulphonic acid groups (SO_3H^+) exchange with other cations in the solution and the excess protons in the solution causing it to become acidic very rapidly and the pH of the solution can become very low and therefore unsuitable for any plant growth.

I experimented with methods described by Van Nguyen et al. (2007) for chemically treating the surface of the Nafion particles in order to remove inorganic impurities and ensure the full conversion to the H^+ form before occupying the surface exchange sites with common soil cations. It was found that by repeatedly washing a 10 g sample of the hydrolysed Nafion particles with a concentrated plant nutrient solution (MSR medium at stock concentration (Strullu & Romand, 1986)) by immersing the particles in a beaker with a volume sufficient to cover the particles, cations from the nutrient solution bound to the exchange sites, replacing the protons, which were discarded by changing the washing solution. The process was monitored by measuring the pH after each wash using a using a desktop pH meter (Mettler Toledo FE20). Eventually, the pH remained stable, showing that the exchange sites were saturated with cations such as Mg^{2+}, K^+, Ca^{2+}, and Na^+.

This process resulted in the development of the following protocol which was used for preparing Nafion particles for transparent soil and was used throughout the thesis.

Cation exchanging Nafion particles were made by ensuring full conversion to the acid form by washing in a solution of 15% w v^{-1} KOH, 35% v v^{-1} DMSO and 50% dH_2O at 80 °C for 5 hours, then with dH_2O (milliQ) at room temperature for 30 minutes followed by several dH_2O rinses. This was followed by 2 washes in 15% v v^{-1} nitric acid in dH_2O at room temperature: 1 wash for 1 hour and 1 wash overnight. The particles were treated with 1M sulphuric acid for 1 hour at 65 °C, and the acid was removed and replaced with dH_2O at 65 °C for 1 hour. After cooling, the particles were washed several times with dH_2O. They were then washed in a 3 wt % H_2O_2 solution at 65 °C for 1 hour and allowed to cool. The particles were rinsed again multiple times with fresh dH_2O (Van Nguyen et al., 2007). To titrate the particles with mineral ions, concentrated (i.e. undiluted) MSR medium (Strullu & Romand, 1986) was used to immerse the particles. These were shaken at 30 °C in an incubator shaker (New Brunswick Scientific, Enfield, USA) for 30 minutes before renewing the nutrient solution. This was repeated until the pH of the nutrient solution was neutral and stable after adding it to the particles. pH was measured using a desktop pH meter. The particles were rinsed with dH_2O to remove excess MSR medium. Before use, the particles were autoclaved submerged in dH_2O for sterilisation using a Boxer 220/40LR benchtop autoclave (Lab3 Ltd. Northampton, UK) for 20 minutes at 121 °C and 2 bar. This regime and machine was used throughout the thesis.

Nafion also has the useful capability to be chemically converted from the precursor form to the cationic form (exchanging anions) using a method developed by Salerno et al. (2012) (Figure 2.6). This was done by using a bridging cation, dimethylpiperazinium (DMP), which ionically binds to the Nafion exchange sites, and provides further exchange sites where initially fluoride ions were available for exchange. To do this, acid form Nafion particles were added to DMP in a beaker (with enough DMP to cover the particles) at room temperature for 3 hours. The DMP was removed by pouring it from the beaker and the particles were rinsed several times in dH_2O and left overnight in dH_2O. The Nafion was then treated with KOH, where the F^- ions were exchanged with hydroxide ions. This was done by removing the dH_2O and flooding the particles with 3M

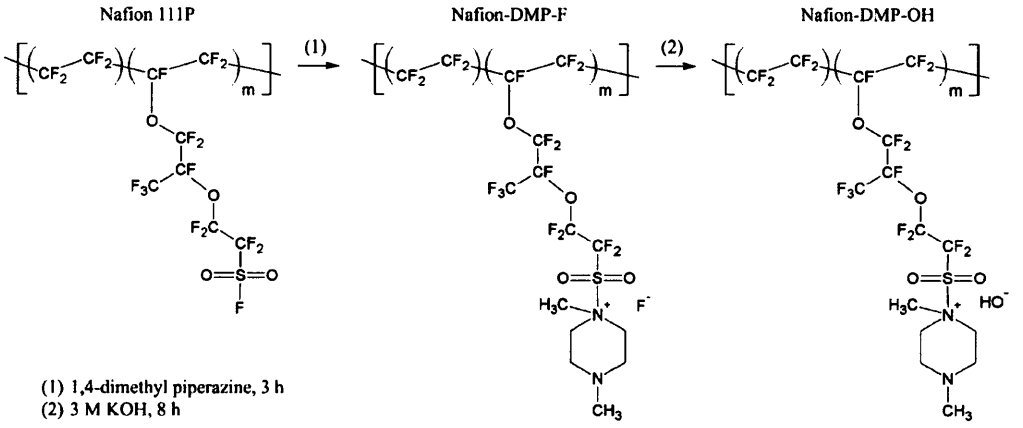

Figure 2.6. Schematic diagram of the steps taken to produce cationic Nafion. DMP is added to precursor Nafion, which exchanges with the fluoride ions. KOH is then used to hydrolyse the Nafion, leaving an exchangeable hydroxide ion. Reproduced from Salerno et al. (2012) with permission from John Wiley and Sons.

KOH. This was left at room temperature for 8 hours and then rinsed multiple times in dH_2O over 24 hours. The nutrient titration of the Nafion was then carried out in the same way as with the anionic Nafion, described in the previous paragraph.

2.7 Labelling

2.7.1 Visualising transparent soil particles

When applying fluorescent imaging to biological structures such as roots in a transparent granular substrate, it is beneficial to be able to locate the transparent particles by making images of them. To achieve this using transparent soil, one approach was to use fluorescent dyes. In fluorescent imaging, there are many fluorescent dyes available with a range of absorption and emission wavelengths. Dyes with peak emission in the red range of the spectrum (>580 nm) were tested with Nafion and FEP particles. Red dyes were chosen to avoid overlap with GFP, the most common fluorescent protein used as a marker in live organisms, and because there is good availability of red fluorescent dyes (Gurr, 1971).

In terms of image visualisation and image processing, it is most desirable for the dyes to be adsorbed on the surface of the particles. The advantage of this is that when the 3D image is produced, the boundaries of the particles can be easily visualised in relation to the plant roots and in image analysis; having the particle boundaries delineated facilitates measuring the particle dimensions and locations. We tested several red fluorescent water soluble dyes by making up an aqueous solution of the dye, where the concentration was based on previously used concentrations in the literature. The dyes

tested were sulphorhodamine B (5×10^{-6} M), sulphorhodamine 101 (5×10^{-6} M), Rhodamine 6G (1×10^{-3} M) (all from Invitrogen) and Pyronin Y (3.3×10^{-3} M, Sigma).

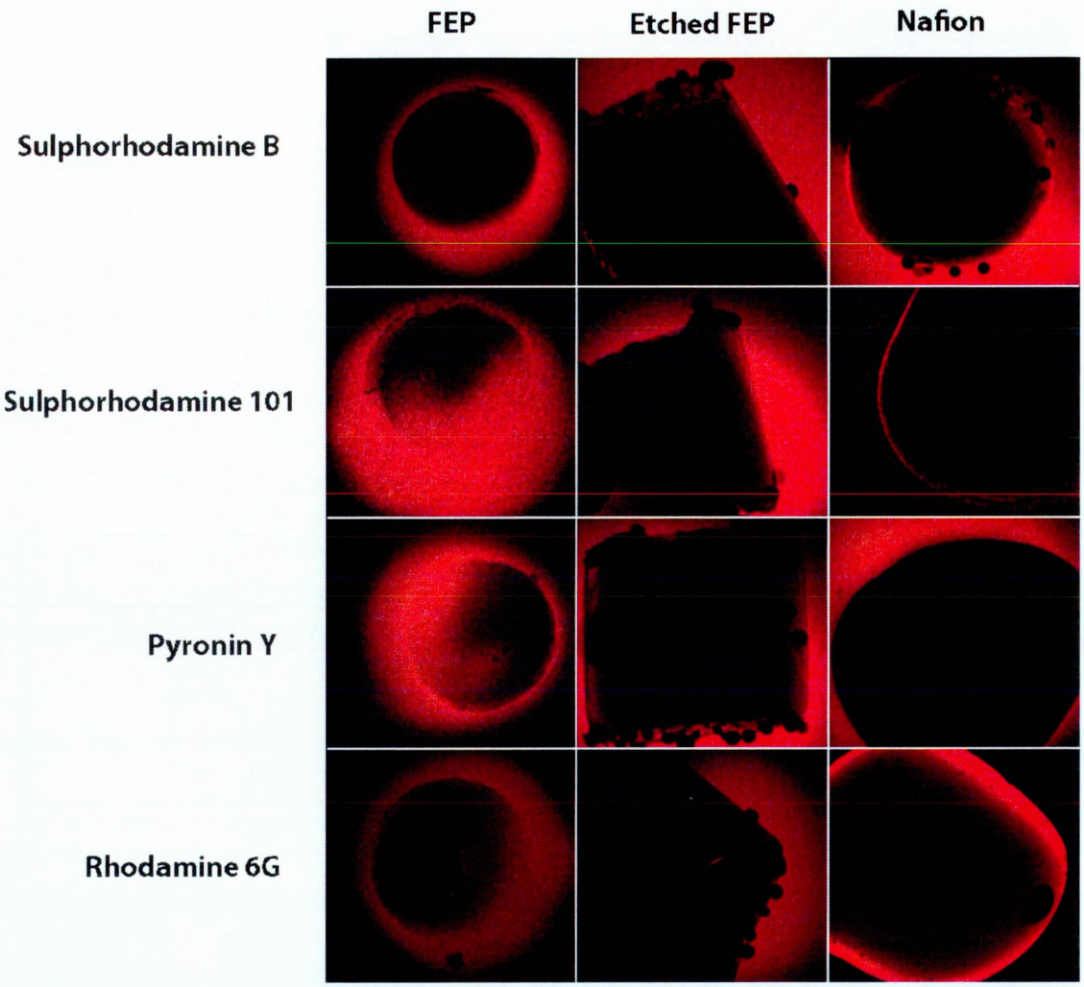

Figure 2.7. CLSM images showing the interaction between red fluorescent dyes and FEP, etched FEP and Nafion particles. Binding was evident where there was a bright red region around the surface of the particle. Sulphorhodamine B, sulphorhodamine 101 and Rhodamine 6G bound to the Nafion particles, but in all other cases, the dye did not bind to the material.

500 µl of the dye solution was added to single particles of FEP, etched FEP and H^+ form Nafion in wells of 96 well flat bottom 400 µl microplates (Fisher) and images of the dye surrounding the particles were captured using a Leica TCS SP2 confocal laser scanning microscope with a 10× / 0.30 dry objective lens. This confocal microscope was used throughout the thesis. The results showed that none of the dyes bound to FEP; the dyes sulphorhodamine B (5×10^{-6} M), sulphorhodamine 101 (5×10^{-6} M) and Rhodamine 6G (1×10^{-3} M) (all from Invitrogen) bound to Nafion in the anionic form. Pyronin Y (3.3×10^{-3} M, Sigma) did not bind to anionic Nafion (Figure 2.7). None of the dyes were tested with cationic Nafion, and so dyes which do not bind to anionic Nafion may bind to cationic Nafion.

Several blue dyes were also considered and tested for labelling the Nafion particles in order to complement experimental setups where there would be emission from biological structures with fluorescent proteins in the red (c. λ 630 – 700 nm) and green (c. λ 515 – 555 nm) parts of the spectrum. 7-amino-4-methyl coumarin (Sigma) was not tested because it is not water soluble. Alexafluor 350 hydrazide (Invitrogen) may have been suitable but was not tested because there was no 350 nm laser available on the CLSM setup used, which was required for excitation of alexafluor 350 hydrazide. Another potential dye, Alexafluor 450 cadaverine was tested by making a 1 µg ml^{-1} solution in dH_2O, adding the solution to 2 or more Nafion particles and checking for binding on the surface using the confocal microscope. Imaging was carried out using 450 nm laser excitation and collecting emitted light between 480 and 580 nm. The dye did not efficiently label anionic, titrated Nafion, but was slightly more effective when it

was added to the acid particles, before the nutrient solution was added. The bond between the dye and the particles' surface was certainly not as strong as that between the particle and the red dye sulphorhodamine B. It was not tested with cationic Nafion and this may be another route for development.

None of the dyes tested bound to FEP, etched or non-etched (Figure 2.7), however there may be other ways of carrying out fluorescent imaging of materials such as FEP. For example, it might be possible to introduce the dye at the stage of processing the polymer by making the dye lipophilic by means of ion pairing with a water soluble ionic surfactant with the opposite charge to the dye molecule (Mohr, 2006). It was possible to image FEP particles with the confocal microscope by adding the red dye, sulphorhodamine B to the liquid saturating the pore spaces of the matrix at a concentration of 5×10^{-6} M in water, with the mixture in a 3.5 ml fluorometer cuvette

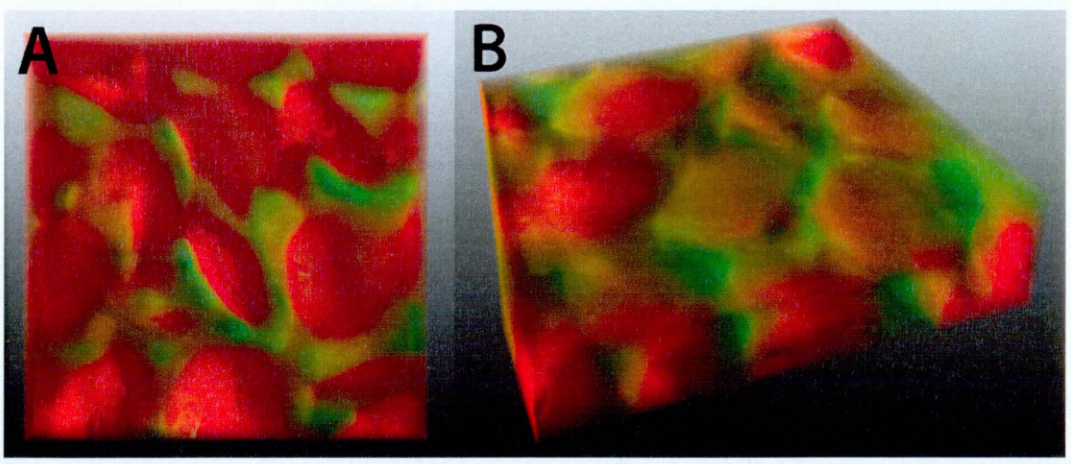

Figure 2.8. FEP granulates (red) and pore spaces (green). Top view (A) and oblique view (B) of 3D reconstruction of confocal image stack.

(Figure 2.8) where the volumes with no fluorescence were determined as the particles but image analysis of these images is more difficult than where the dye labels the particle-pore boundaries directly.

2.7.2 Imaging rhizosphere pH

The study of root-mediated pH balance of the rhizosphere is an important topic in root research because of the effect of rhizosphere pH on the solubility and bioavailability of plant nutrients and toxic elements (Blossfeld et al., 2011). The fluorescent pH indicator dye fluorescein, conjugated to 10 kDa dextran (Sigma) (Monshausen et al., 2007) was tested for imaging rhizosphere pH. This was carried out by growing lettuce plants prepared as described by Monshausen et al. (2007) and cultured in anionic Nafion transparent soil (set up as described in section 2.6, page 41). Immediately before confocal imaging, 30 μg ml^{-1} fluorescein in water was added to saturate the samples. Confocal excitation was alternated between 458 and 488 nm and emitted light between 530 and 600 nm was collected (Monshausen et al., 2007). Two samples were tested and by qualitative examination of the images of the dye, no difference or gradient in fluorescence in the liquid in the pore spaces or around the roots could be detected using this method. This may have been due to an interaction between the dye and the Nafion which affected the chemistry of the dye molecules. The function of a dye may not be preserved once it is bound to Nafion.

2.8 Conclusion

This Chapter has explored different ways in which transparent soils could be engineered in order to construct a transparent granular substrate that is suitable for culturing plants, has a low refractive index and is amenable to engineering of its physical and chemical properties. After much consideration over the materials that would be suitable for this application, Nafion emerged as the material with the greatest potential for this application for the following reasons. Engineering of Nafion was found to be achievable with common lab equipment. For example, manipulating the particle size of Nafion could be done with a freezer mill, whereas to achieve a similar result with FEP, we would most likely have required the use of industrial equipment for melt extrusion and perhaps custom-made parts.

Nafion has properties that are extremely useful in replicating soil factors, including its ion exchange capacity, which allows the sorbed nutrients to buffer the substrate solution, and its water retention properties. Its good transparency and reaction with fluorescent dyes enable effective optical imaging. FEP was less transparent, did not exchange ions and could not be labelled directly using any of the fluorescent dyes tested. For these reasons, Nafion was used as the building block of transparent soil in the experiments described in the following Chapters of this thesis. However, Nafion is expensive (Nafion in this study was obtained from Ion Power Inc., Delaware USA, cost in the range of $4 – 5.70 per gram) and there may still be a place for a FEP-based substrate, subject to more method development to address the points raised above. For

example, it was possible to make some 3D images of FEP granulates in a RI matched solution where a fluorescent dye was added to the solution to allow visualisation of the pore spaces (Figure 2.8) and water retention may be improved by chemical etching. In conclusion, we have developed one configuration of a transparent granular substrate for this application, but there may be other ways of achieving a similar end product using different materials, but the same principles described here, taking into consideration the points raised in this Chapter.

Chapter 3. Development of a transparent soil for imaging roots

This Chapter is based on the article Downie H, Holden N, Otten W, Spiers AJ, Valentine TA, et al. (2012) Transparent Soil for Imaging the Rhizosphere. PLoS ONE 7(9): e44276. See appendix (page 203) for the full article.

3.1 Introduction

We present the development of a substrate that consists of particles of the transparent ionomer (synthetic polymer with ionic properties) Nafion. The Nafion particles have ions required for plant growth adsorbed on their surfaces and the matrix includes water with plant nutrients in the smaller pore spaces and air in the larger pore spaces. By matching the refractive index (RI) of the solid Nafion particles and a liquid, the boundaries between the materials become invisible, thus revealing non-transparent structures within the solid–liquid matrix such as plant roots, which can then be imaged.

Imaging of roots at different scales is important because at the whole root system scale, it is possible to measure parameters of the root system architecture, which can also be influenced by environmental factors (Malamy, 2005). Equally, imaging at the cellular scale must be performed in order to gain information on fine structures such as root hairs (Prieto et al., 2011) and cellular chemical processes such as the chemistry of the apoplasm (fluid occupying space in cell walls and intercellular spaces) and the cytosol is important for the regulation of nutrient uptake. Fluorescent probes injected into living plants have been used to measure spatial differences in apoplastic pH in relation to corn

root gravitropism (Taylor et al., 1996) and Ca^{2+} (Monshausen et al., 2008). Often 3D imaging provides more spatial information than imaging in 2D. In this Chapter, two different 3D optical imaging approaches have been tested for imaging plant roots in transparent soil. Optical projection tomography (OPT) and confocal laser scanning microscopy (CLSM) (both described in Chapter 1) were used for imaging whole roots and root sections to a cellular level, respectively.

The heterogeneous physical structure and availability of oxygen in transparent soil are thought to provide an environment that more closely represents a soil substrate than the gel substrates that have previously been used to image root structures (e.g. Fang et al., 2009). To test this, the aim was to grow plants in transparent soil, phytagel, sand and soil and measure parameters of the resulting root system architectures (RSA) from each substrate and then compare these to find similarities and differences. The second aim was to build on the method development from Chapter 2 focussing on the systems for imaging roots in transparent soil and to test the applicability of optical projection tomography (OPT) and confocal laser scanning microscopy (CLSM) to imaging plant roots in transparent soil.

3.2 Materials and methods

3.2.1 Construction of transparent soil

Nafion (Ion Power Inc., USA) in the form of 4 mm × 3 mm pellets in acid (NR50 1100) and precursor (R1 100) forms were used. Size reduction of Nafion particles was performed using a freezer mill (6850, SPEX SamplePrep, UK). The final particle size range was 200–

1600 µm. Cation exchanging Nafion particles were made by ensuring full conversion to the acid form by washing in a solution of 15% v v^{-1} KOH, 35% v v^{-1} DMSO and 50% dH_2O at 80 °C for 5 hours, then with dH_2O (milliQ) at room temperature for 30 minutes followed by several dH_2O rinses. This was followed by 2 washes in 15% v v^{-1} nitric acid at room temperature: 1 wash for 1 hour and 1 wash overnight. The particles were treated with 1M sulphuric acid for 1 hour at 65 °C, and the acid was removed and replaced with dH_2O at 65 °C for 1 hour. After cooling, the particles were washed several times with dH_2O. They were then washed in a 3 wt % H_2O_2 solution at 65 °C for 1 hour and allowed to cool. The particles were rinsed again multiple times with fresh dH_2O (Van Nguyen et al., 2007). To titrate the particles with mineral ions, concentrated (i.e. undiluted) MSR medium (Strullu & Romand, 1986) was used to immerse the particles. These were shaken at 30 °C for 30 minutes before renewing the nutrient solution. This was repeated until the pH of the nutrient solution was neutral and stable after adding it to the particles. The particles were rinsed with dH_2O to remove excess MSR medium. Before use, the particles were autoclaved, submerged in dH_2O for sterilisation.

3.2.2 **Refractive index matching**

To determine the best refractive index match between the particles and liquid, plastic cuvettes were filled with acid Nafion particles and saturated with a range of concentrations of sorbitol solutions from 0–13% (w v^{-1}) to achieve a range of refractive indices. On one side of each cuvette, a straight line was drawn from top to bottom and a projection image was taken through the solid / liquid mix. There were 5 replicate images taken at each sorbitol concentration at 20 °C. The straightness of the line for each image

was used as an indicator of the light path distortion by refraction. A threshold was applied to each image to remove background and to get the clearest possible image of the line. The image was then skeletonized, where the line was thinned until it was 1 pixel in width and a bounding box was created around this line. The straightness was calculated as straightness = height of bounding box / area of bounding box. This was carried out using ImageJ (National Institutes of Health, USA). Nutrient-titrated Nafion particles were also tested in this way, but with a larger range of sorbitol concentrations. The refractive index of the sorbitol and percoll solutions was measured at 20 °C using a hand refractometer (N-series, Atago Co., Ltd).

3.2.3 Characterising the properties of transparent soil

Water retention was measured in samples of transparent soil with 3 size categories of Nafion particles (200–500 μm, 500–850 μm and 850–1250 μm, n = 3 for each category), with a dry mass of 10.3 ± 0.1 g. The dry bulk density of each particle size category was measured by drying samples (n = 3 for each size category) of each particle size category at 60 °C in a drying oven for 24 hours, measuring 3 10 cm^3 samples of each particle size category using a falcon tube, which was gently tapped on the bench for uniform packing and recording the mass of each sample. The dry bulk density for each particle size is shown in Table 3.1.

For saturation and packing, the samples were submerged in dH_2O, gently shaken and left submerged for at least 2 hours. The samples were not compressed as this was found not to change the volume. Water saturated samples were placed on ceramic plates in

Particle size category	Mean sample mass (g)	Dry bulk density (g cm^{-3})
Small (200 – 500 µm)	9.51 ± 0.17	0.95 ± 0.02
Medium (500 – 850 µm)	9.92 ± 0.34	0.99 ± 0.03
Large (850 – 1250 µm)	10.16 ± 0.09	1.02 ±0.01

Table 3.1. Dry bulk density of 10 cm^3 samples of Nafion with different particle size categories. Error margins are shown in standard error.

glass funnels, which were connected to hanging water columns. Different suctions were achieved by moving the water level in the water column to a specific height (from 0–1 m). At each pressure, the water content of the sample was allowed to equilibrate and the mass was recorded by moving the sample to a balance to allow calculation of volumetric water content. Data on water retention in vermiculite and sand from other studies were used for comparison with our data on water retention in transparent soil (Schroth et al., 1996, Schmidt, 2011).

Exchangeable cations were extracted using the ammonium acetate method (Thomas, 1982) on titrated Nafion samples with a particle size range of 500–1600 µm, where 2 g air dried, anionic Nafion treated with nutrient solution, as described in section 3.2.1 (page 53), was added to a 50 ml tube with 20 ml 1M NH_4OAc. The sample was swirled in a shaker for 2 hours at room temperature, after which the NH_4OAc was removed and retained for chemical analysis. Cation exchange capacity was quantified by inductively coupled plasma mass spectrometry (ICP-MS analysis, carried out by Macaulay Analytical

at the James Hutton Institute, Aberdeen, UK). To measure anion exchange capacity, sorbed chloride ions were exchanged with nitrate ions and exchange capacity was determined by measuring the extracted chloride ions (Pansu & Gautheyrou, 2006). These chemical analyses were carried out by Macaulay Analytical at The James Hutton Institute.

3.2.4 **Plant culture**

Arabidopsis thaliana expressing 35S:LTI6b- EGFP (constitutively expressed enhanced green fluorescent protein targeted to the plasma membrane), in the C24 background (originally obtained from Dr. J. Haseloff, University of Cambridge, UK) (Kurup et al., 2005) and auxin reporter lines (Federici et al., 2012) were used for confocal microscopy. *Nicotiana benthamiana* (tobacco, from SCRI stocks) and *Lactuca sativa* (lettuce, var. capitata, Seed Parade, UK) seeds were surface sterilized by washing in 10% bleach (Domestos, Unilever, UK) for 20 minutes followed by several sterile dH_2O washes. *Arabidopsis thaliana* seeds were sterilized on filter paper by adding 70% ethanol, allowed to dry slightly and addition of 90% ethanol before allowing to air dry. MSR nutrient medium (Strullu & Romand, 1986) was used for culturing tobacco seeds and half-strength (2.2 g L^{-1}) Murashige and Skoog (M&S) basal medium (Sigma) was used for lettuce and *Arabidopsis* seeds. Seedlings were germinated before use in experiments by sowing seeds in Petri dishes with 5 g L^{-1} phytagel (Sigma) with MSR or M&S nutrient medium. Plants were incubated at 20°C with 16 hours light: 8 hours darkness.

3.2.5 **Plant growth comparison**

The substrates used for analysing plant growth were: 1. Sandy-loam soil from Lower Pilmore field, The James Hutton Institute, Dundee, UK. The soil was sieved to 3 mm and packed to a density of 1.2 g cm^{-3} with a gravimetric moisture content of 20% (n=9) by weighing-out soil dried at 70 °C for 24 hours using a digital lab balance (Ohaus PA114, Nänikon, Switzerland), adding it to the sample holders, compressing to 20 cm^3 with a smaller cylindrical tube and adding the appropriate volume of water with a pipette. 2. Horticultural grit sand (Gem, UK), packed to a density of 1.5 g cm^{-3} and MSR plant nutrient medium to achieve a gravimetric moisture content of 15.2% (n=9) in the same method as described for soil. 3. 4 g L^{-1} phytagel (Sigma) with MSR medium was prepared by autoclaving and poured into the samples holders (n=9). 4. Transparent soil with a Nafion particle size range of 500–1600 µm was prepared as described in section 3.2.1 (page 53) and packed to a density of 1.03 g cm^{-3} (n=6). Wild type tobacco (*Nicotiana benthamiana)* plants were used in this experiment and the growth period was 2 weeks after transferring the seedlings to the medium in cylindrical glass sample holders, diameter = 2.5 cm, height 7.5 cm. The growth room conditions were 20 °C, 16 hours light: 8 hours darkness. All plants were excavated, the roots were washed and they were mounted onto acetate sheets for scanning using a flatbed scanner (Epson Expression 1640 XL). Primary and lateral roots lengths and numbers were measured using the segmented line function from ImageJ software (National Institutes of Health, USA). After imaging the plants' roots and shoots were separated using a pair of forceps, placed in 2

ml pierced eppendorf tubes and dried at 60 °C in a drying oven for ≥ 24 hours, after which the dry mass was recorded using a Sartorius microbalance.

3.2.6 3D imaging of roots in transparent soil

For OPT imaging the samples were prepared in glass cylindrical specimen tubes (2.5 cm in diameter, 7.5 cm in height) with a substrate volume of 15 cm^3. Duration of growth was dependent on plant species but in general, imaging was performed before the roots reached the base of the tube. Tobacco plants used for OPT were imaged 10 days after sowing. Immediately prior to imaging, the samples were saturated with MSR medium with 13% sorbitol (wv^{-1}). The OPT setup was built in-house and consists of a light box, stage for sample with rotating stepper motor, stereo microscope (Leica MZ 16 FA) and camera (Leica DFC 350 FX). The stage and camera were controlled by software also built in-house, allowing control of the number of images acquired for each sample. The projection images were reconstructed to produce 3D data using a filtered backprojection algorithm with the Iradon function in Matlab (The MathWorks, Inc.). *Arabidopsis* plants used for confocal imaging were imaged 10-14 days after sowing.

3.2.6.1 *Construction of 3D slides*

For CLSM, plants were grown in purpose-built chambers, constructed using a microscope slide and long cover glass with a 4 mm spacer made using a cable tie between them on 3 sides and an opening at the top (Figure 3.1). The spacer was glued to the slide and cover glass using Araldite glass and ceramic adhesive (Huntsman International). These growth chambers will be referred to as 3D slides throughout the

thesis. The chambers were covered with aluminium foil on the outside during growth to exclude light from the roots. Foil was removed immediately before imaging. Before imaging, transparent soil was saturated with MSR containing 13% (wv^{-1}) sorbitol or 98% Percoll (Sigma) with 2% MSR medium (vv^{-1}) at stock concentration (Strullu & Romand, 1986). The refractive index of the solution matches the refractive index of the Nafion particles used here to provide complete transparency in the substrate. Sulphorhodamine B (Sigma) at 1 µg ml^{-1} RI matching liquid was used to dye the particles in situ before imaging by saturating the transparent soil. A Leica TCS SP2 confocal laser scanning microscope and objective lenses 2.5× / 0.07, 10× / 0.30 (dry), 20× / 0.50, 40× / 0.80 and 63× / 0.90 (water dipping) were used to obtain the confocal scans. To image GFP, a 488 nm laser was used for excitation and the emitted light was collected between 500 and 530 nm. To image the RFP and sulforhodamine B, a 561 nm laser was used for excitation and light was collected between 580 and 620 nm. To image the calcofluor light was collected between 430 and 470 nm. For the signal from the lettuce roots, a 405 nm laser was used for excitation and the emitted

3.2.7 **Data analysis**

Analysis of variance and multiple comparisons were carried out using Genstat 13th Edition (VSN International Ltd.). Sigmaplot 12 (Syststat Software, Inc.) was used for non-linear and linear regressions. Avizo software (VSG) was used for visualisation of CLSM images. Image analysis for root tracking and 2D root measurements was carried out using Mevislab (Koenig et al., 2006) and Fiji Software (Preibisch et al., 2010) respectively. Root tracking used an algorithm by Friman et al. (2008).

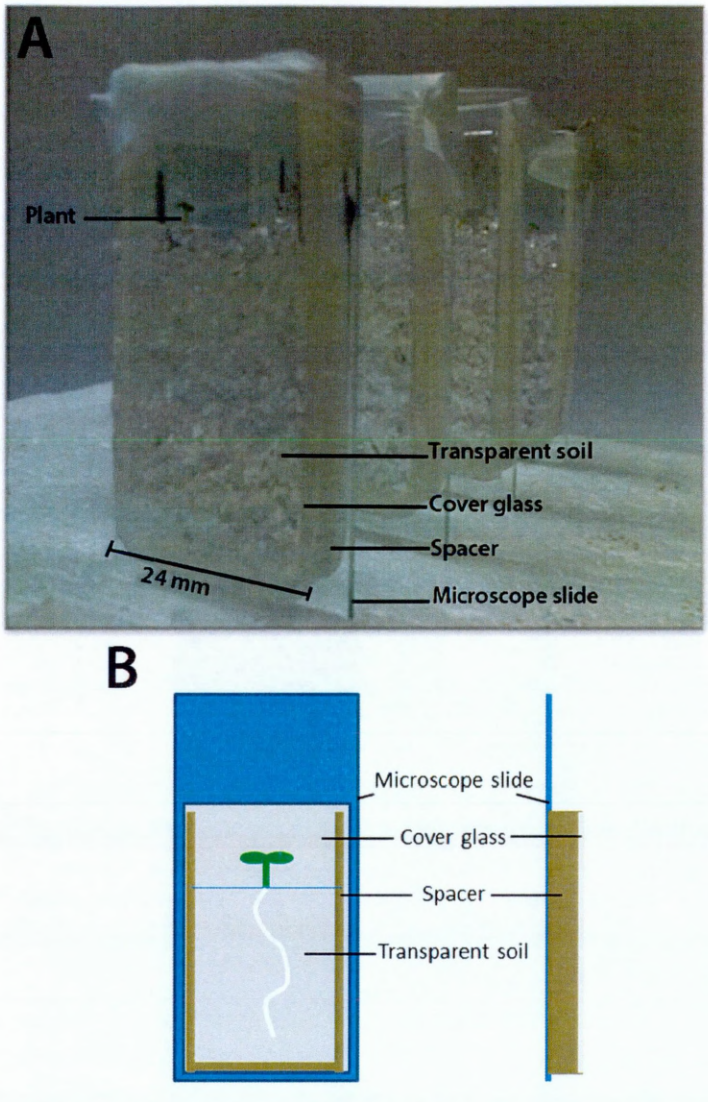

Figure 3.1. A) Samples that were prepared for confocal imaging with transparent soil in 3D slides including Arabidopsis thaliana *plants. B) Schematic diagram of 3D slides (not to scale).*

3.3 Results

3.3.1 Selection of materials

Nafion was selected as the material to use as the basis of transparent soil partly because of its low refractive index (RI, 1.34), which is close to that of water (1.33) and therefore matching can be achieved with an aqueous solution. The refractive index of hydrated Nafion films has previously been reported as 1.3366 to 1.3433 (Leis et al., 2005), however because Nafion is available in many different forms and because pellets rather than films are being used here, a method to measure the refractive index was developed. Using this method, data on refractive index was obtained, a curve was fitted to the data and the maximum value was used. It was found that the refractive index of acid Nafion pellets (NR50 1100) was 1.340 (Figure 3.2, A). Figure 3.2, B shows refractive indices for other common transparent materials (Polyanskiy, 2008-2012) in order to contextualise these values. This demonstrates that the refractive index of Nafion is very close to that of water, in comparison with other transparent materials.

During the experiments for calculating the RI of Nafion, solutions of a range of sucrose concentrations in water were used in order to find a solution with a refractive index matching that of the Nafion particles. Sucrose was ideal for this application because of the well-described relationship between sucrose concentration and refractive index (the Brix scale) (Rosenbruch et al., 1974). However, sucrose is not always an ideal substance to use because of its effect on root growth (Bahmani et al., 2009) and so other options investigated were sorbitol and Percoll. Sorbitol solutions have RIs very close to those of

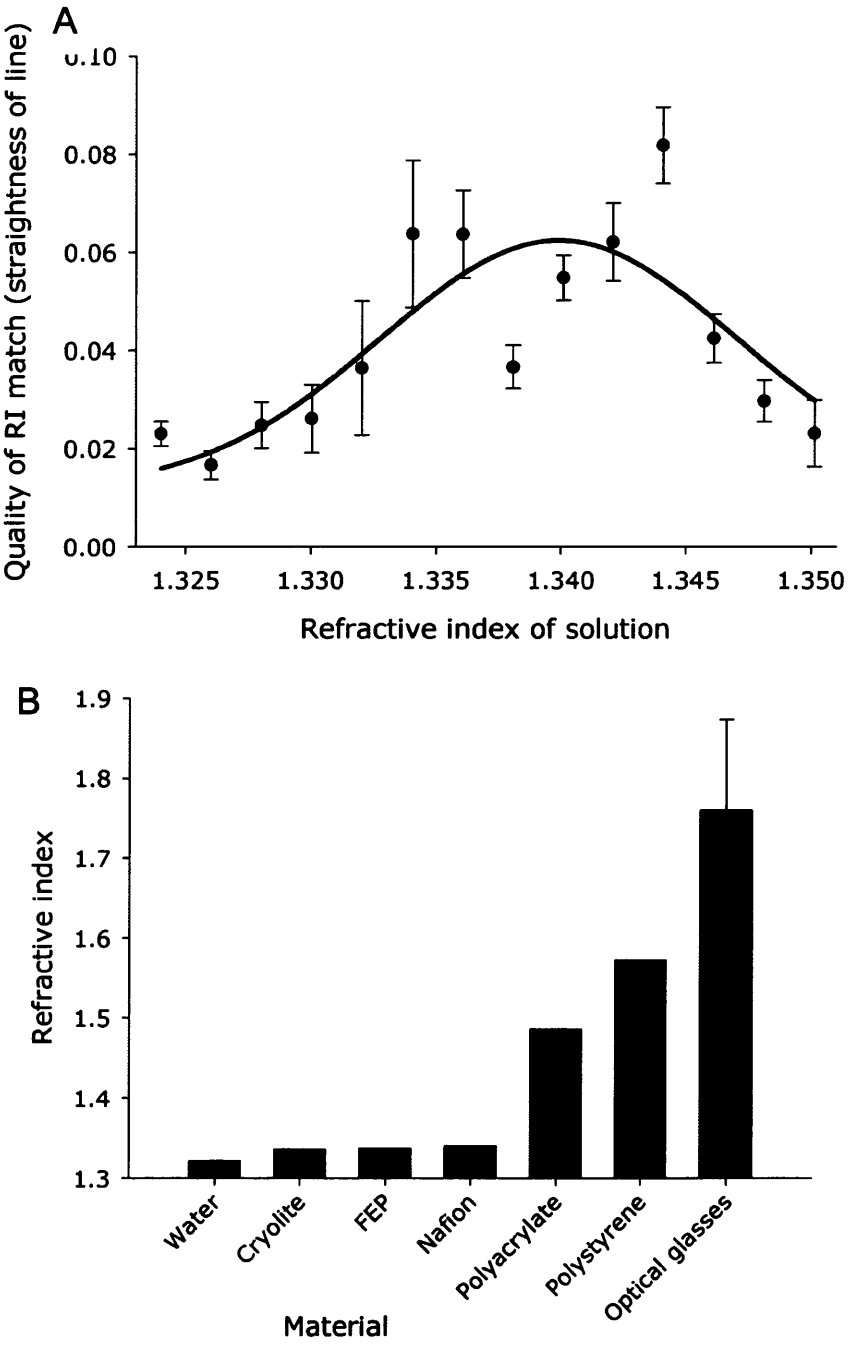

Figure 3.2. Refractive index of Nafion. A) Optimal RI of nutrient solution for RI matching with Nafion using projected straight line images deformed by the substrate. Curve shows Gaussian non-linear regression (R^2 = 0.38). B) Refractive index of common transparent materials and Nafion. Error bar shows standard error.

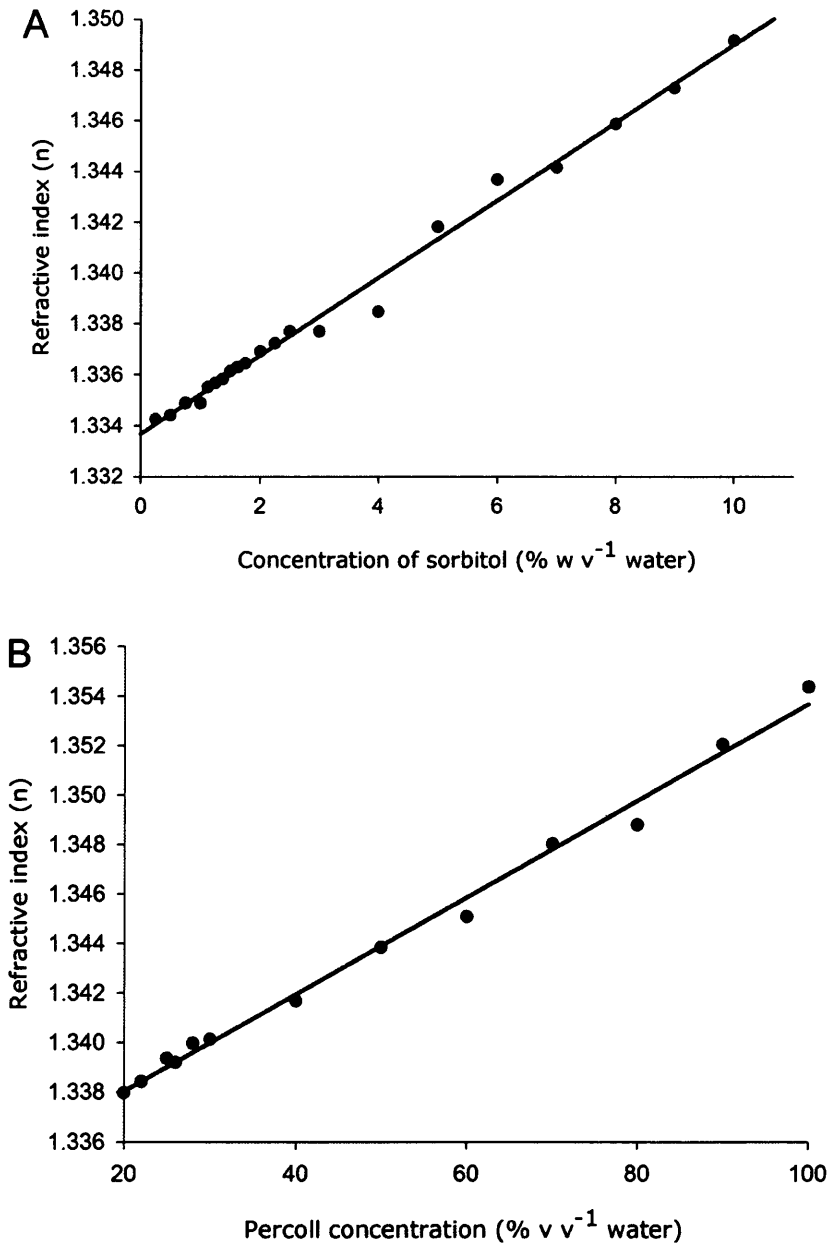

Figure 3.3. Refractive indices of solutions used for RI matching with Nafion. A) Sorbitol solutions have RIs very similar to sucrose solutions. A linear regression is shown where $R^2 = 0.99$. B) The range of RIs that can be achieved using Percoll covers the value required for matching with Nafion. A linear regression is shown where $R^2 = 0.99$.

the equivalent sucrose solutions (Figure 3.3, A). Percoll, the silica-based colloid suspension, has a smaller range of possible refractive indices, but nevertheless the refractive index of Nafion (equivalent to 10% sucrose) is within this range (Figure 3.3, B).

3.3.2 Transparent soil

By physically and chemically engineering Nafion particles and by using a RI matching technique, a new substrate has been developed for the purpose of observing plants and soil organisms. During the period of plant growth, pores were partially saturated with a plant nutrient solution and air spaces were maintained for aerobic respiration. Immediately before imaging, the substrate was saturated using a RI matched liquid plant nutrient solution, containing either Percoll or sorbitol, so that imaging of roots could be carried out in situ (Figure 3.4).

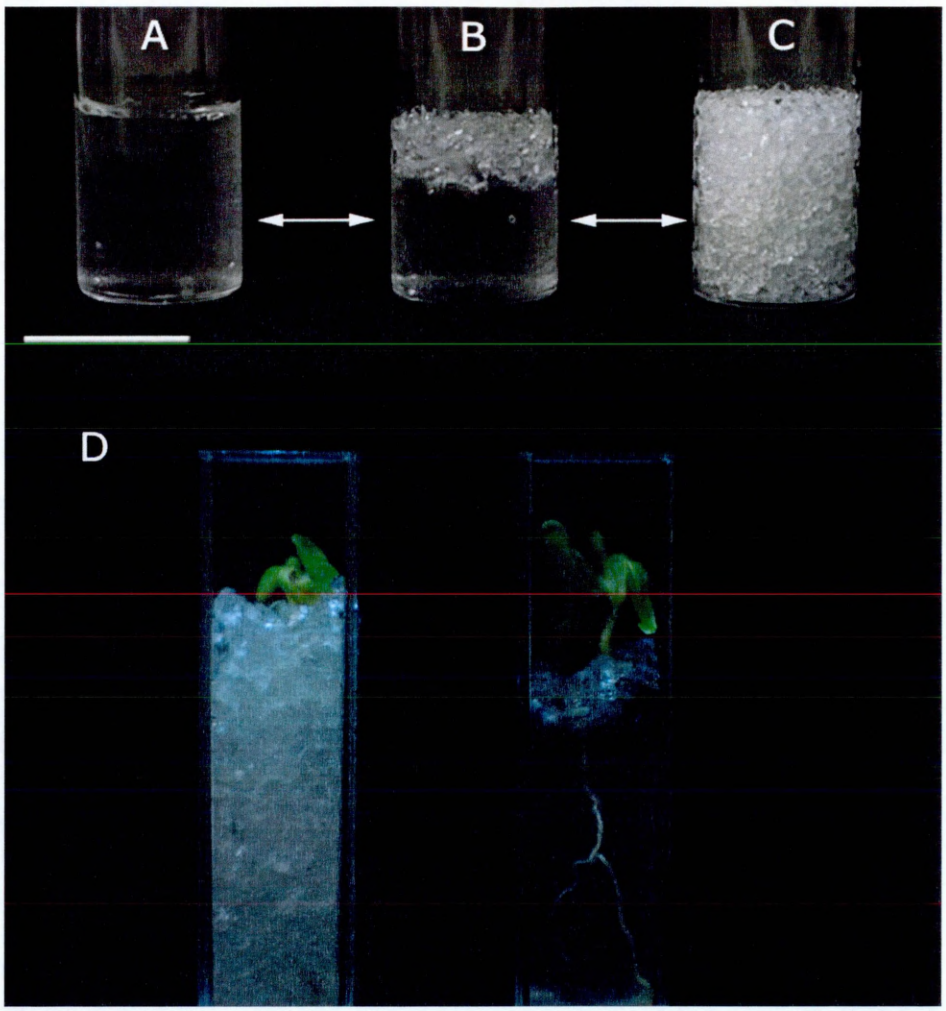

Figure 3.4. Samples of transparent soil. A) Fully saturated with RI matching solution. B) Large pores partially drained. C) Large pores fully drained. Scale bar = 2.5 cm. D) Latuca sativa *plants growing in transparent soil and saturated with RI matched liquid for imaging making the roots visible (right).*

3.3.3 Characterisation of transparent soil

Water retention is an important soil characteristic because it can determine the availability of water for plants under non-saturated conditions. Water retention of transparent soil with 3 particle size categories was measured using the hanging water column technique (Warrick, 2003) and compared to water retention in vermiculite and sand (Figure 3.5). In the 2 smallest size categories, and in vermiculite, the sharpest release of water occurred between -1.5 and -5 kPa. The water release in the largest

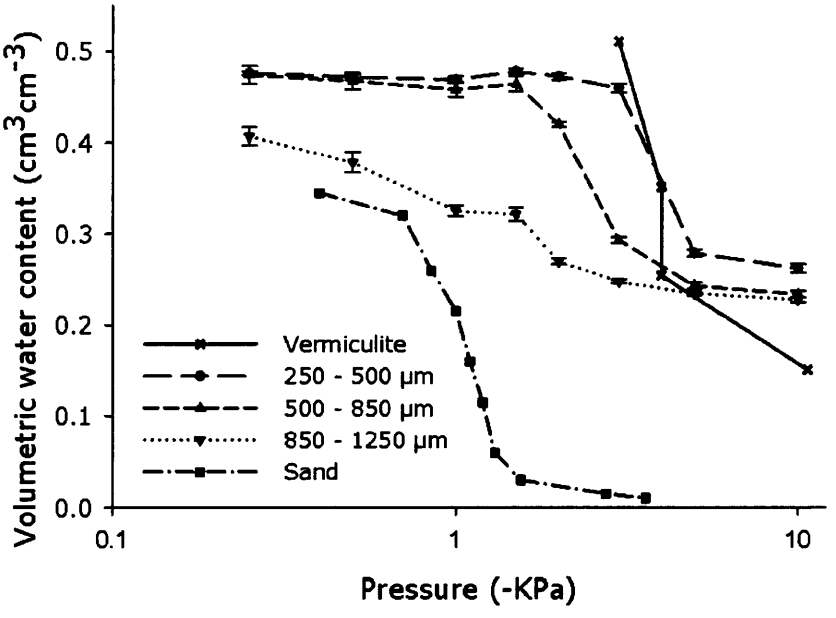

Figure 3.5. Water retention in transparent soil, sand and vermiculite. Water retention in 3 different particle size categories of transparent soil was plotted along with water retention data for sand from Schroth et al. (1996) and vermiculite from Schmidt (2011).

sized particles was more gradual but in all sizes, a levelling off of water release occurred towards -10 kPa and the residual water content measured in transparent soil ranged from 0.23 to 0.26 cm^3 cm^{-3} at -10 kPa. This value was higher than is usual in sand (Schroth et al., 1996), despite the similarity in particle size.

The cation exchange capacity (CEC) of transparent soil was quantified by extraction using the ammonium acetate method (Pansu & Gautheyrou, 2006) and subsequent Inductively coupled plasma mass spectrometry (ICP-MS) analysis and was found to be 81 meq $100g^{-1}$. This is within the range that could be expected for vermiculite (80–150 meq $100g^{-1}$ (Lal, 2002)). It was found that Nafion could be converted to the cationic form (details in section 2.6, page 41), and therefore would exchange anions rather than cations (Salerno et al., 2012). After carrying out the conversion, the anion exchange capacity (AEC) of cationic Nafion was 47 meq 100 g^{-1} as quantified by saturating the exchange sites with Cl^-, exchanging them for nitrate ions and measuring the Cl^- concentration in the exchanged solution by ICP-MS (Pansu & Gautheyrou, 2006).

3.3.4 Root growth in transparent soil

Primary root length and diameter and lateral root number and length of the root systems of *Nicotiana benthamiana* plants grown in transparent soil, soil, sand and phytagel were measured after excavation and scanning of the plants (Figure 3.6). Root and shoot dry weights were also measured and a general ANOVA showed that there was a significant difference in root dry weight ($F_{3,31}$=6.04, p=0.003) and shoot dry weight between the substrates ($F_{3,31}$=5.87, p=0.003). The results of a Fisher's protected least

significant difference (LSD) test showed that although there was no significant difference between root weight of plants from transparent soil (TS) and phytagel and roots from TS and soil, the root dry weights were different between the two pairs. Roots from plants grown in sand were significantly heavier than the roots from the other treatments, with the exception of those grown in soil, which were not significantly different (Figure 3.7). Similarly, the results of a Fisher's protected LSD test on the shoot dry weight measurements showed that there was no significant difference between shoot weight of plants from transparent soil (TS) and phytagel and roots from TS and soil or sand although there was a difference between these two pairs (Figure 3.7).

Lengths of the plants' primary roots were measured, along with the lengths of each of the lateral roots. A general ANOVA showed that there were significant differences in primary root lengths ($F_{3,31}$=11.75, $p<0.001$) and cumulative lateral root length ($F_{3,31}$=4.19, $p=0.014$) between the plants grown in different substrates. Primary root length was not significantly different in plants from soil and sand, but the measurements were significantly smaller than the measurements of primary root length in plants grown in TS and phytagel, which were not significantly different from one another. Total lateral root length was not significantly different in plants from soil, sand and TS, but was significantly smaller in plants from phytagel (Figure 3.8).

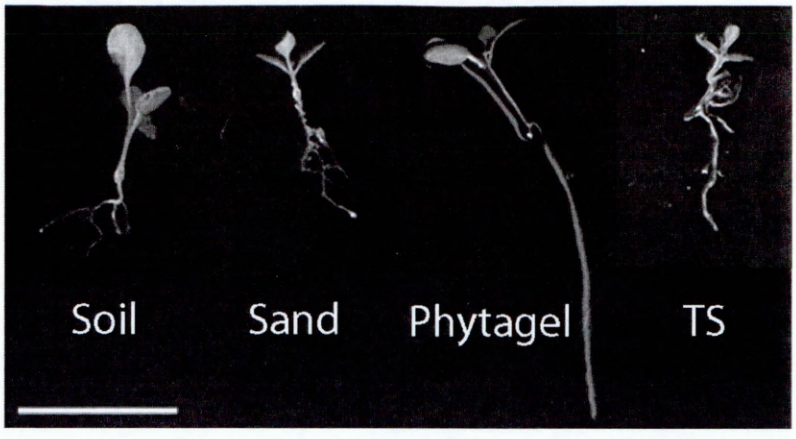

Figure 3.6. Images of plants after excavation from soil, sand, phytagel and transparent soil (TS). Plants grown in soil and sand have short primary roots but numerous long lateral roots. Plants grown in phytagel have long primary roots and usually no lateral roots and plants grown in TS have long primary roots but more lateral roots than plants grown in phytagel. Scale bar = 1 cm.

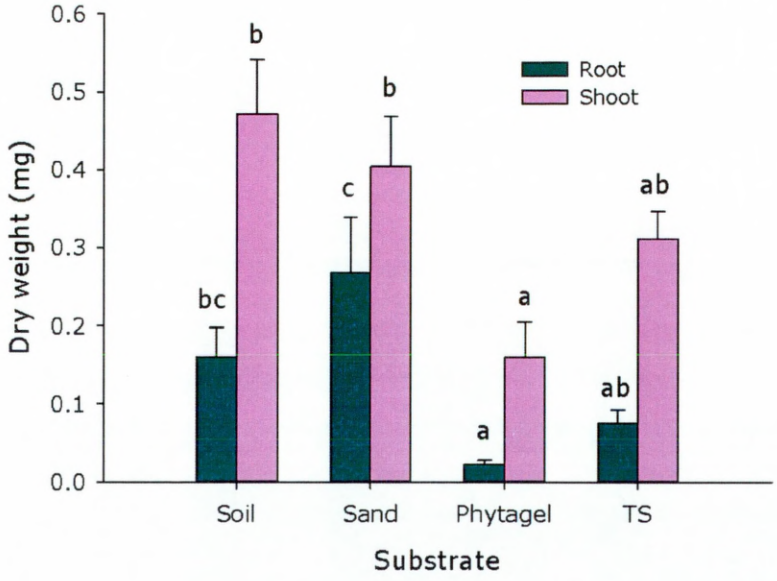

Figure 3.7. Root and shoot dry weights of plants grown in soil, sand, phytagel and transparent soil (TS). Letters above the bars correspond to the results from the Fisher's protected LSD test. Error bars signify standard error.

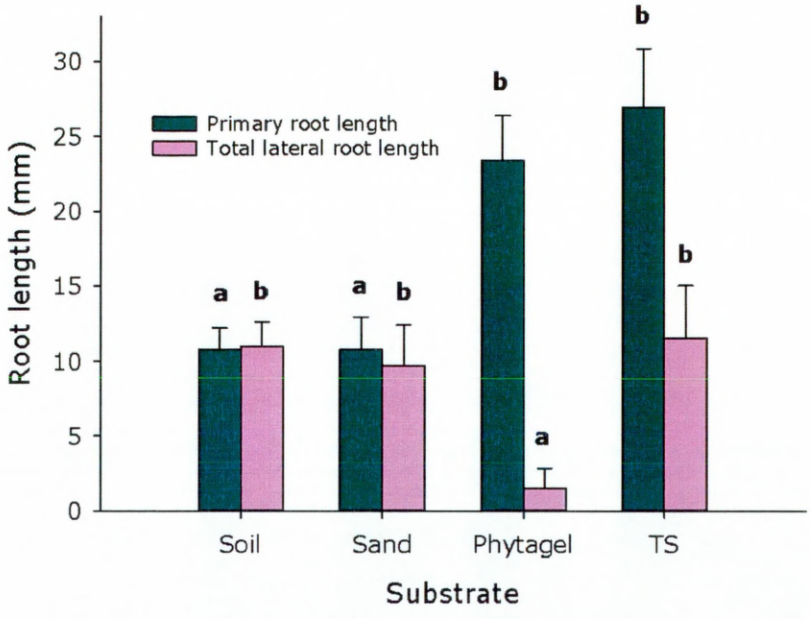

Figure 3.8. Mean primary root lengths and cumulative lateral root lengths of plants grown in soil, sand, phytagel and TS. Letters above the bars correspond to the results from the Fisher's protected LSD test. Error bars signify standard error.

The number of lateral roots were also recorded and there was a significant difference in the number of lateral roots between plants from different substrates ($F_{3,31}$=9.64, p<0.001). Plants grown in phytagel had a significantly smaller number of lateral roots than the plants from the other substrates, and the median number of lateral roots in plants grown in phytagel was 0. Plants grown in sand and TS had a similar mean number of lateral roots to one another, and plants grown in soil had a lateral root number significantly greater than that of plants from all other substrates (Figure 3.9). The mean primary root diameter was also significantly different between plants from the different substrates ($F_{3,31}$=3.69, p=0.026). Plants from soil and sand had root diameters not

significantly different from one another. These diameters were also not significantly different from the root diameter of plants grown in phytagel or TS, but the diameter of roots grown in TS was significantly larger than that of plants grown in phytagel (Figure 3.9).

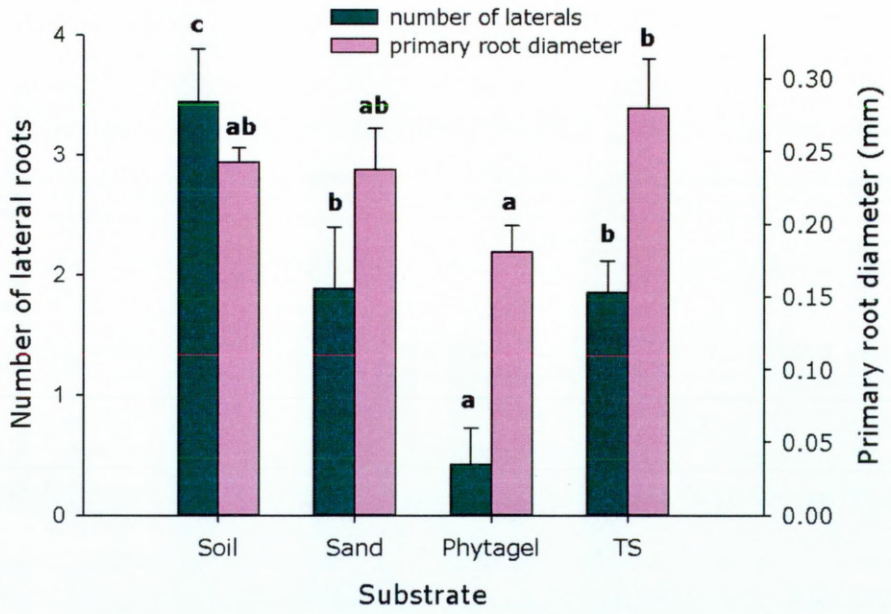

Figure 3.9. Mean number of lateral roots and primary root diameter in plants grown in soil, sand phytagel and TS. Letters above the bars correspond to the results from the Fisher's protected LSD tests. Error bars signify standard error.

Overall, plants grown in phytagel developed very different root systems from plants grown in soil or sand (which had quite similar root systems). The main differences in the root systems were the length of the primary root, which was short in plants from soil and sand and long in plants from phytagel and the number and length of lateral roots,

which were lower in plants from phytagel than in plants from soil or sand. Root systems of plants grown in transparent soil were different still because they had primary roots in the same length range as plants from phytagel but the number and length of lateral roots was comparable with plants from soil or sand.

3.3.5 **3D imaging of roots in transparent soil**

To assess the utility of the system for imaging root: particle interactions at various scales we imaged *Nicotiana benthamiana* and *Arabidopsis thaliana* using OPT and CLSM. Imaging at the whole root level (< 5 cm) was achieved using OPT and the root was segmented from the 3D image using a root tracking algorithm (Figure 3.10). Confocal

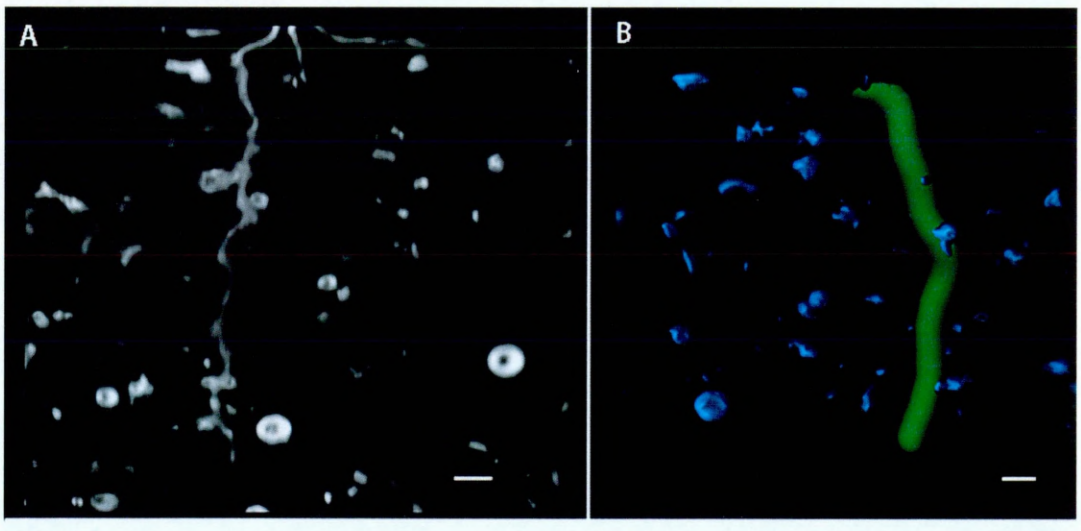

Figure 3.10. OPT images of Nicotiana benthamiana *roots in transparent soil. A) Projection image of roots and small air bubbles trapped in the substrate. B) Root (green) and air bubbles (blue) after application of the root tracking algorithm. Scale bars = 1 mm.*

imaging was also applied to image roots in transparent soil to a cellular level (Figure 3.11, Videos S1-S3, Appendix 2 & enclosed CD). Plants with plasma membrane localized reporter gene-encoded GFP expression were imaged at a range of scales to visualise root architecture in relation to Nafion particles (Figure 3.12, A), lateral root initiation (Figure 3.12, B) and root epidermal cells and root hairs (Figure 3.12, C). The 3D distribution of the hormone auxin in *Arabidopsis thaliana* root tips was also visualised (Figure 3.12,D) using auxin reporter lines (Federici et al., 2012).

Confocal imaging relies on detecting fluorescence in the sample, therefore to visualise the Nafion particles a fluorescent dye, Sulphorhodamine B was mixed with the RI matching solution (either 10 wt % sorbitol or 100% percoll) and added to the substrate immediately before imaging. This allowed consecutive imaging of the roots and the surrounding Nafion particles, which could then be combined later to visualise the path of the roots among the Nafion particles (Figure 3.11).

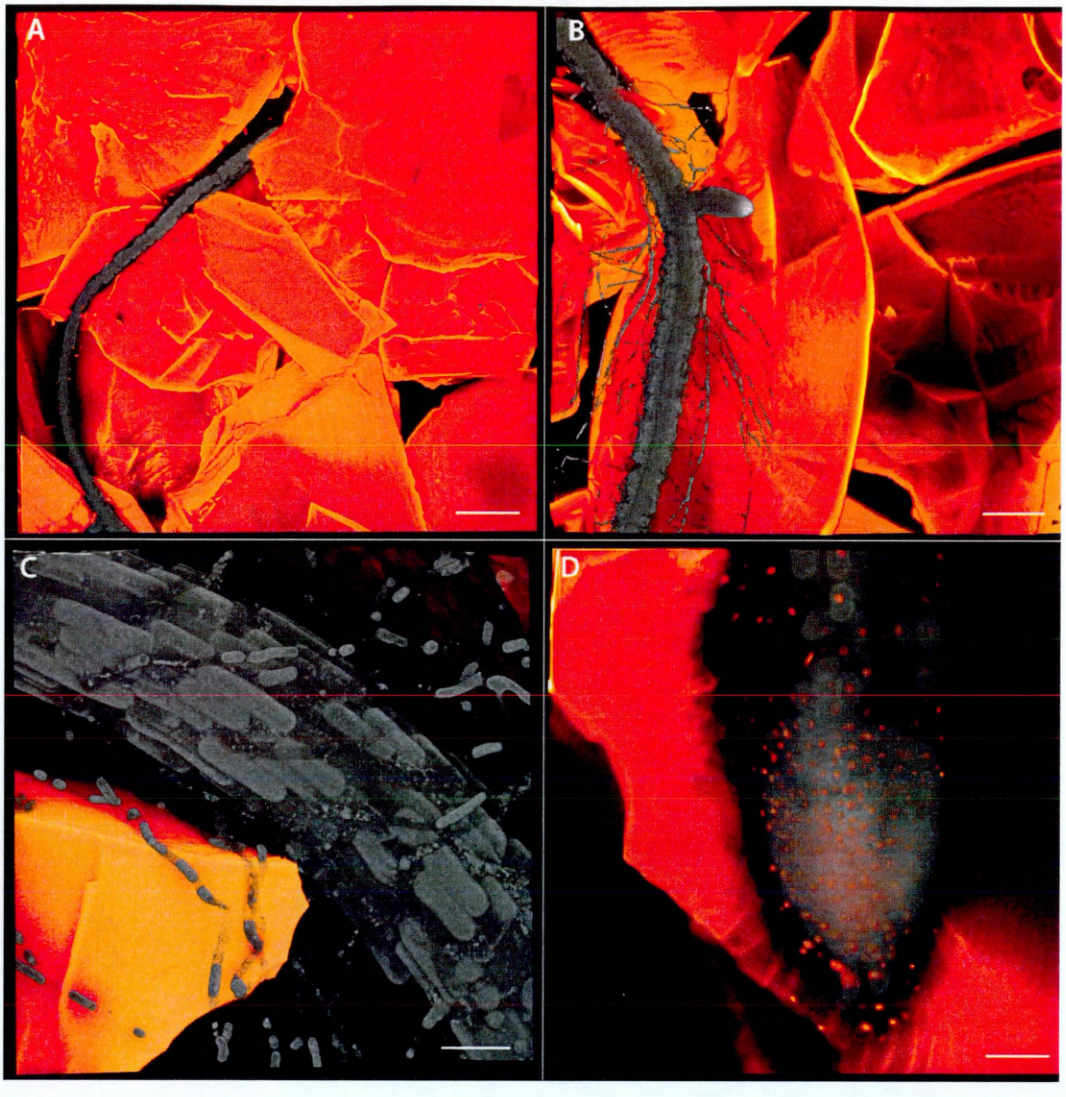

Figure 3.11. 3D volume renderings of confocal images of Arabidopsis thaliana *roots (grey) in transparent soil with Nafion particles dyed with sulphorhodamine B (orange). A–C) Arabidopsis thaliana roots with plasma membrane localised expression of GFP in transparent soil at a range of scales where the scale bars represent 300 µm (A), 170 µm (B) and 40 µm (C). D) Root tip with nuclear RFP expression linked to auxin reporter (Federici et al., 2012).*

3.4 Discussion

The main advantage of transparent soil over field soil is, of course, that its transparency allows the application of optical imaging techniques to observe biological structures in the substrate in 3D. However, transparent soil has a number of further advantages over the other transparent substrate that has been used for this purpose. The other transparent substrate that has allowed 3D optical imaging of roots is phytagel (gellan gum) (Fang et al., 2009, Fang et al., 2011, Clark et al., 2011). Phytagel is a homogeneous and very transparent (Maizel et al., 2011) agar substitute in which plants can grow. It is also inexpensive and quick to prepare, compared with transparent soil. However the results presented here show that using phytagel as the growth substrate for *N. benthamiana* plants had a strong influence on the growth of the plants (Figures 3.6–3.9).

Firstly, the plant biomass is significantly smaller in plants from phytagel than in plants from soil or sand (Figure 3.7). This could be because the phytagel is effectively a water saturated substrate, which necessitates anaerobic respiration in the root tissues, rather than more efficient aerobic respiration, resulting in lower biomass for plants with oxygen-deprived root systems in phytagel (Blackwell & Wells, 1983). Secondly, phytagel caused significant differences in the architecture of the root systems, compared with plants grown in soil and sand (Figure 3.6, Figure 3.8 & Figure 3.9). There are many factors that are known to influence the root system architecture (RSA) including water

availability (Giuliani et al., 2005), and contact between roots and solid obstacles which promotes lateral root initiation in the primary root (Goss & Russell, 1980).

Because of these factors, transparent soil represents an improvement on phytagel as a transparent substrate for growing plants for root imaging. As shown in the results, root and shoot biomass (Figure 3.7), total lateral root length (Figure 3.8) and number of lateral roots (Figure 3.9) were not significantly different in plants grown in transparent soil and plants grown in soil or sand. This may relate to the points outlined above: the substrate is not saturated and so aerobic respiration can occur in transparent soil, and the roots are making contact with solid obstacles and so the initiation of lateral roots may be stimulated (Goss & Russell, 1980).

Nafion particle size of transparent soil affects the water retention, particularly at low pressures (Figure 3.6). Finding the best particle size to use is a trade-off between having small particle sizes which more closely represent soil or sand particles and having larger particles which makes saturation of the substrate before imaging more efficient because trapping air bubbles is less of an issue. The Nafion particle size range used here falls into the same category size as sand (50–2000 μm (Jahn et al., 1990)), however the water retention curve shows that there is a large amount of residual water present in the substrate at the highest pressure measured. The residual water content is not significantly different in the 2 largest particle size categories and is only slightly higher in the smallest particle size category. This may be due to the networks of hydrophilic nano-channels present in Nafion. Although the exact nature of these networks is still unclear,

it is estimated that the diameter of the channels varies between 1 and 6 nm (Ceynowa, 1984, Xue et al., 1989, Rieberer & Norian, 1992). At this range of scales, the hydrogen bonds holding the water molecules are extremely strong and it is unlikely that the water sorbed in the Nafion particles could be accessed by most biological organisms.

Transparent soil has enabled the production of images with low levels of noise (Figures 3.11 & 3.12) and opens avenues for automated analyses of genetic screens (French et al., 2009). In addition, the availability of fluorescent signals eases the discrimination of biological structures where separation of the different wavelengths provides much of the segmentation of the biological structures. Transparent soil can also be used to capture cellular events using plants with plasma membrane and nucleus-localized reporter gene-encoded proteins (Figure 3.12, Videos S1-S3, Appendix 2 & enclosed CD), which could be used for automated analysis of multicellular development (Dumais & Kwiatkowska, 2002, Dupuy et al., 2010a).

Chapter 4. Measuring the effects of substrate physical factors on 3D root growth trajectories

4.1 Introduction

4.1.1 Root tropisms

The architecture of root systems influences the effectiveness of the plant at taking up resources from the soil (Yang et al., 2012), at anchoring itself securely and at providing stability to the soil (Stokes et al., 2009). Tropisms play an important part in regulating the direction of growth of the root tip and the resulting trajectory or path of root tips over time in turn determines the morphology of the root system. Tropisms can be defined as differential growth responses that reorient the plant organs in response to the direction of environmental stimuli (Esmon et al., 2005). The best described responses are gravitropism (gravity), thigmotropism (touch), hydrotropism (water) and phototropism (light).

Roots tend to grow in the direction of gravitational pull (Moore et al., 1998a). As well as being considered a model response with which to study the molecular basis of sensing and signalling in plants (Boonsirichai et al., 2002), gravitropism plays a substantial role in determining the trajectory of a plant root. There have been several studies measuring gravitropically induced bending of roots after reorientation of the whole plant. Mullen et al. (2000) maintained a constant gravitropic stimulus on *Arabidopsis* roots using a rotating platform to show that the root response time was around 10 minutes. Experiments investigating the response of cucumber roots to light and gravity showed

that root systems alter their entire architecture based on the sensing and signalling of a small part of the root system (Otreba, 2009). The plasticity of gravitropism in *Arabidopsis* roots has also been quantified (Brooks et al., 2010). Root bending also occurs due to negative phototropism, and the curvature of rice roots has been measured in 2D after photo-stimulation (Wang et al., 2002). Some root analysis software incorporate functions to automate the measurement of root bending, such as RootTrace (French et al., 2009) and KineRoot (Basu et al., 2007).

4.1.2 Endogenous trajectories

The trajectories taken by growing root tips are thought to be partly determined by inherent, genetically regulated mechanisms. In order to investigate what these trajectories might be, plants have been grown in microgravity during space flight experiments. It was found that *Arabidopsis* roots exhibit less stochasticity in their growth patterns and a higher degree of skewing, where the root deviates from vertical, when they were grown on agar plates in space than when they were grown on Earth, but their growth was not random (Millar et al., 2011). Moss cell populations have been found to default to a spiral growth pattern in microgravity (Kern et al., 2005) and so it could be the case that these organisms have endogenous growth patterns that are masked by the usual gravitational conditions on Earth along with their interaction with the substrate.

Roots also exhibit movements that are independent of a directional stimulus, which are known as nastic movements (Moore et al., 1998a) and it has been possible to record

these movements. Darwin (1880), for example, carried out experiments where he grew plants in darkness along inclined, smoked glass plates, where the roots left a track of deep and smooth waves. He interpreted these findings by explaining that the root inherently makes a 3D spiralling movement during growth, which he called circumnutation.

Since then, other studies have shown that this is the case through experiments, mostly with *Arabidopsis*, where the root is grown along an inclined agar surface. This results in a waving pattern of growth which is a result of a flattened right-handed circumnutational spiral (Simmons et al., 1995). A combination of waving and root skewing has also been observed on inclined agar plates (Oliva & Dunand, 2007). Root–gel interactions may also play a role in determining the waving growth pattern (Thompson & Holbrook, 2004). The inclined surface of an agar plate is, however, a highly unrealistic environment for root growth and so translating these results to plant growth in soil remains a challenge.

4.1.3 Substrate effects on root trajectories

It has been observed that the characteristics of a substrate in which plants are grown have an effect on the growth pattern of the roots. For example, Antonsen et al. (1999) used nuclear magnetic resonance (NMR) to image the gravitropic response of oat seedling after reorientation. The plants were grown and imaged in different substrates, namely soil, glass beads and in humid air. They found that the substrate had an effect on the time taken for the roots to make the full 90° curvature and, in particular, the plants

grown in soil took the longest time to re-orientate. They concluded that this was because of the greater touch stimuli induced by the soil. Indeed, Massa and Gilroy (2003) showed that the gravitropic response is overridden by a touch response when roots touched a barrier and began to grow agravitropically to navigate around the barrier.

Images of roots from X-ray μCT studies have been used to measure some aspects of 3D root geometries. For example, the ratio of root length: the distance between the 2 extremities of the root has been used as a global measure of root tortuosity (Perret et al., 2007). Tracy et al. (2012) calculated root tortuosity as the ratio of primary root length : linear rooting depth and found that tomato plants grown in compacted soil had more tortuous primary roots than plants grown in less compacted soil.

In this Chapter, the effects of two substrate characteristics are investigated. These are substrate particle size and compaction. Land use can have a significant effect on soil particle size distribution (Tian et al., 2008) and the soil particle size can affect nutrient supply to the roots by mass flow and diffusion (Oliveira et al., 2010). Compaction is a problem on agricultural land caused by surface pressure by, for example, farming machinery. Root growth is impeded by compacted soils (Bengough et al., 2011, Valentine et al., 2012) and results in lower leaf elongation rates of cereal plants than in non-compacted soils (Young et al., 1997). It is evident that the growth trajectory of a root is influenced by responses to many different factors, including environmental factors such as gravity and light and local factors linked to the substrate such as

mechanical stimulation, nutrients and water. There also seems to be endogenous growth patterns, revealed by microgravity and inclined gel experiments but the role these have in determining growth trajectories in soil is unknown.

4.1.4 Aims

In the experiments described in this Chapter, lettuce roots were grown and imaged in transparent soil with the aim of performing local and global measurements of root trajectories in 3D. The second aim was to determine the effects of the substrate texture and compaction on the 3D root trajectories.

4.2 Materials and methods

4.2.1 Seed preparation

Lettuce (*Lactuca sativa*) is a globally important fresh produce dicotyledonous crop plant and it is favourable to use in plant growth experiments because of its fast germination time and growth rate. On the day before setting up the samples, *Lactuca sativa* (lettuce, var. capitata, Seed Parade, UK) seeds were surface sterilized by washing in 10% bleach (Domestos, Unilever UK Ltd.) for 20 minutes followed by 4–6 sterile dH_2O washes. The seeds were sown in Petri dishes containing 7 g L^{-1} phytagel (Sigma) with half-strength (2.2 g L^{-1} dH_2O) M&S basal medium (Sigma).

4.2.2 Sample set up

4.2.2.1 *Substrate compaction experiment*

Plants were set up in cylindrical glass vials (diameter = 2.5 cm, height 7.5 cm) with transparent soil consisting of anionic Nafion particles with a size range of 500–1600 µm. The Nafion particles were prepared as previously described (from page 53). Nafion particles were dried in an oven for 2 days at 50 °C and were then weighed and the appropriate mass of particles was added to each vial in order to set up the substrate treatments, as detailed in Table 4.1.

Distilled H_2O was added to the vials to cover the particles and they were autoclaved in dH_2O for sterilisation. The water on top of the particles was poured off and replaced with sterile half-strength Murashige & Skoog basal medium (Sigma) and the substrate was mixed. Much of the solution in the pore spaces between particles was removed using a Pasteur pipette with a pipette tip. The resulting particle mix was left in a laminar flow cabinet for around 3 hours to allow further evaporation of water to achieve the final gravimetric water content of the substrate, detailed in Table 4.1. For this reason, it was not possible to achieve precisely the same water content in each sample.

After measuring the gravimetric water content by weighing each sample using a digital lab balance (Ohaus PA114, Nänikon, Switzerland), the different compaction densities of the substrate were set up by mixing and then compressing the transparent soil, in all cases, to a final volume of 14 cm^3, so that the samples which had the highest

Treatment – substrate density (g cm^{-3})	Number of samples	Gravimetric water content (%)	Final substrate volume (cm^3)
0.78	3	Unsaturated: 34.9 ± 0.4	14
0.7	3	Unsaturated: 35.9 ± 0.7	14
0.62	3	Unsaturated: 34.8 ± 0.6	14

Table 4.1. Details of the setup of transparent soil samples for comparing root growth at different compaction levels.

compaction had a smaller final pore volume than the samples with lower compactions. One pre-germinated seedling was then transferred to the surface of the substrate at the centre of each vial.

4.2.2.2 *Substrate particle size experiment*

Four different substrates were prepared as shown in Table 4.2. The three transparent soil samples were prepared as described previously (page 53) and were separated into size categories 250–500 µm, 500–850 µm and 850–1250 µm by sieving. The particles were autoclaved in dH_2O for sterilisation and then much of the water was removed using a Pasteur pipette with a pipette tip. Murashige and Skoog basal medium (Sigma)

was added to Percoll (Sigma) at 10: 90% (v v^{-1}) and the pH was adjusted to pH 6.with 1 M HCl. This RI matching solution was then added to the particles to saturate the pore spaces. For the other treatments, phytagel (Sigma) was prepared at a concentration of 5 g L^{-1} or 10 g L^{-1} dH_2O to create 2 different gel densities and in each case, the phytagel contained half-strength Murashige and Skoog basal medium (Sigma). In this experiment, the transparent soil samples were saturated throughout the growing period in order to have a closer comparison with the phytagel treatments. One pre-germinated seedling was then transferred to the surface of the substrate at the centre of each vial.

Treatment – substrate composition	**Number of samples**	**Water status**	**Final substrate volume (cm^3)**
Small particles – 250 – 500 µm	4	Saturated	14
Medium particles – 500 – 850 µm	4	Saturated	14
Large particles – 850 – 1250 µm	4	Saturated	14
Soft phytagel – 5 g L^{-1}	4	Saturated	14
Hard phytagel – 10 g L^{-1}	4	Saturated	14

Table 4.2. Details of the setup of transparent soil and phytagel samples for comparing root growth in substrates with different textures.

4.2.3 **Plant culture**

In all cases, the "below ground" part of the sample was covered with aluminium foil on the outside of the vial during the growth period to eliminate light from the roots. The samples were kept in a controlled temperature room at 20 °C with 16 hours light: 8 hours darkness each day. In all cases the plants were grown for 6 days in the substrates before imaging.

4.2.4 **Imaging**

For the experiment comparing the effect of substrate compaction on root growth, the samples were prepared by adding a RI matching solution with 20% sorbitol (w v^{-1}),

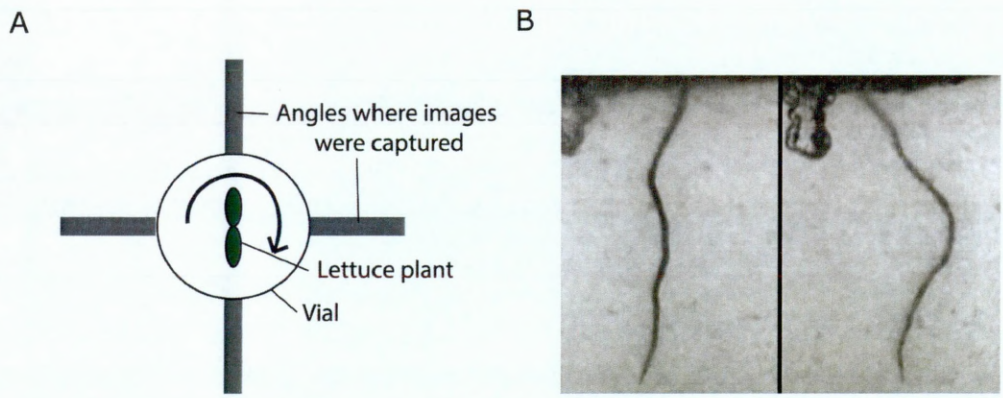

Figure 4.1. Imaging process. A) Top view diagram of the plant sample, where 4 projection images were taken at 90° intervals by rotating the sample. B) Examples of 2 consecutive images of a root system. Only 2 out of 4 images were used because the image pairs were mirror images of one another. The images that were used were selected based on how clearly the roots appeared.

accounting for the dilution effect of the water already present in the samples. The saturated samples from the experiment comparing the effect of gels and particle size on root growth required no extra preparation for imaging.

Imaging was carried out using the optical projection tomography (OPT) system at The James Hutton Institute. For each sample, 4 projection images at a resolution of 900 pixels mm^{-2} were taken with 90° of separation between them (Figure 4.1).

4.2.5 **Image analysis**

The root systems studied in this experiment were not old enough to have developed lateral roots and so only the primary roots were analysed. In order to calculate the 3D trajectories of the roots, the images were processed using the open-source software FIJI (Schindelin et al., 2012). Of the 4 images captured, 2 consecutive images were selected based on how clearly the roots appeared (Figure 4.1). The background was subtracted using the "subtract background" tool, and then the primary root was traced using the pencil tool, which gave a black line, 1 pixel in diameter. All of the XY coordinates along the line were extracted by an edge tracking algorithm and saved for subsequent 3D reconstruction.

Once this had been carried out for both of the images of a root, the 3D co-ordinates were calculated using the following procedure. One 2D image provided XZ, the other YZ co-ordinates. The Z co-ordinates common to both images were picked to find the complete X, Y and Z co-ordinates for each point This was done using a custom program

written by Lionel Dupuy (The James Hutton Institute, Invergowrie, UK) in Python 2.7.3 (Python Software Foundation).

4.2.6 **Data analysis**

The 3D coordinates were joined together to form a representation of the root trajectories 1 voxel in diameter consisting of a series of small straight sections. The total combined length of the sections could be calculated to estimate the root length. The length of the sections was not always the same because the distance between the coordinates was set using a determined number of pixels between the Z coordinates of each point. There were 15 pixels (0.5 mm) between each point in the Z dimension, therefore the 3D distance between each point varied (Figure 4.2). Root length, vertical curvature (the angle of deviation from a straight line along consecutive sections of the root) and 3D verticality (angle of deviation from vertical, where 0 = vertical, of each root section) were calculated from the 3D coordinates using a custom Python program written by Lionel Dupuy (Figure 4.2). Distances between root extremities were calculated from the 3D vector given by the coordinates at the beginning and end of each root trajectory.

4.2.6.1 *Statistical analysis*

Means and standard errors were calculated using Sigmaplot 12.3 (Systat Software, Inc.). The data on root curvature from the substrate density experiment were log transformed and the curvature data from the substrate texture experiment were square root transformed in order to satisfy the requirements of normality for the statistical tests.

General analyses of variance, restricted maximum likelihood (REML, linear mixed models) and Spearman's rank correlation were performed using Genstat, 14th edition (VSN International Ltd.). For the analysis of variance, all of the measurements for each treatment (i.e. multiple plants and multiple measurements from each plant) were pooled and the overall means for each treatment were used. For the REML estimation, a linear mixed model was used. Treatment and distance along the root were used as the fixed effects. Distance along the root was also squared in order to allow curves in the model and was also added to the fixed effects. The individual plant was used as the random model. There was assumed to be no interaction between individual plant and distance along the root. The curvature or verticality was considered as a variate. Simple linear regression was used to compare pooled data with the fitted values from models and a simple linear regression with groups was used to compare data grouped by individual plant with the fitted values from models.

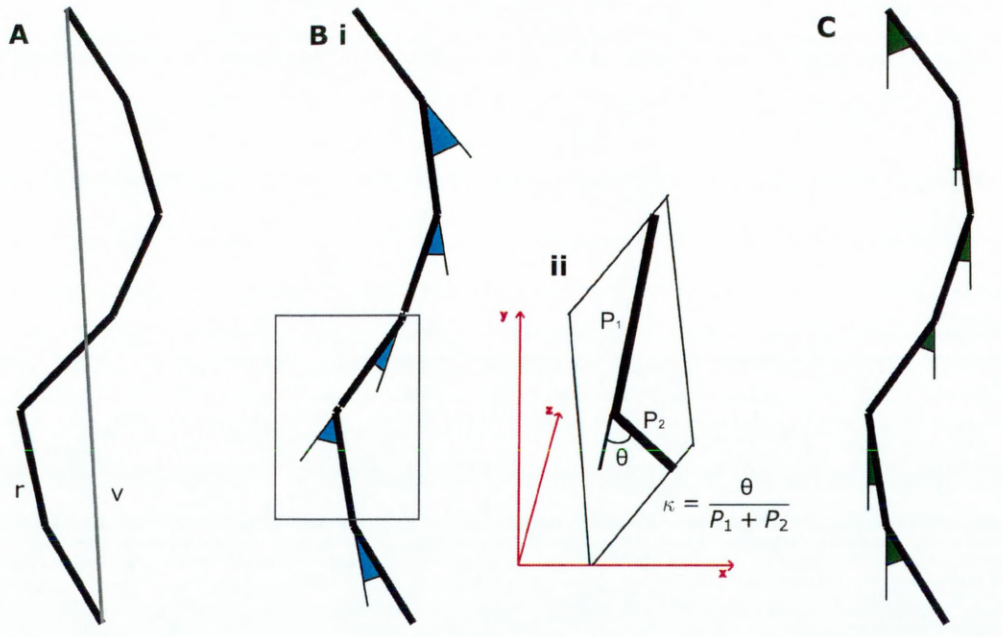

Figure 4.2. Representation of the method by which root length, curvature and verticality were measured along the roots. A) Root length was the length of the 3D trajectory representing the root (r), which was compared with the vector representing the Euclidean distance between the root extremities (v). B) Curvature was a measure of the change in direction of the root, where the blue sections (i) represent the angles measured along the root. The 2 vectors representing sections of the root, P_1 and P_2, occupy a 2D plane in 3D space and curvature (K) is calculated in this plane. C) Verticality was a measure of how far the root trajectory deviated from vertical. The green sections represent the angles that were measured.

4.3 Results

4.3.1 The effect of substrate compaction on primary root trajectories

3D root trajectories were reconstructed from plants grown in transparent soil at densities of 0.62 g cm^{-3} (n = 3), 0.70 g cm^{-3} (n = 3) and 0.78 g cm^{-3} (n = 2). Primary root lengths were measured and the Euclidean distance between the base of the root and the root tip was calculated for plants grown in transparent soil at the different compaction levels (Figure 4.3). The overall mean primary root length was 36.4 ± 3.5 mm

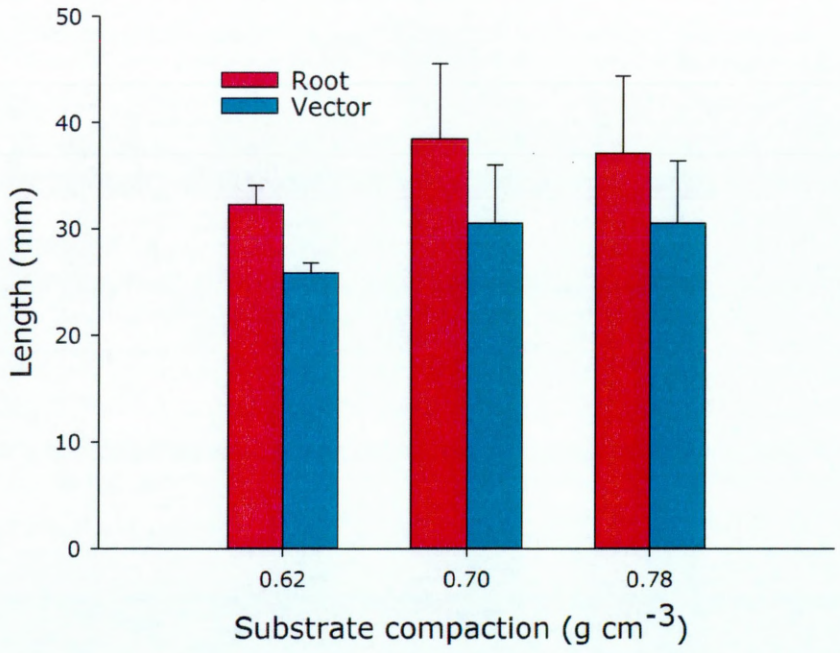

Figure 4.3. Mean primary root lengths and distance between root extremities (vector) of lettuce plants grown in transparent soil with 3 different substrate compactions. Error bars represent standard error.

and a general analysis of variance (ANOVA) showed that there was no significant difference in primary root length between the plants grown in substrates with different compactions ($F_{2,7}$ = 0.25, p = 0.785). Likewise, there was no significant difference in distance between the root extremities of the plants from different treatments ($F_{2,7}$ = 0.28, p = 0.766). In the present study, the mean root: vector length was 1.24 and there was no significant difference in this ratio between the plants grown at different compaction levels ($F_{2,7}$ = 0.22, p = 0.811) (Figure 4.4).

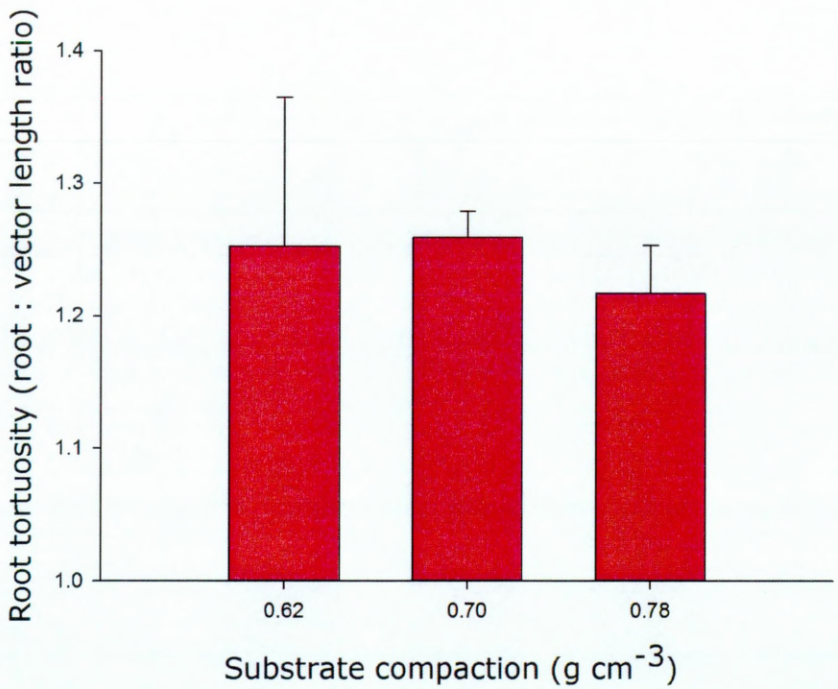

Figure 4.4. Ratio between the root length and the length of the distance between the root extremities. This was used as a global measure of root tortuosity of plants grown in transparent soil with 3 different levels of compaction.

Curvature was found to vary along the trajectory of the root and a list of angles of curvature was collected for each root trajectory and at each substrate compaction level. A general ANOVA was used to compare the variance in curvature of roots grown at different substrate compaction levels by pooling all of the measurements for each treatment. There was no significant difference in overall root curvature between roots from the different substrates ($F_{2,342} = 2.74$, $p = 0.066$). The spread of the data on root curvature was also visualised (Figure 4.5). The root curvatures in the substrates with the highest compaction (0.78 g cm^{-3}) had a wider range than those from the substrates with

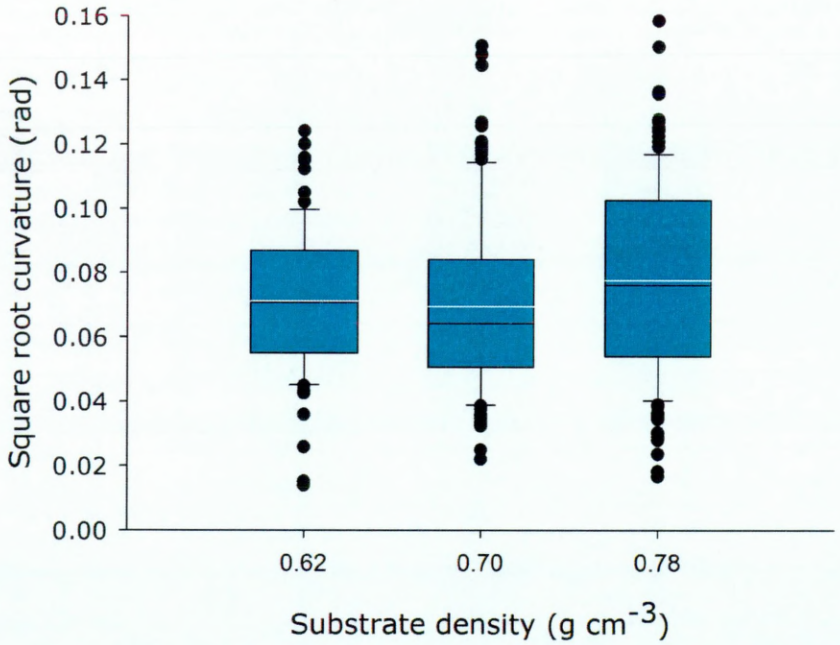

Figure 4.5. Box plot showing the spread of data on root curvature in substrates with different compaction levels. The black line inside the box denotes the median and the white line denotes the mean. The data shown have been square root transformed.

lower compaction levels, and in particular, the difference between the upper and lower quartiles was highest at the highest compaction. The standard deviation of the curvature of roots grown at a substrate compaction of 0.62 g cm^{-3} was 2.2×10^{-2}, at 0.70 g cm^{-3} the standard deviation was 2.7×10^{-2} and at 0.78 g cm^{-3}, the standard deviation of root curvature was 3.0×10^{-2}.

Restricted maximum likelihood (REML) variance component analysis was used to allow the incorporation of a spatial factor along the roots into the analysis. Using this method, it was found that the compaction treatment had no effect on root curvature ($F = 0.31$, $p = 0.748$, Table 4.3). However, the measurements' distance along the root (sequence) did influence root curvature and there was an interaction effect between the treatment and distance along the root (Table 4.3). The linear mixed model could be fitted to the curvature data, incorporating distance along the root. The goodness of fit of the model was tested using a simple linear regression, which showed that the model (with 95% confidence intervals) accounted for 54.1% of the variation in the data (Figure 4.6). Another linear regression was carried out where the treatment levels were included as groups (Figure 4.7). In this case, the model could account for 79.2% of the variation in the data. Generally, there were no clear patterns in the way in which curvature varied between the treatments. Verticality along the root trajectories was also measured (Figure 4.8) and a general ANOVA showed that there was no significant difference in mean root verticality between the different substrates ($F_{2,374} = 0.54$, $p = 0.586$, Figure 4.8). REML variance component analysis was used again for analysing the verticality along the roots. It revealed that the treatment had no effect on root verticality ($F = 0.16$,

p = 0.859, Table 4.4), yet the measurements' distance along the root did influence the verticality and there was an interaction effect between the treatment and distance along the root (Table 4.4). A linear regression, grouped by treatment level, showed that the model accounted for 38.7% of the variation in the data (Figure 4.10). Again, there was no clear trend in verticality along the root between the treatments.

Fixed term	n.d.f.	F statistic	F pr.
Treatment	2	0.31	0.748
Sequence	1	26.60	<0.001
Sequence^2	1	41.98	<0.001
Treatment.sequence	2	21.90	<0.001
Treatment.sequence^2	2	21.45	<0.001

Table 4.3. Fixed effects from the REML component analysis on root curvature in roots grown in transparent soil with different compaction levels. "Sequence" is the distance along the root and n.d.f. = the number of degrees of freedom. The sequence^2 term was used to allow non-linear fitting.

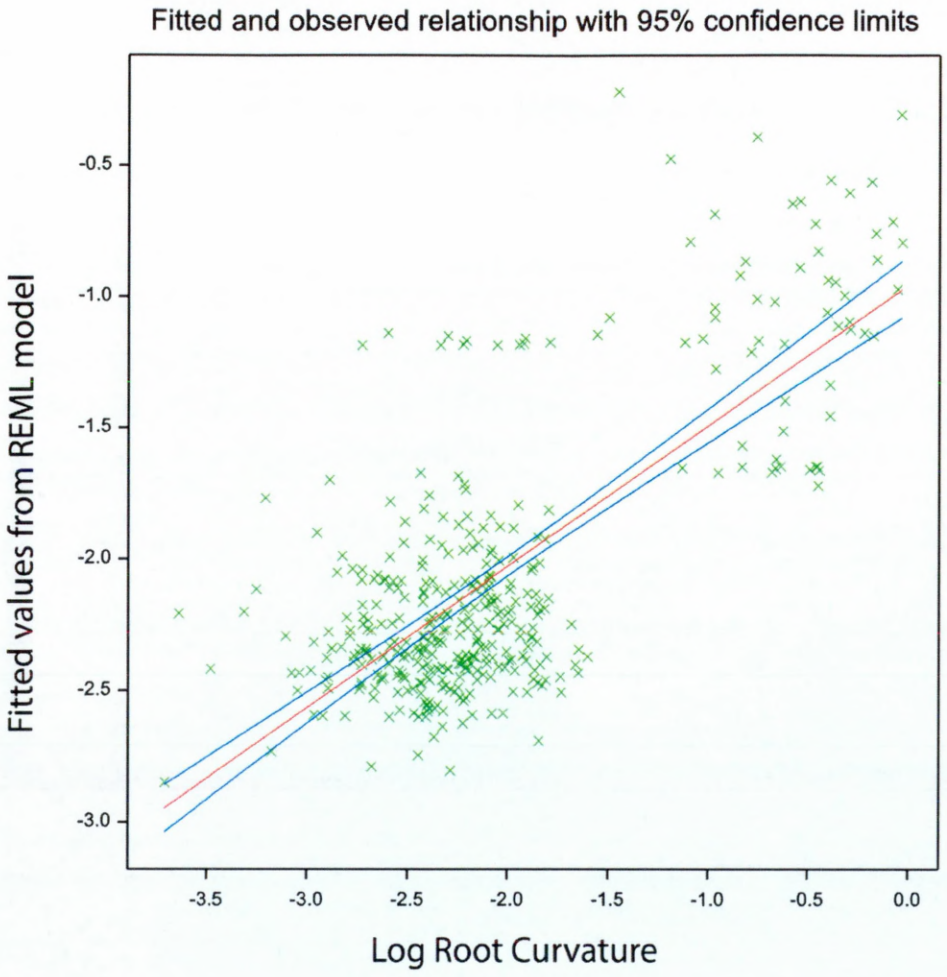

Figure 4.6. Relationship between the log transformed curvature values of roots grown in transparent soil with 3 different densities (data from all roots have been pooled in this plot) and the fitted values from the REML variance component analysis. The red line shows the linear regression with 95% confidence limits (blue lines) where $p < 0.001$.

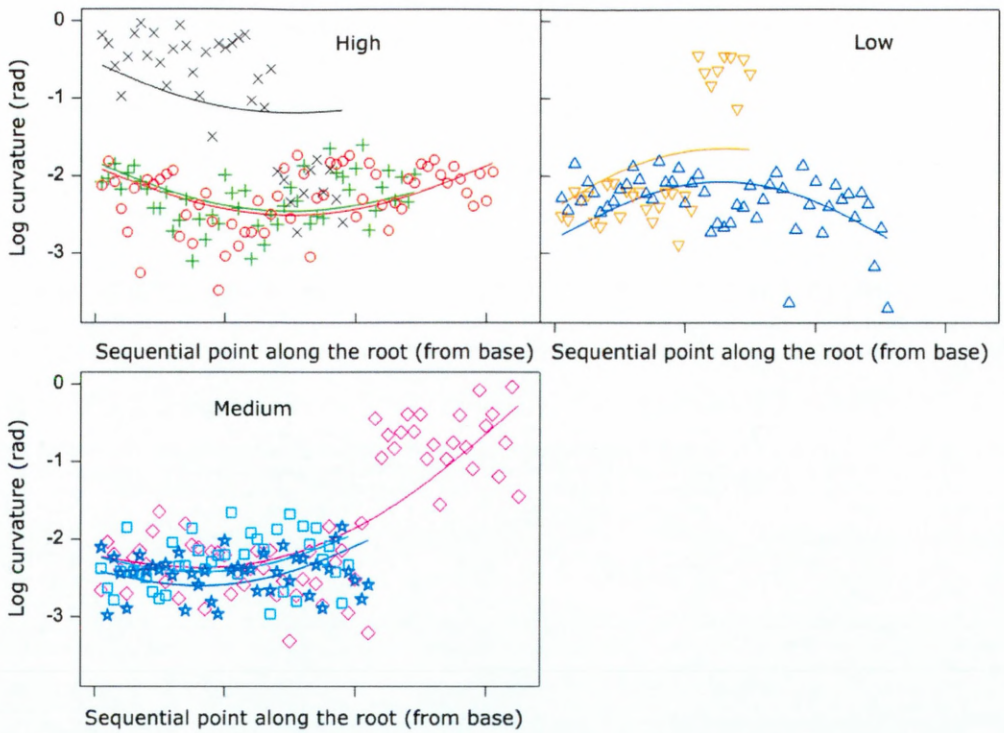

Figure 4.7. Linear mixed model from REML variance component analysis (curves) as applied to curvature data from each plant (data points) from the three substrate density treatments: high density (0.78 g cm^{-3}), low density (0.62 g cm^{-3}) and medium density (0.70 g cm^{-3}). The different symbols signify data from different individual plant samples.

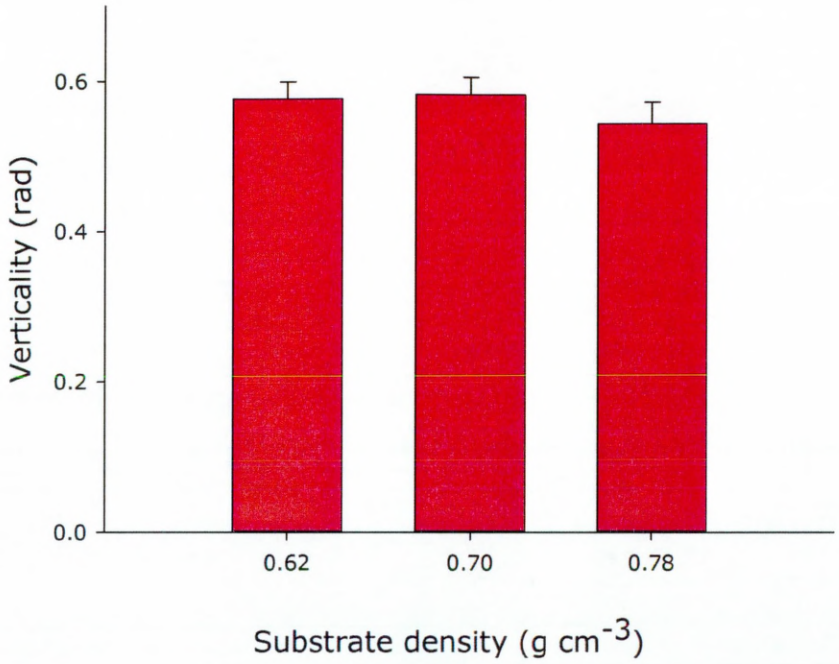

Figure 4.8. Overall mean verticality in lettuce roots grown in transparent soil with different compaction levels. Error bars show standard error.

Fixed term	n.d.f.	F statistic	F pr
Treatment	2	0.16	0.859
Sequence	1	6.03	0.015
Sequence^2	1	8.36	0.004
Treatment.sequence	2	16.36	<0.001
Treatment.sequence^2	2	3.16	0.043

Table 4.4. Fixed effects from the REML component analysis on root verticality in plants grown in transparent soil with different compaction levels. "Sequence" is the distance along the root and n.d.f. = the number of degrees of freedom. The sequence^2 term was used to allow non-linear fitting.

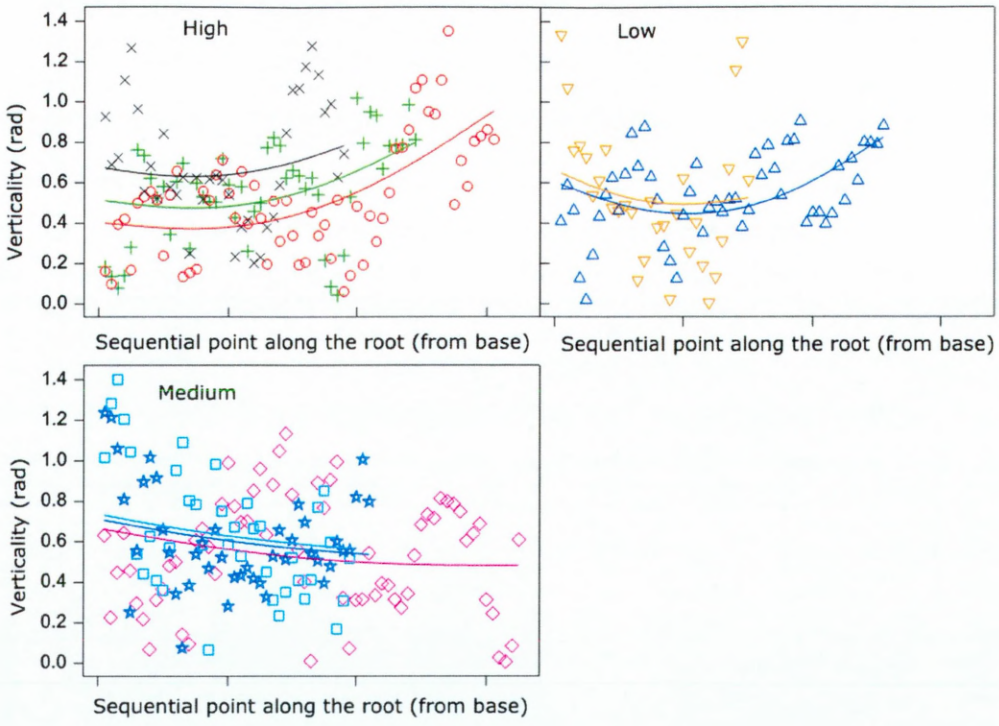

Figure 4.9. Linear mixed model from REML variance component analysis (lines) as applied to verticality data from each plant (data points) from the three substrate density treatments: high density (0.78 g cm^{-3}), low density (0.62 g cm^{-3}) and medium density (0.70 g cm^{-3}). The different symbols signify data from different individual plant samples.

4.3.2 The effect of substrate texture on root growth trajectories

Plants were grown in transparent soil with 3 different particle size categories (small 250–500 μm, medium 500–850 μm and large 850–1250 μm) and in phytagel with two different densities (5 g L^{-1} and 10 g L^{-1}). The plants grown in the transparent soil with the smallest particle sizes (250–500 μm) could not be imaged because the substrate became opaque over time. These samples were therefore excluded from further analyses. Primary root length was measured and a general ANOVA showed that there was no significant difference in primary root length ($F_{3,12}$ = 0.32, p = 0.810) and distance between the root extremities ($F_{3,12}$ = 0.53, p = 0.671) between the plants grown in any of the substrates (Figure 4.10). The overall mean root length: root vector ratio was 1.12 and the ratios from the different substrate types were not significantly different from one another ($F_{3,12}$ = 1.10, p = 0.398, Figure 4.11).

Similar to the experiment investigating the effects of compaction on root trajectories, there was variation in curvature along the roots and between the substrate treatments in this experiment comparing the effects of substrate textures on roots (Figure 4.12). A general ANOVA confirmed that there was a significant difference in root curvature between the substrates ($F_{3,532}$ = 10.02, p < 0.001) and a post-hoc Fisher's protected LSD test showed that the roots grown in hard phytagel had the lowest curvatures. Roots grown in soft phytagel and in transparent soil with small particles had the next lowest curvatures and the curvatures of roots grown in transparent soil with large particles had

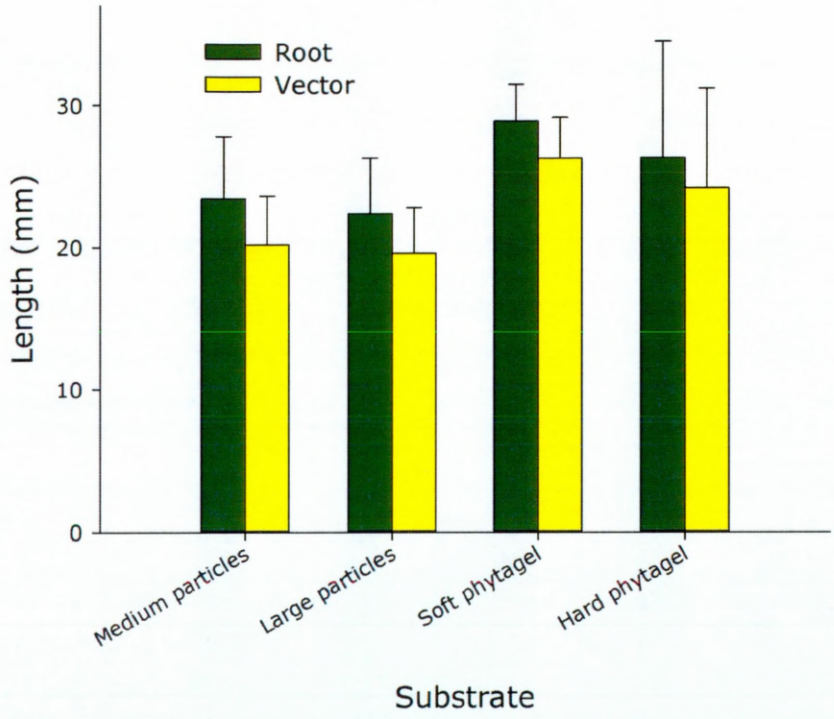

Figure 4.10. Mean primary root lengths and distance between root extremities (vector) of lettuce plants grown in transparent soil with different particle size categories and phytagel with two different densities. Error bars represent standard error.

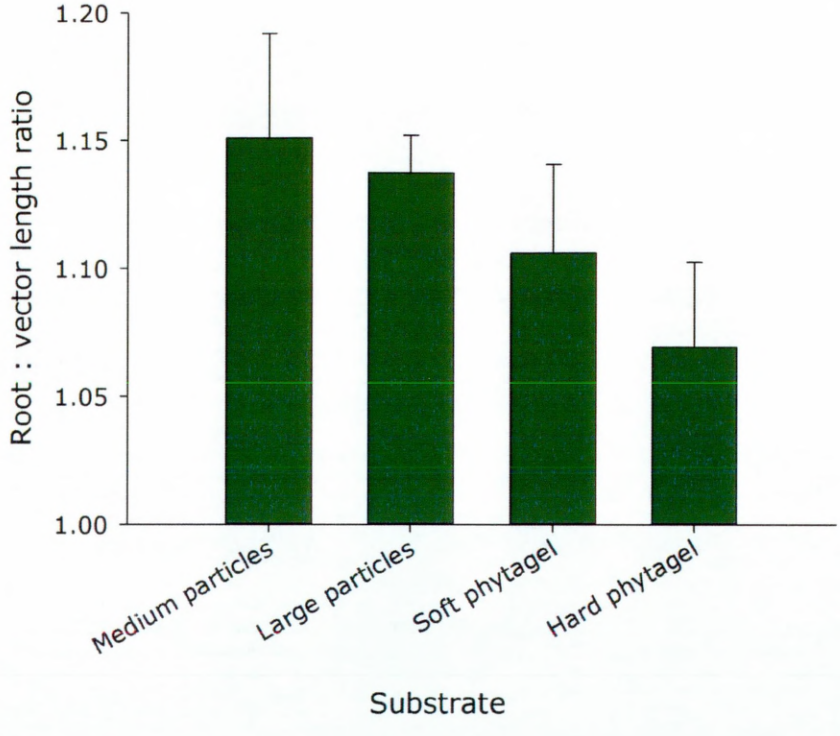

Figure 4.11. Root length : vector length ratio as a global measure of root tortuosity of plants grown in transparent soil with two different particle size compositions and in phytagel of two different densities.

of

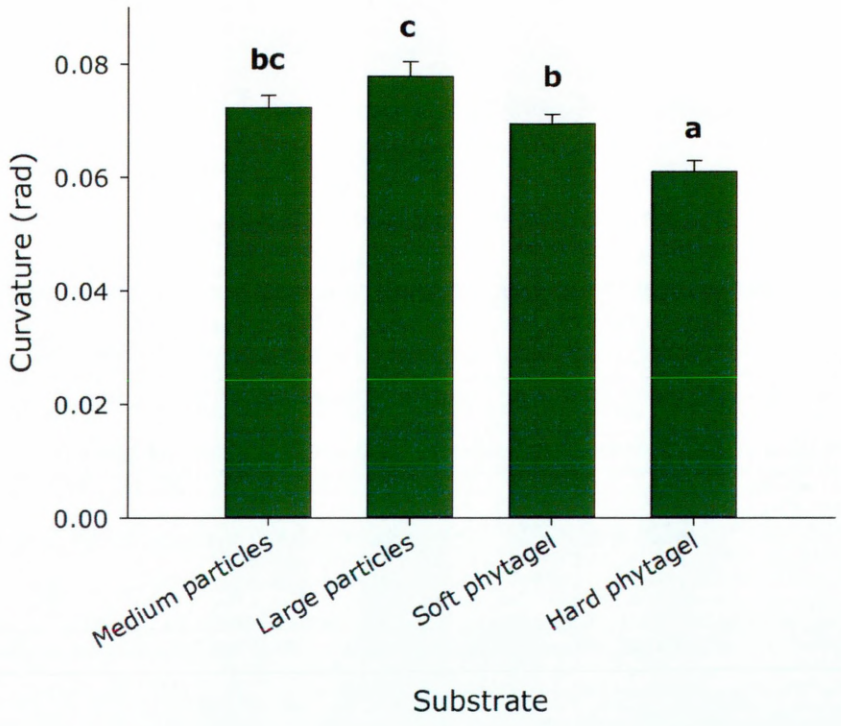

Figure 4.12. Overall mean root curvature in substrates with different textures. The data shown has been square root transformed and the error bars represent standard error. The letters above the bars indicate the results from a Fisher's protected least significant difference test.

curvatures higher than all of the other treatments, with the exception of the transparent soil with small particles, between which there was no difference (Figure 4.12).

REML variance component analysis also showed that there was a difference in curvature between roots from the different substrates ($F = 9.76$, $p = 0.014$, Table 4.5). The curvature did not depend on the measurements' distance along the root but there was an interaction effect between the treatment and the distance along the root (Table 4.5). A simple linear regression was used to compare the data with the fitted values from the model, which accounted for 10.1% of the variation in the data (Figure 4.13). When the linear regression was grouped using the treatment levels, the model could account for 60.1% of the variation in the data (Figure 4.14).

Fixed term	**n.d.f.**	**F statistic**	**F pr**
treatment	3	9.76	0.014
Sequence	1	0.29	0.592
Sequence^2	1	1.45	0.228
Treatment.sequence	3	5.83	<0.001
treatment.sequence^2	3	2.40	0.067

Table 4.5. Fixed effects from the REML component analysis on root curvature in plants grown in transparent soil with different substrate textures. "Sequence" is the distance along the root and n.d.f. = the number of degrees of freedom. The sequence^2 term was used to allow non-linear fitting.

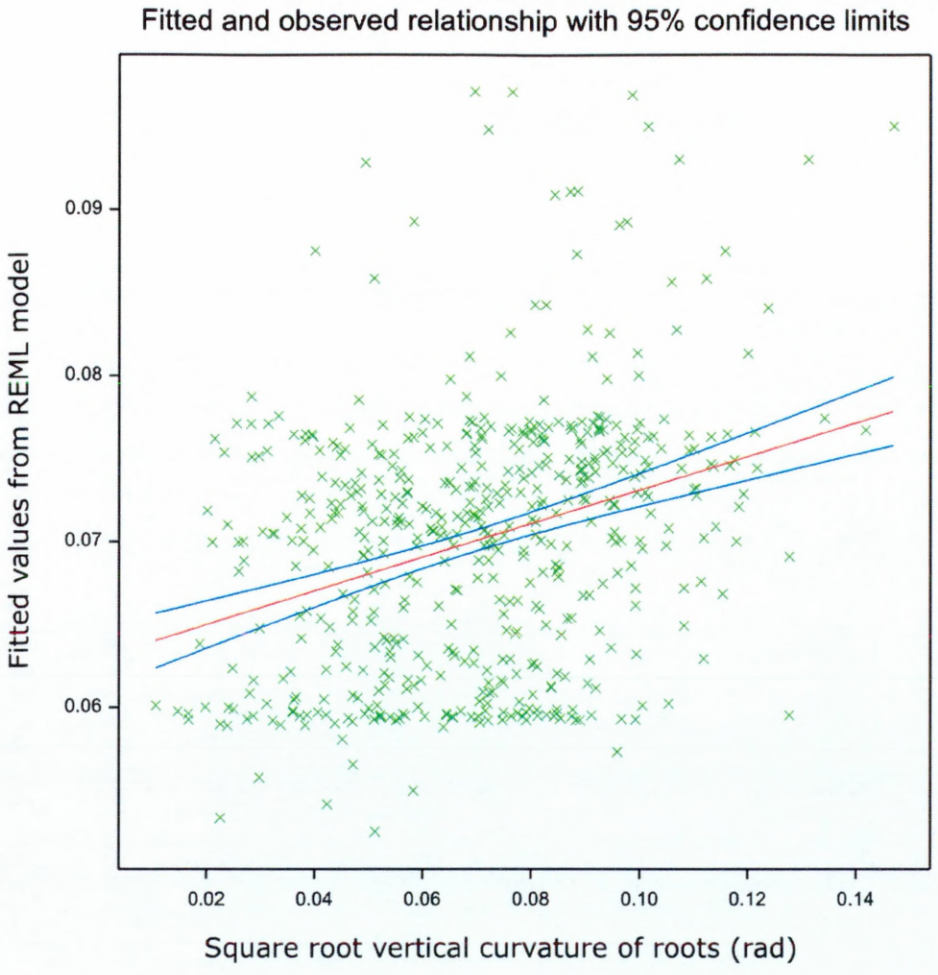

Figure 4.13. Relationship between the square root transformed curvature values of roots grown in transparent soil with four different textures (data from all roots has been pooled in this plot) and the fitted values from the REML variance component analysis. The red line shows the linear regression with 95% confidence limits (blue lines) where $p < 0.001$.

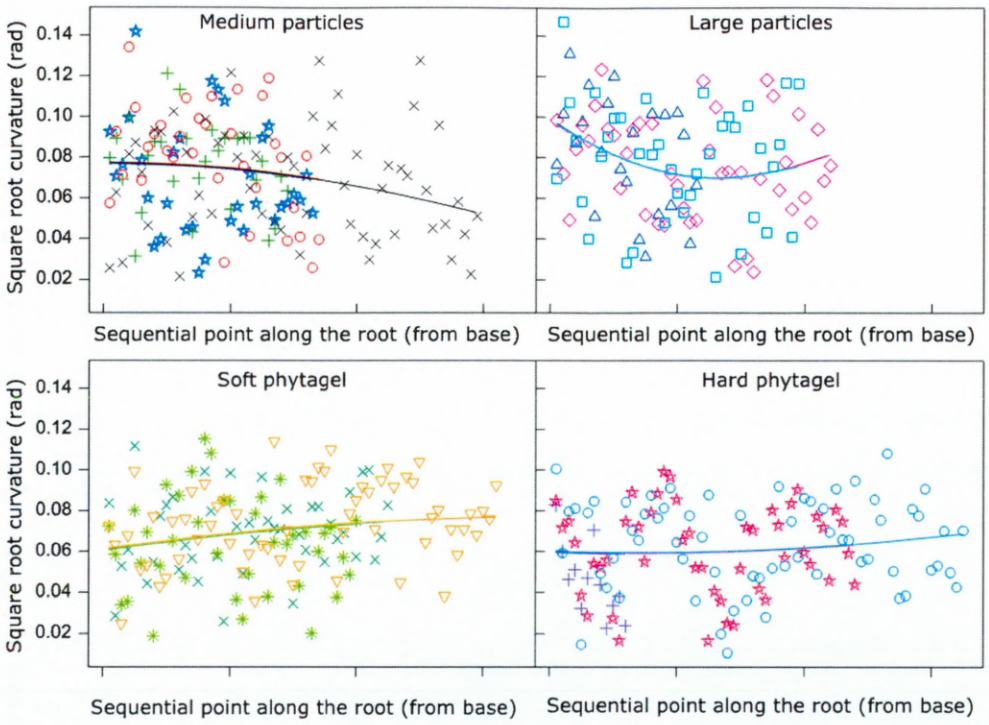

Figure 4.14. Linear mixed model from REML variance component analysis (lines) as applied to square root transformed curvature data from each plant (data points) from the four substrate texture treatments: medium particles, large particles, soft phytagel and hard phytagel. The different colours signify data from different individual plant samples.

Verticality also varied along the roots and between substrate treatments (Figure 4.15). A general ANOVA showed that there was a significant difference in mean verticality between the treatments ($F_{3,532} = 4.33$, $p = 0.005$, Figure 4.15). The roots of plants grown

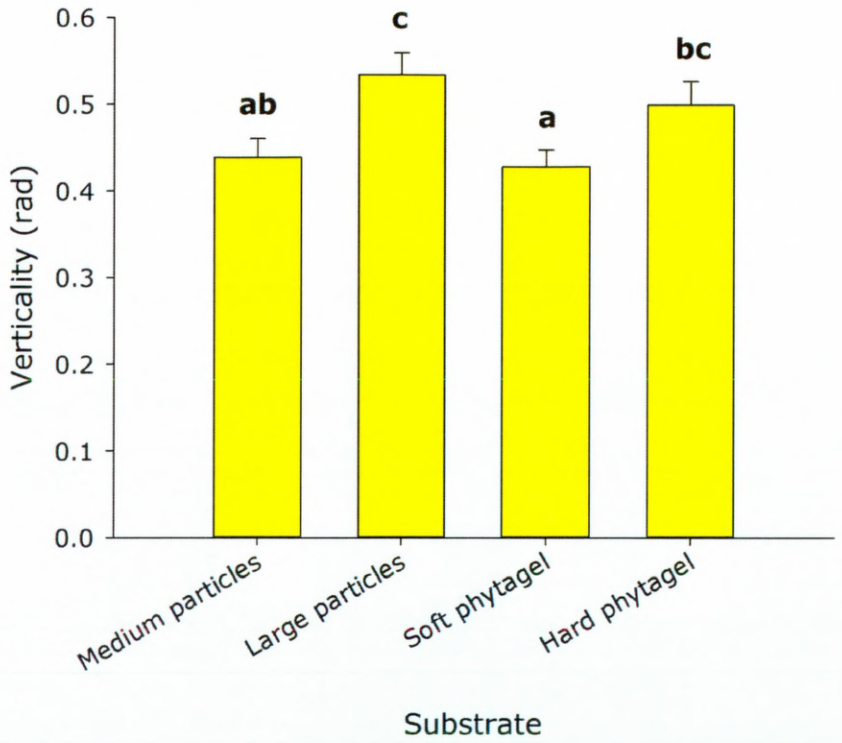

Figure 4.15. Mean verticality in lettuce roots grown in transparent soil with different substrate textures. Error bars show standard error. The letters above the bars indicate the results from a Fisher's protected least significant difference test.

in soft phytagel and in transparent soil with small particles had the mean verticalities closest to zero (where 0 = vertical). The roots of plants grown in transparent soil with large particles had a mean verticality furthest from zero and roots of plants grown in hard phytagel had a mean verticality that was not different from that of plants grown in transparent soil with small or large particles.

However, when the measurements' distance along the roots was incorporated into the analysis using REML variance component analysis, it was found that the substrate had no effect on the roots' verticality ($F = 0.83$, $p = 0.513$, Table 4.6) but the distance along the root did have a significant effect on the verticality and there was an interaction effect between distance along the root and treatment. A grouped simple linear regression showed that the model accounted for 57.6% of the variation in the data (Figure 4.16), and there was a positive correlation between verticality and (distance along the root)^2 (correlation: 0.233, $p < 0.001$).

Fixed term	n.d.f.	F statistic	F pr
Treatment	3	0.83	0.513
Sequence	1	75.85	<0.001
Sequence^2	1	11.58	<0.001
Treatment.sequence	3	4.76	0.003
Treatment.sequence^2	3	11.31	<0.001

Table 4.6. Fixed effects from the REML component analysis on root verticality in plants grown in transparent soil with different substrate textures. "Sequence" is the distance along the root and n.d.f. = the number of degrees of freedom. The sequence^2 term was used to allow non-linear fitting.

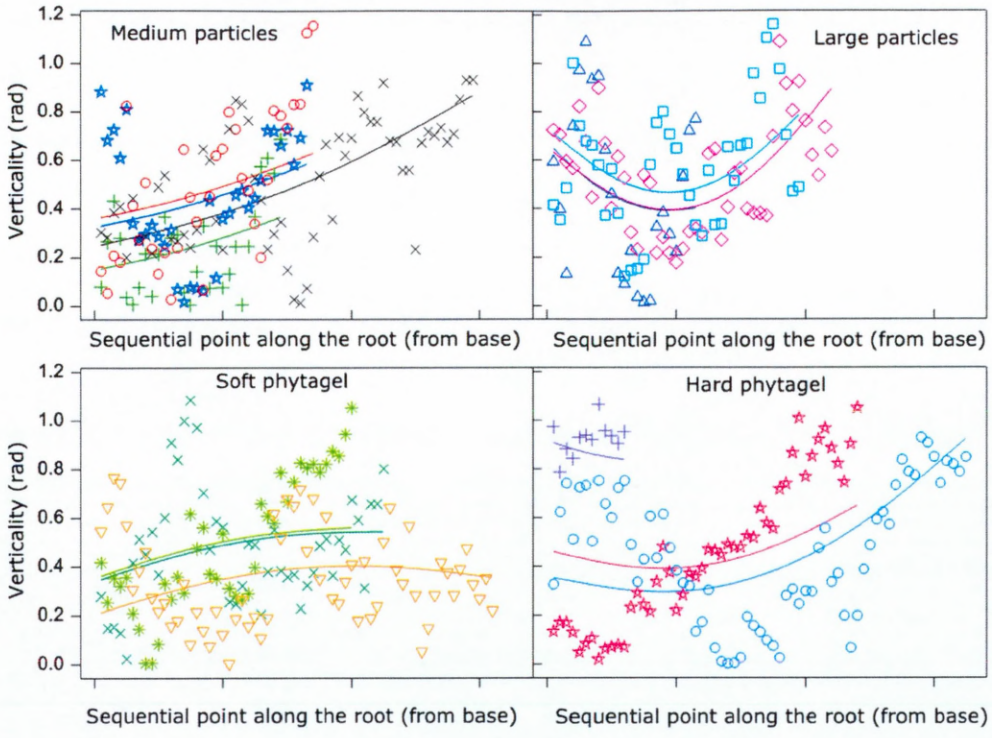

Figure 4.16. Linear mixed model from REML variance component analysis (lines) as applied to square root transformed curvature data from each plant (data points) from the four substrate texture treatments: medium particles, large particles, soft phytagel and hard phytagel. The different colours signify data from different individual plant samples.

4.4 Discussion

4.4.1 The effect of substrate compaction on root trajectories

In the experiment comparing root trajectories in substrates with different compaction levels, there was no difference in primary root tortuosity (Figure 4.4). These results are contrasting with data presented by Tracy et al. (2012) where they found that soil compaction increased the tortuosity of the primary root. There could be several reasons for this discrepancy. The calculation of tortuosity by Tracy et al. compared the vertical rooting depth, rather than the Euclidean distance between the root extremities, with the root length. There was also a greater difference in compaction between the soils used in the experiments by Tracy et al. than there was here. Perhaps more fundamentally, plants from different genera were used in the two experiments and Tracy et al. used a real soil rather than a soil analogue.

Regarding root curvature at different densities, it might have been expected that there would be a trend in mean root curvature with different levels of compaction; however that was not the case here. There was a difference in the range of curvatures between the treatments and by visualizing the data in the form of a box plot, it was evident that the range of measurements was larger with higher compaction (Figure 4.5) and correspondingly the standard deviation is higher with higher compaction levels. This could be because with higher compaction, the particles in the substrate have a greater influence on the trajectory of the root. At low compaction, the root would be more able to push soil particles aside as it followed a trajectory based on the inherent growth

pattern and tropic responses, whereas at high compaction it would have to grow around the particles more often and the trajectory would be more subject to thigmotropic responses. The data presented here show how this leads to root trajectories with a greater range of curvatures. The angle of curvature was influenced by the distance along the root, as confirmed by the REML component analysis (Table 4.3), but the shape of the curves varied greatly between individual plants (Figure 4.7). Because the curvatures were not dependent on the substrate compaction, it is not valid to generalise on root curvature between substrate treatments.

It was expected that higher levels of compaction would increase the mechanical impedance experienced by the roots and would result in shorter, more tortuous roots (Goss & Russell, 1980, Tracy et al., 2012), which would perhaps also have higher curvatures. In order to further examine the relationship between root growth and the transparent soil with different compactions, it would be possible to quantify the pore volumes, diameters and tortuosities of the transparent soils with different properties. This could be achieved using X-ray μCT and subsequent image analysis. Also, higher compactions could perhaps be achieved using transparent soil with smaller particle sizes, and so this would be one option for further studies.

No difference was found in the mean root verticality in plants grown at different levels of compaction (Figure 4.8). The distance of the measurement along the root did have an influence on the verticality and this effect also depended on the treatment (Table 4.4). From this, we can conclude that compaction did not affect the straightness of the

growth trajectory because the treatments did not have an influence on the gravitropic response of the root tips. However, the verticality did change with distance from the root base, which could perhaps be due to the timing of gravitropism in root development (Barlow, 2002) and because of the decreasing influence of the initial seed direction over time on the growth direction of the root tip.

4.4.2 The effect of substrate texture on root trajectories

In the experiment comparing root trajectories in substrates with different particle sizes and gel densities, no difference was found in the root lengths or in the global tortuosity of the primary roots (Figure 4.10 & Figure 4.11). These results are in agreement with the results presented in Chapter 3 (section 3.3.4, page 68) which showed that tobacco plants grown in transparent soil have primary roots the same length as plants grown in phytagel. Despite the similarities in root length and global tortuosity between the plants, there were some interesting differences in root curvature between the treatments (Figure 4.12). Overall, the mean curvature was higher in plants grown in transparent soil than in phytagel. This could represent the smoother root trajectory that was possible in gel where the roots were not navigating around objects, as they were in transparent soil.

The roots of plants grown in the hard phytagel had less vertical growth trajectories than plants grown in soft phytagel (Figure 4.14). This corresponds with the studies by Antonsen et al. (1999) and by Massa & Gilroy (2003) which showed that the gravitropic response in roots can be overridden by touch stimuli. This may happen to a greater

extent with the harder phytagel than the soft phytagel because of the increased resistance experienced by the root tip. Further experiments with a greater number of replicates, where the samples could be reoriented during growth would be required to fully test this hypothesis.

In both of the experiments presented in this Chapter, verticality varied with distance along the root. This could be because immediately after emergence, the direction of root growth could be influenced by the direction in which the seed was facing as the root emerged. The discrepancy of verticality along the root could also be because of the time lag between gravity perception and gravitropic response exhibited by roots (Kiss et al., 1996), however there was a strong positive correlation between distance along the root and verticality, which suggested that the roots deviated further from vertical near the root tip, which could be caused by a responses to the substrate. These hypotheses would require further experimental testing, ideally with a larger sample number, to be validated.

4.4.3 Future directions

4.4.3.1 *Manipulating transparent soil for mimicking soil physical conditions*

The methods presented in this Chapter have described some simple ways in which transparent soil can be manipulated to replicate different soil compaction levels and soils with different particle sizes. As discussed, it may be possible to increase the range of compaction levels possible by using smaller particle sizes than were used here.

Another potential way of increasing the resistance experienced by roots would be to apply pressure to the surface of the substrate so that the particles could be less easily displaced by the roots (Clark et al., 2001). Similarly, a larger range of particle sizes could be tested, the upper limit being the size of the particulate raw material (2–3 mm), and the minimum possible size would be determined by practical considerations (very small particle sizes are difficult to work with and the substrate becomes difficult to saturate effectively for imaging).

In the longer term, if the transparent soil system could be scaled up sufficiently for high throughput root system analysis, the analysis techniques presented in this Chapter could be very useful. For example, in a crop breeding program to select plant varieties with deep rooting systems even in compacted soil, compacted transparent soil could be used and the root systems imaged. Subsequent 3D root measurements could be carried out, including 3D verticality, an indicator of deep rooting (Kato et al., 2006).

4.4.3.2 *Image analysis and data analysis*

Analysis of root trajectories could benefit from techniques developed for analysing the 3D path of living organisms taken over time, rather than as a growth trajectory as studied in this Chapter. Crenshaw et al. (2000) presented a method for standardising the analysis of 3D curved trajectories called the Finite Helix Fit (FHF) and applied the technique to the analysis of the movement of diverse living things including a flagellate, a ciliate, spermatozoa and a larvae. The 3D trajectories of sperm cells have received some attention, particularly with advances in 3D microscopy (Woolley & Vernon, 2001,

Corkidi et al., 2008, Su et al., 2012). Various approaches have been used to analyse and categorize their trajectories. It would be interesting to find out how the approach employed by root tips to explore a 3D volume compares to the trajectories taken by other organisms to explore a volume, taking into account the vast scale differences in time and space. More generally, techniques for analysing movement trajectories could be applied to describing root trajectories, particularly if time series data was available.

With more data, advanced analysis techniques could be used to describe the data more effectively. Time series analysis techniques, for example, could be used to elucidate any patterns in geometry along the roots, rather than using average measures. These techniques are commonly used for analysing many types of data accumulated over time, such as changes in landscape cover taken from satellite image data (e.g. Jakubauskas et al., 2001, Stow et al., 2004, Beck et al., 2006). However, because the data presented in this Chapter are not strictly time series data, this should be accounted for in the analyses. Eventually, with data from many plant species and in many substrate conditions, it would become possible to use such data to parameterize and improve the accuracy of crop models for predicting the growth of roots under given sets of conditions (Dupuy & Vignes, 2012, Fourcaud et al., 2008).

4.4.4 Conclusions

Overall, these results show that global root measures of root morphology such as tortuosity are merely approximate descriptors of root geometry. Alternatively, by measuring geometric parameters along the roots, it was possible to describe the

trajectory and directional growth of a root tip in greater detail, including how the root geometry can change with distance along the root. The method presented in this Chapter of using transparent soil to grow plants for 3D imaging of the root system followed by analysis of the root trajectories represents a starting point for sophisticated analyses of root growth in a complex soil-like system. The analysis presented here, particularly the REML component analysis, demonstrated that the root trajectories can be analysed in novel ways, incorporating the distance along the root. This meant that behaviour of the root tip during the growing period and with depth in the substrate could be assessed.

Chapter 5. High resolution 3D distribution of living *Pseudomonas fluorescens* on and around lettuce (*Lactuca sativa*) roots

5.1 Introduction

Soil contains a high concentration and diversity of bacteria that perform essential functions such as decomposition of organic matter and nitrification (van Elsas et al., 2007). The way in which bacteria interact with plant roots is of interest because of the role of bacteria in plant growth promotion through biological control against plant pathogenic microorganisms (Whipps & Gerhardson, 2007) and through processes which provide plants with resources, such as during nitrogen fixation (Garg & Geetanjali, 2007). The interaction can occur indirectly in the rhizosphere – the zone of soil that is influenced by the roots by, for example, root exudates, or directly on the surface of the root – the rhizoplane. Pseudomonads are Gram-negative generalist species and can be found in most soils. They are also among the best root colonisers and have a high rhizosphere competence (Lugtenberg et al., 2001).

Biofilms consist of bacteria embedded within a stable matrix of extracellular polymeric substances (EPS). These can form on plants, where they play an important role in the ecology of the species involved as well as the soil ecosystem at large (Danhorn & Fuqua, 2007). The biofilm's integrity is dependent on a number of other factors including bacterial surface appendages such as pilli and flagella and lipopolysaccharide (LPS) coatings and the composition of the colonised surface (Donlan, 2002). Wheat root

colonisation by *Pseudomonas* species and other native bacteria was quantified and biofilms were found within 11 μm of the root surface and could be found on 40% of root surfaces (Watt et al., 2006). Exopolysaccharides of rhizosphere biofilms of *Pseudomonas* species contribute to biofilm survival and fitness under water-limiting conditions (Nielsen et al., 2011). The biofilm structure and composition of *Pseudomonas fluorescens* can be influenced by chemical factors such as the presence and concentration of metals (Koza et al., 2009).

After inoculation of seeds with *Pseudomonas fluorescens* and subsequent plant growth, bacterial cells can be found on the seeds and at the base of the root (Unge & Jansson, 2001). After colonisation they remain as single cells or grow into microcolonies, including rhizoplane biofilms, sometimes covered in mucigel (Chin-A-Woeng et al., 1997), which are usually found at root epidermal cell junctions (Rovira, 1956) and lateral root emergence sites (Unge & Jansson, 2001). Regarding the distribution of *P. fluorescens* cells and microcolonies along the root, there have been few conclusive studies. Dandurand et al. (1997) conducted a quantitative study on the spatial patterns of *P. fluorescens* strains in the rhizoplane of pea seedlings and found that there was a large amount of variation in the distribution between their samples and the distribution often seemed random. Humphris et al. (2005) found that border cells and mucilage produced by maize roots prevented colonization of the root tip by *P. fluorescens* SBW25, which was also the case in tomato and oat plants (Rovira, 1956). In other studies, wave-like fluctuations in bacterial density along roots have also been described (van Bruggen et al., 2000, van Bruggen et al., 2008).

Pseudomonas fluorescens releases various metabolites, some of which have a positive effect on plant growth through biological control (Dowling & O'Gara, 1994, Lakshmanan et al., 2012). Siderophores are among the metabolites produced, which allow the bacteria to take up iron from the soil solution and it is thought that this gives the bacteria a competitive advantage over some plant pathogenic fungi, whose pathogenicity can be significantly reduced in the presence of *P. fluorescens* (Raaijmakers et al., 1995). Plant protection by pseudomonads can also be through an indirect route, by stimulating the plant's own defence mechanisms inducing systemic resistance to pathogens (Preston, 2004). The plant growth promotion effect of *P. fluorescens* colonization of the roots may be pertinent under stress conditions, evidenced by a study showing that the biomass yield of *Catharanthus roseus* was enhanced by *P. fluorescens* under drought stress conditions (Jaleel et al., 2007).

Biological control conferred by plant growth promoting bacteria has yielded inconsistent results in the field, often due to poor root colonization (Weller, 1988). In order to engineer successful plant–bacteria associations for this purpose, further information is required on their ecological associations so that the bacteria's location along the root can be optimised so that it coincides with the regions favourable for the pathogenic microorganisms (Gamalero et al., 2003). Root colonization by *Pseudomonas fluorescens* in the field will undoubtedly be influenced by the soil properties, although these factors have not been studied.

The first aim of this Chapter is to use transparent soil to gain insight into the colonisation of lettuce roots by *Pseudomonas fluorescens* SBW25 and in doing so demonstrate the potential of transparent soil as a tool for quantitatively studying plant–microbe interactions. The second aim is to develop image analysis protocols to investigate how the particle size range of the transparent soil affects root colonization and bacterial density adjacent to the root surface.

5.2 Materials and methods

5.2.1 Bacterial culture

Pseudomonas fluorescens SBW25 marked with GFP-ASV (mini-Tn7 (Gm, gentamycin resistant) PrrnB P1 gfp.ASVa) (Lambertsen et al., 2004) was from A. Spiers. The bacteria were cultured in Luria–Bertani (LB) medium (Sambrook et al., 1989) with 1 mg L^{-1} gentamycin at 28 °C in a shaking incubator. Bacterial culture density was determined from the colony forming units (cfu) counted from LB plates, which were incubated at 28 °C for 48 hours before counting the colonies. The bacterial suspension used contained 6×10^7 cfu ml^{-1}.

5.2.2 Plant preparation

Lactuca sativa (lettuce, var. capitata, Seed Parade, UK) seeds were surface sterilised by washing in 10% bleach (Domestos, Unilever UK Ltd.) for 20 minutes followed by several sterile dH_2O washes. The seeds were sown in Petri dishes containing 7 g L^{-1} phytagel and half-strength (2.2 g L^{-1}) Murashige and Skoog (M&S) basal medium (both from Sigma) for pre-germination one day prior to transfer to transparent media.

5.2.3 Sample set up

16 samples were set up as summarised in Table 5.1. 3D slides were constructed as previously described (Section 3.2.6.1, Page 59) and were used as sample containers. Transparent soil with two different anionic Nafion particle size ranges (500–850 and 850–1200 µm) were prepared as described in Section 3.2.1, Page 53.

Prior to transferring the transparent soil to 3D slides, the substrate was saturated with dH_2O and autoclaved. The water that could be poured off was removed and replaced with sterile half-strength M&S medium and mixed. This was repeated twice so that the liquid in the pore spaces contained plant nutrients. The liquid occupying larger pores was removed using a 3 ml sterile Pasteur pipette to achieve an approximate gravimetric water content of 35% (verified by weighing the samples).

Per gram of transparent soil (in working state, i.e. not saturated and not dry), 50 µl of

Nafion particle size range (µm)	Plant status	Number of replicates
500 – 850 (A)	Present	4
500 – 850 (A)	Absent	4
850 – 1200 (B)	Present	4
850 – 1200 (B)	Absent	4

Table 5.1. Summary of sample set up for experiment comparing bacterial distribution under different conditions.

bacterial suspension in LB medium was added and then mixed to evenly distribute the bacteria. The transparent soil was then added to the 3D slides and compacted by tapping the slide on the bench. One pre-germinated seedling was added to the transparent soil in each sample using a pair of forceps. The substrate part of the samples were then covered in aluminium foil and placed in a growth room at 20 °C with 16 hours light: 8 hours darkness.

Imaging was carried out after 5 days and on the day before imaging, all samples were saturated with a half-strength M&S medium containing 1 mg ml^{-1} fluorescent brightener (calcofluor) (Sigma) in order to stain the root tissue. Immediately before imaging, this solution was removed and replaced with pure Percoll (Sigma) containing 1 μg ml^{-1} sulphorhodamine B (Sigma). The Percoll was for RI matching with the Nafion particles and the sulphorhodamine B was for staining the surface of the particles.

5.2.4 Image acquisition

Images were taken with a Leica TCS SP2 confocal laser scanning microscope using a 20× / 0.50 n.a. water dipping objective lens so that the whole diameter of the roots could be captured in an image. Imaging was carried out at a resolution of 1849 pixels mm^{-2}. The same laser intensity and gain settings (gain = 600) were maintained for GFP acquisition. GFP fluorescence was excited by illumination with the 488 nm wavelength line of an argon laser and detected between 500 and 530 nm. 2 × line averaging was used. In some cases, high resolution imaging of the root surface was carried out using a 63× / 0.90 n.a. water dipping objective lens.

In each sample, 27 points, distributed in 3D, were sampled by imaging. This meant that the effect of position along the root and perpendicular to the root could be quantified. In samples with plants present, the root tip was located using the bright field settings on the confocal microscope and 3 images were acquired at this position (labelled R1,Figure 5.1), where the first image represented the upper surface of the root, and the last image was 90 μm further down in the Z direction, with one image taken in between (Figure 5.1,B). This procedure was repeated at each of the sampling points shown in Figure 5.1. In samples with no plants, the same imaging sample points were used as in the samples with plants. Position R1 was chosen to mimic the approximate area where the root tips were in samples with plants (Figure 5.1).

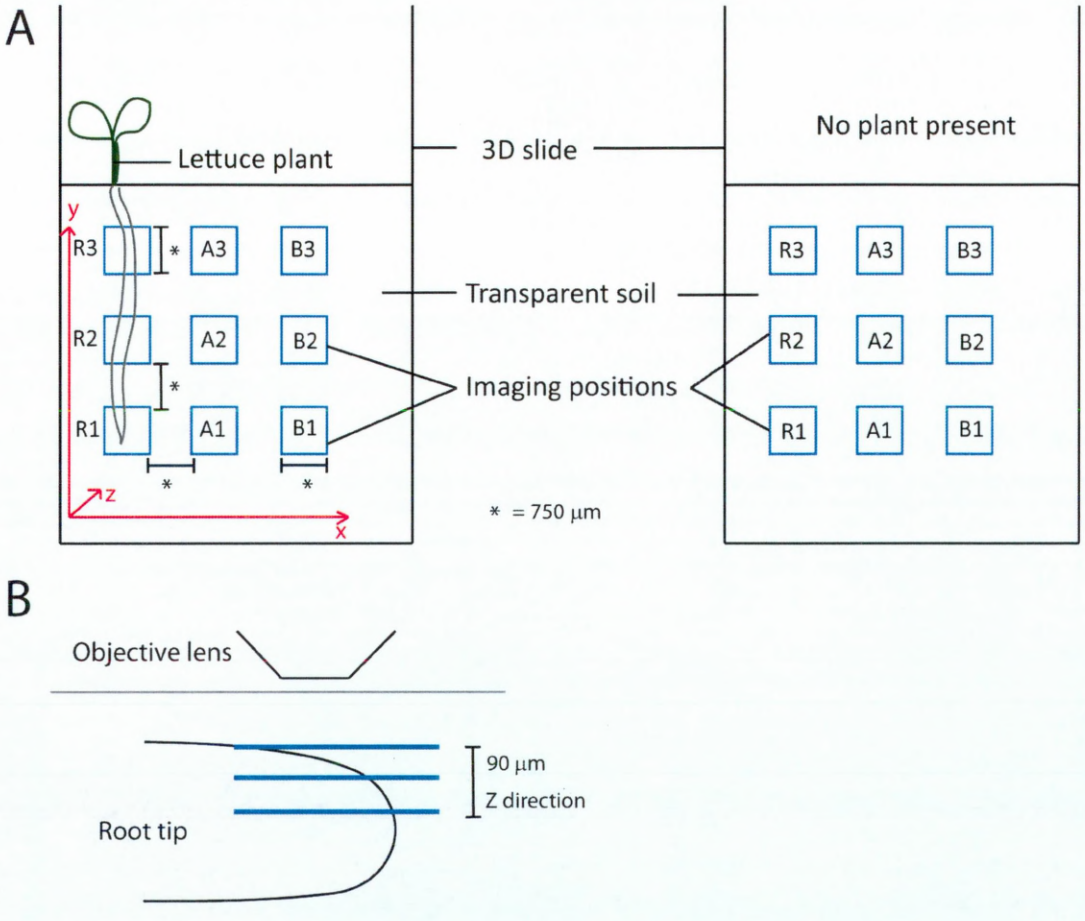

Figure 5.1. Diagram representing spatial distribution of points where images were acquired. A) Distribution of points in X (horizontal) and Y (vertical) directions on samples with and without plants. The naming convention for the sampling positions is also shown (R1, A1, etc.). B) At each point shown in (A), 3 images were taken in the Z direction to a depth of 90 µm from the first image.

5.2.5 Biomass measurement

After imaging, the plants were removed from the transparent soil by gently pulling and then rinsing with water to remove remaining Nafion particles. The roots were separated from the shoots using sharp forceps. Roots and shoot were placed in individual 2 ml Eppendorf tubes which were pierced in the lid to avoid the tubes opening during autoclaving. The samples were autoclaved for decontamination for 20 minutes at 121 °C and then placed in a drying oven for 72 hours at 60 °C. The samples were then weighed on a Sartorius micro balance and the dry mass for each root and shoot was recorded.

5.2.6 Image processing and analysis

5.2.6.1 *Quantifying bacterial abundance*

GFP expression from the bacteria was captured during imaging (Figure 5.2, A & B) and a number of steps were taken to process these images for consistent quantification. Firstly, the images were despeckled in order to remove background noise. The despeckle function is a median filter which replaces each pixel with the median value of its 9 × 9 pixel neighbourhood (Figure 5.2, C). A fixed threshold (min. 14, max. 255) was then applied to the image resulting in a binary image with multiple separate groups of individual white pixels representing the fluorescence from bacterial aggregates (Figure 5.2, D). In order to quantify these aggregates, these groups of pixels were selected. The images were automatically scanned to find white pixels and an edge tracking algorithm was used to find neighbouring adjacent white pixels until the perimeter of a group was delineated (Figure 5.2, E). This was carried out for the whole image, which enabled

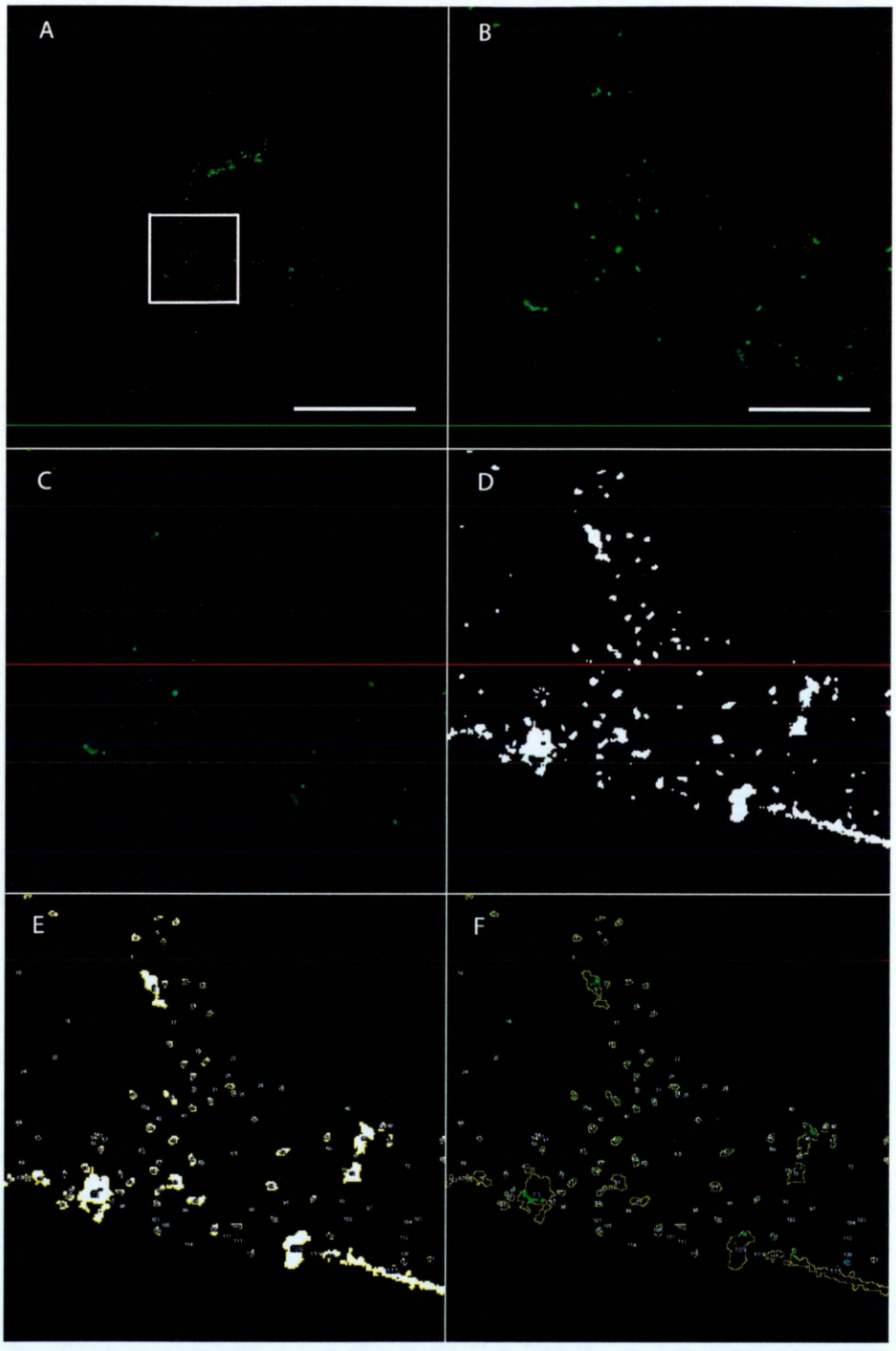

Figure 5.2. Image analysis steps taken in order to analyse and quantify bacterial GFP expression. A) Example of original confocal image from the GFP channel. Scale bar represents 200 µm. B) Magnification of image (A) (white window). Scale bar represents 40 µm. C) Image after despeckle filter has been applied. D) Binary thresholded image – fluorescent aggregates are shown in white. E) Areas where P. fluorescens *were detected. Outlines of fluorescent bacterial aggregates are in yellow. F) Outline of units has been overlaid on the unprocessed original image.*

a number of measurements to be carried out. The measurements were number of fluorescent bacterial aggregates per image, average aggregate size and area occupied by bacterial fluorescence. Individual bacterial cells could not be resolved from the images and counted and therefore the measurements were based on the number of pixels with significant GFP fluorescence, which was not adjusted for cell numbers.

5.2.6.2 *Correcting results for available area*

The vast majority of images analysed had volumes where bacterial occupation was not possible. These areas were either inside Nafion particles or inside roots. The fraction of the images that were unavailable for the bacteria was highly variable and so the area was quantified and an available volume correction was applied to all of the bacteria quantification data (Figure 5.3). To make an estimation of the area inside Nafion particles, images of sulphorhodamine B on the particles' surface were used. Firstly a fixed threshold was applied (min. 25, max. 255) followed by the despeckle filter. Further noise reduction was applied using a median filter where a pixel value was replaced if it deviated from the neighbourhood median by more than the threshold value. In this case, the settings were median = 5, threshold = 50 (Figure 5.3, B). A skeletonisation of the binary image was then applied where the objects in the image are thinned until they are 1 pixel in width. The image was then inverted (Figure 5.3, C) so that the regions inside the Nafion particles could be selected using a magic wand, where a region around

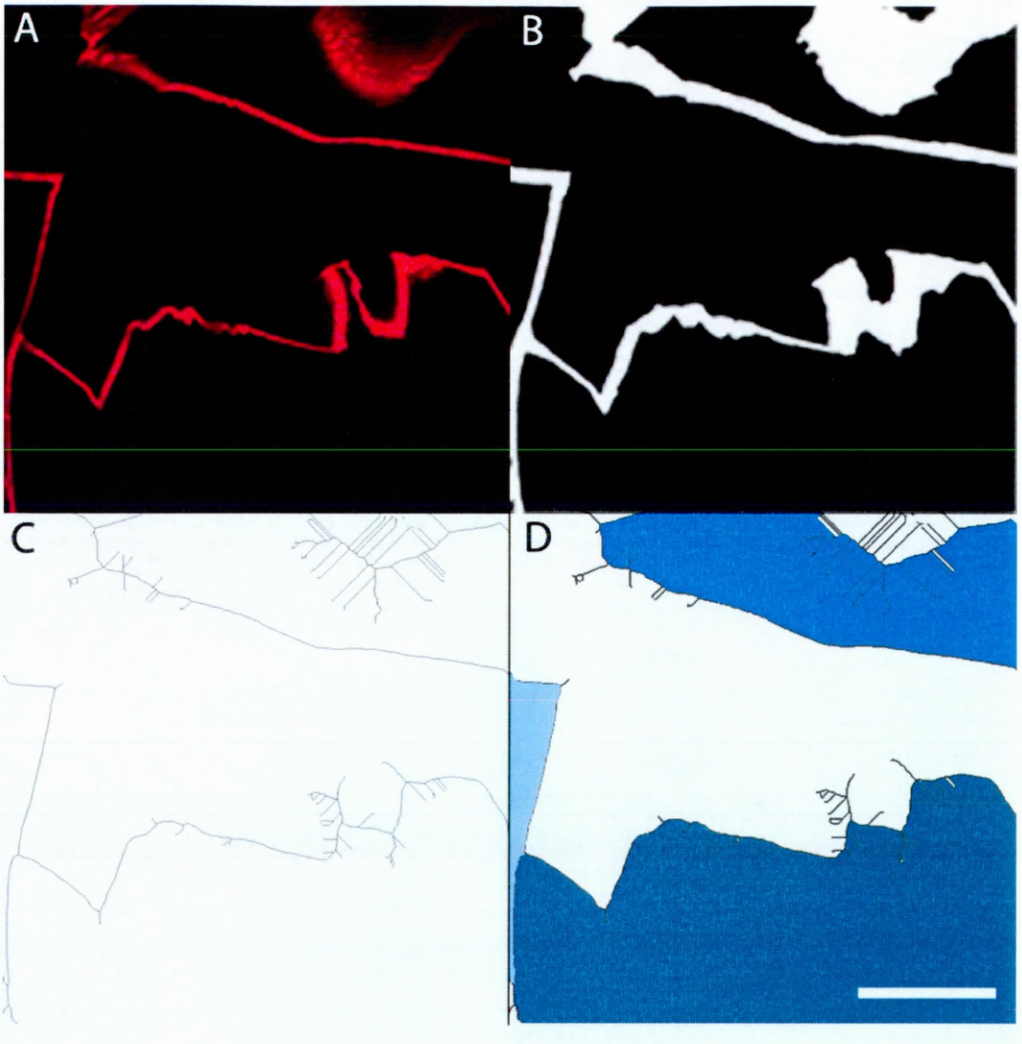

Figure 5.3. Method for estimation of the volumes of the image where bacteria could not be detected. A) Original confocal image of Nafion particles stained with sulphorhodamine B. B) Transformed image after processing by thresholding, despeckling and application of a median filter. C) Inverted skeleton of the thresholded image. D) Selection of areas of the image occupied by Nafion particles. Here three shades of blue are used to represent the areas occupied by the particles. Scale bar represents 200 µm.

a given position is flooded until no pixels with the same value are found at the edge of that region and these areas were then measured (Figure 5.3, C).

In some cases, images also included root sections and so areas inside roots occupied a proportion of the image. Similarly to the inside of particles, it was assumed that these volumes could not contain bacteria and so they were manually selected by creating a polygon which occupied the internal part of the root, and the areas were measured.

Once the areas inside particles and roots were measured for each image, the fraction of the image occupies by bacterial fluorescence was calculated using the following equation:

$$x = \frac{N}{A}$$

where N = original measurement of bacterial fluorescence and A = area of the image which is available for bacteria (%).

5.2.6.3 *Measuring the perimeter of Nafion particles*

To measure the perimeter of the Nafion particles, the thresholded images produced as described in section 5.2.6.2 were used. In a second step, a series of morphological erosions, where white pixels were turned to black when pixels in a neighbourhood were black, was applied to the image in order to reduce the thickness of the particle perimeters. Erosion was stopped before the edges were being disconnected. A Gaussian filter was then applied, and the image was inverted. The areas of high pixel intensity

were then identified using the same method as in 5.2.6.1. The perimeter (including both internal and external edges) of these areas is then halved to find an estimation of the particle perimeter.

5.2.7 Image analysis software

All image analysis was carried out using the open source software FIJI (Schindelin et al., 2012). The specific functions used were "analyse particles" for measuring bacterial abundance and Nafion particle perimeter length. The despeckle function was used for removing noise from images. The median filter "remove outliers" was used and the "skeletonise" function was also used as described in section 5.2.6.2, page 130.

5.2.8 Statistical analyses

For all analyses, the 3 images taken in the Z direction at each position (Figure 5.1, B) were treated as replicates of the XY position because of the small Z distance (90 μm) between each image. Means and standard errors were calculated using SigmaPlot 12.3 (Systat Software Ltd.). This program was also used to perform the linear regression analysis between particle perimeter length and bacterial aggregate number.

Further statistical analyses were performed in Genstat, 14th edition (VSN International Ltd.). The data on number of fluorescent aggregates, average aggregate size and percentage area of image occupied by bacterial aggregates were corrected for available volume and square root transformed for statistical analysis. A general analysis of variance (ANOVA) was used to analyse the effect of the particle size and the presence of plants on the number of fluorescent aggregates, average aggregate size and percentage

area of image occupied by bacterial aggregates at each of the 9 XY positions. The blocking structure was set up in order to create levels where the Z position was a pseudo-replicate of the variate, which was the XY position. The fact that images were taken from different samples was also accounted for. Nafion particle size and whether or not there was a plant present in the sample were independent factors. A general analysis of variance was also used to analyse the effect of the imaging position along the X and Y directions on the number of aggregates, average aggregate size and the percentage area of the image occupied by bacterial fluorescence. In this case, the blocking structure was altered so that X position and Y position were considered as factors independently but otherwise, the blocking structure was the same. Post-hoc Fisher's least significant difference (LSD) tests were applied after analyses of variance to provide means ranking.

5.3 Results

The soil bacterium, *Pseudomonas fluorescens*, survived in transparent soil for a number of days and images were successfully acquired from each sample at each position (Figure 5.1). Fluorescence from the fluorescent brightener staining of the roots, sulphorhodamine B staining of the surface of the Nafion particles and GFP expression from the *Pseudomonas fluorescens* bacteria were captured on separate channels, which could be overlaid to visualise the distribution of roots, Nafion particles and bacteria (Figure 5.4). Dry weights of the roots and shoots of the plants used in the experiment were measured and the mean root dry weight of samples grown with small particles

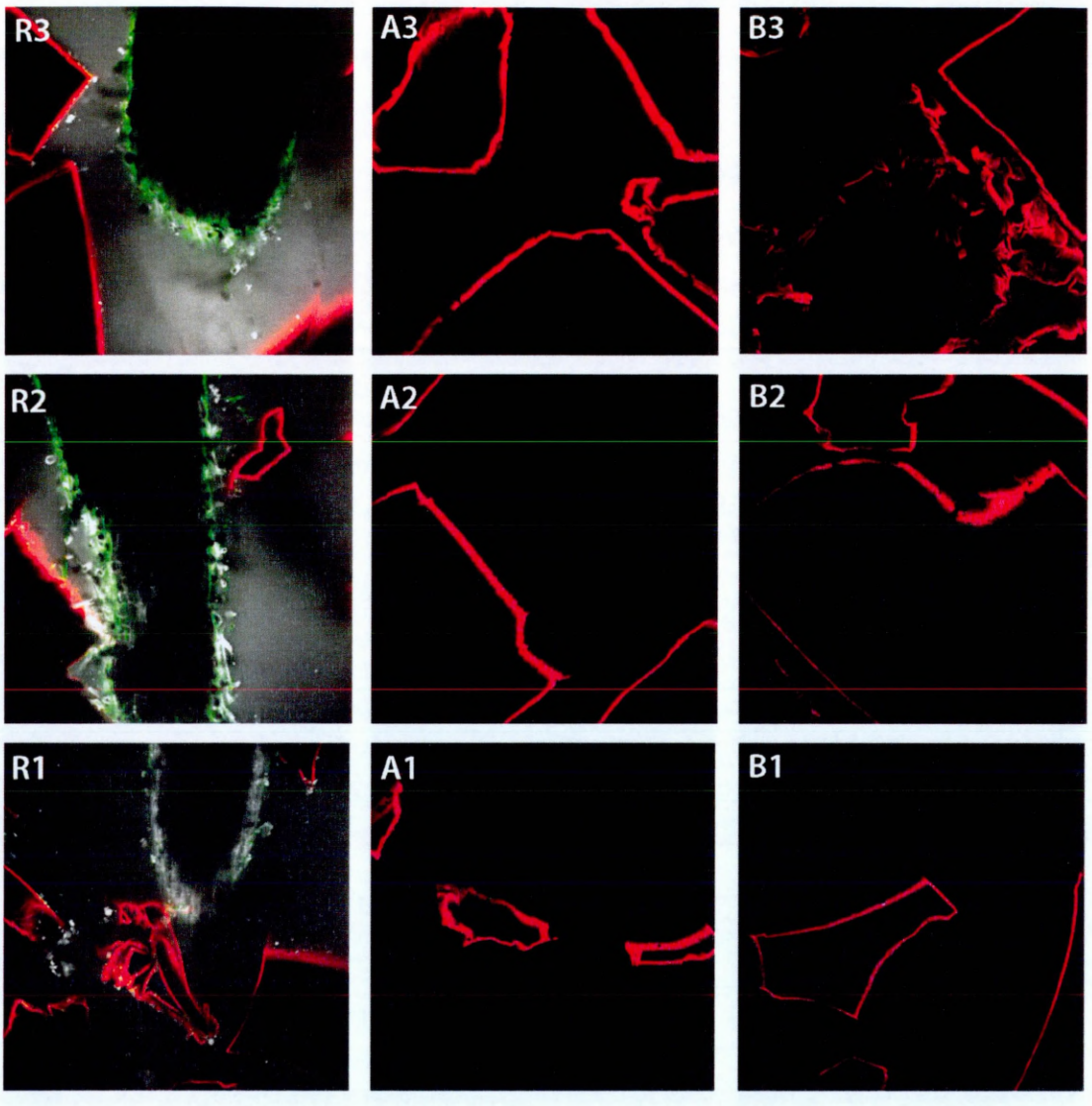

Figure 5.4. Examples of the confocal images taken at each position for one sample with a lettuce plant and small particles. Each image shows a merged image of the channels used. At positions R1, R2 and R3, calcofluor staining on the surface of the root is shown in light grey, GFP detection from P. fluorescens *is shown in green and sulphorhodamine B staining of the Nafion particles is shown in red. At each of the other positions, there was no detection of calcofluor staining but again, the GFP detection from* P. fluorescens *is shown in green and sulphorhodamine B staining of the Nafion particles is shown in red.*

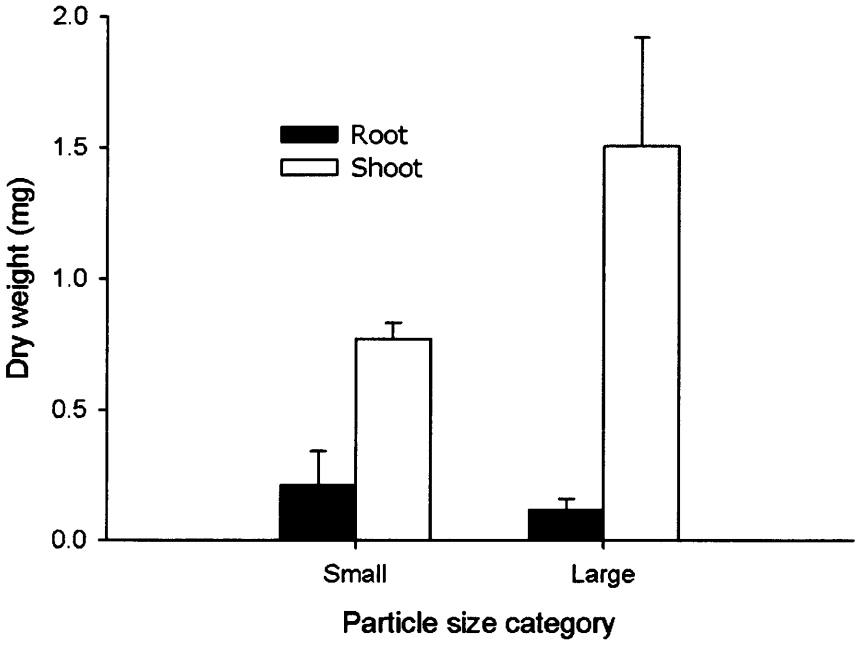

Figure 5.5. Root and shoot dry weights of plants grown in small and large particle size categories. There was no significant difference in root or shoot dry weight between the treatments. n = 4 for each particle size category. Error bars signify standard error.

was not significantly different from the mean root dry weight of plants grown in large particles (overall mean = 0.16 mg, p = 0.512). The mean shoot dry weight was not significantly different in plants grown in large particles from shoot dry weight in plants grown in small particles (overall mean = 1.14 mg, p = 0.130) (Figure 5.5).

5.3.1 Comparative analysis between XY positions

The mean number of aggregates, the mean size of aggregates and the mean area of image occupied by bacterial fluorescence were measured for each 559504 μm^2 image. All measures were significantly higher in samples where a plant was present, at

positions R1, R2 and R3 than in control samples with no plant present and in samples with plants at all A and B positions. Particle size had no significant effect on any of the measures of bacterial distribution at any of the positions (Figures 5.6, 5.7 and 5.8 and Tables 5.2, 5.3 and 5.4). The highest mean for all 3 of the measures of bacterial abundance was at position R2 (1250 µm from the root tip) in samples with plants and large Nafion particles. There was also a consistent pattern through all of the

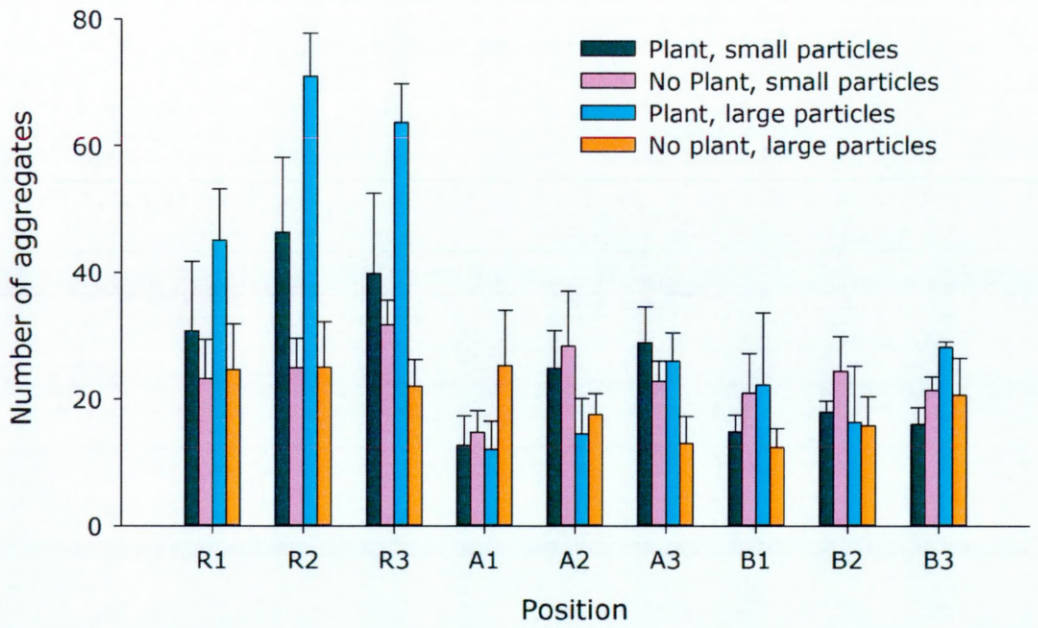

Figure 5.6. Mean number of bacterial aggregates present in the images at each position in samples with plants and small particles, with no plants and small particles, with plants and large particles and with no plants and large particles. The data has been square root transformed and error bars show standard error.

measurements at positions R1, R2 and R3 where the mean was higher in plant samples with large particles than in plant samples with small particles, although the differences were not statistically significant. This pattern does not exist in the no-plant controls.

Position	Particle size	Presence of plant
R1	0.835	0.024
R2	0.174	0.004
R3	0.49	0.016
A1	0.298	0.121
A2	0.106	0.594
A3	0.421	0.234
B1	0.932	0.783
B2	0.423	0.638
B3	0.599	0.507

Table 5.2. Resulting p values from analysis of variance of the effect of particle size and presence of plant on the number of aggregates at each position. Presence of plant had a significant effect on number of aggregates at positions R1, R2 and R3. These p values are shown in red.

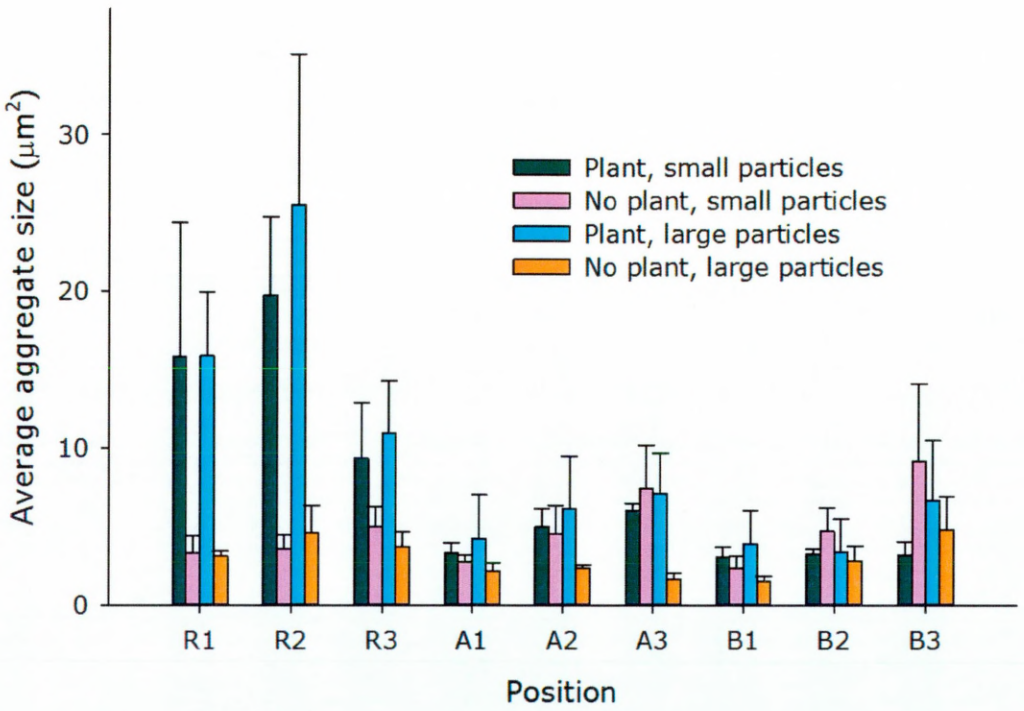

Figure 5.7. Mean average size of bacterial aggregate present in the images at each position in samples with plants and small particles, with no plants and small particles, with plants and large particles and with no plants and large particles. Error bars show standard error.

Position	Particle size	Presence of plant
R1	0.951	0.003
R2	0.718	0.003
R3	0.913	0.02
A1	0.663	0.635
A2	0.607	0.201
A3	0.124	0.187
B1	0.614	0.428
B2	0.355	0.68
B3	0.781	0.409

Table 5.3. Resulting p values from analysis of variance of the effect of particle size and presence of plant on the average size of aggregates at each position. Presence of plant had a significant effect on number of aggregates at positions R1, R2 and R3. These p values are shown in red.

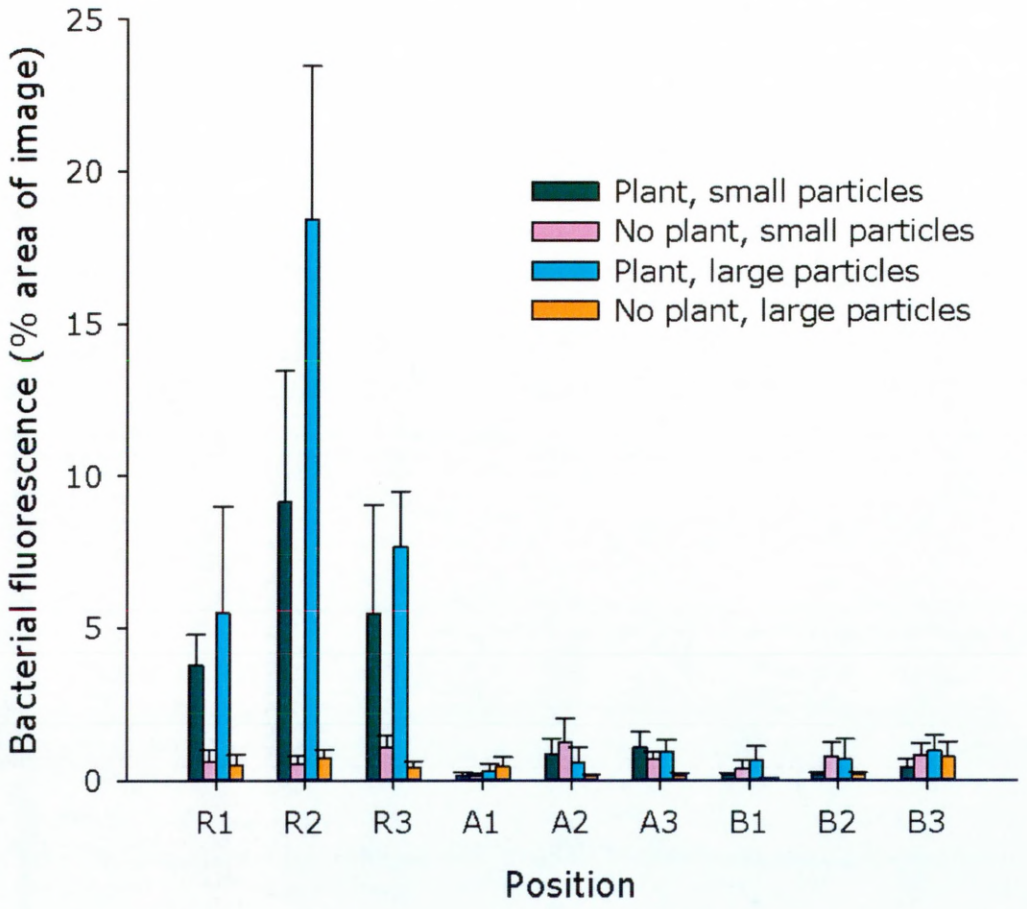

Figure 5.8. Mean area occupied by aggregates classed as bacterial fluorescence in the images at each position in samples with plants and small particles, with no plants and small particles, with plants and large particles and with no plants and large particles. Error bars show standard error.

Position	Particle size	Presence of plant
R1	0.591	0.004
R2	0.202	<0.001
R3	0.694	0.01
A1	0.398	0.579
A2	0.174	0.936
A3	0.195	0.091
B1	0.96	0.441
B2	0.563	0.748
B3	0.843	0.626

Table 5.4. Resulting p values from analysis of variance of the effect of particle size and presence of plant on the % of the image classed as bacterial fluorescence at each position. Presence of plant had a significant effect on the number of aggregates at positions R1, R2 and R3. These p values are shown in red.

5.3.2 **Analysis comparing X and Y directions**

To examine the difference in bacterial density along the X direction (distance from root), and Y direction (distance from root tip), data on the number of aggregates, average size of bacterial aggregate and the area of image occupied by bacterial fluorescence were plotted depending on X position or Y position (Figure 5.9). A general ANOVA showed

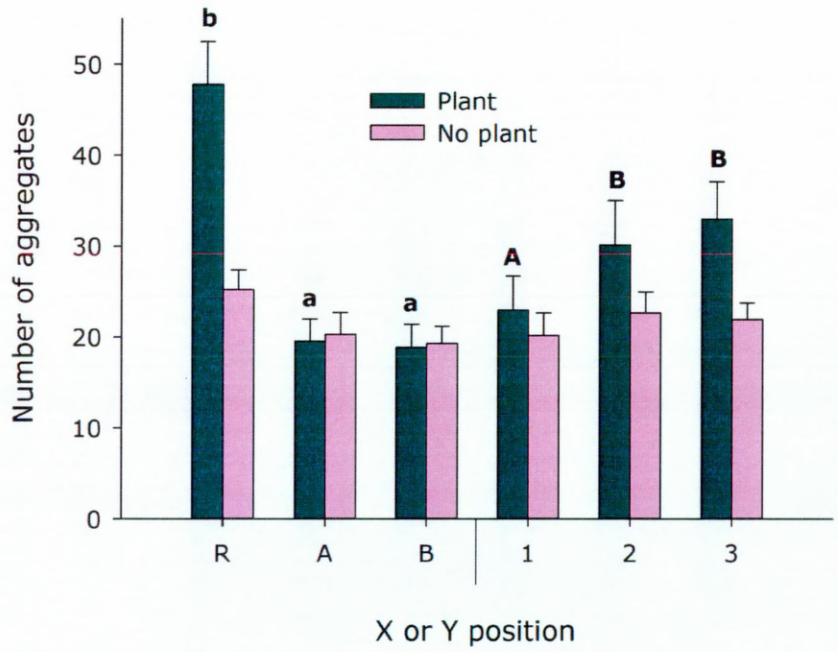

Figure 5.9. Overall mean number of aggregates (square root transformed) at X positions (R, A and B) and Y positions (1, 2 and 3) where there were plants or no plants. Letters above the error bars show the results of a Fisher's protected least significant difference (LSD) tests on the data where there was a significant difference in the means. Lower and upper case letters signify different tests. Error bars signify standard error.

that for the number of aggregates, there was a significant difference between the X positions in samples with plants ($F_{2,200}$=51.18, p<0.001) and the post-hoc Fisher's protected least significant difference (LSD) test confirmed that the images that included the root (position R) had approximately a 6 times higher mean number of aggregates than the non-root images (positions A and B). There was no significant difference in the mean number of aggregates between the non-root positions (A and B) in the presence of plants, despite the difference in proximity to the root in these two imaging positions (Figure 5.1). There was a significant difference in the number of aggregates when the plant was present across the Y positions ($F_{2,200}$=4.88, p=0.012). The post-hoc Fisher's protected LSD test showed that there were significantly less aggregates at position 1 (the root tip) than at positions 2 and 3, between which there was no significant difference (Figure 5.9). There were no significant differences in the number of aggregates in samples with no plants in either of the directions.

Similar patterns were observed in the measurements of average size of aggregate and area occupied by bacterial fluorescence. In both cases, in the X direction, the mean result for position R (on the root) when the plant was present was significantly higher than at positions A and B (average size: $F_{2,197}$=38.18, p<0.001, Figure 5.10, area: $F_{2,200}$=64.02, p<0.001, Figure 5.11). There was no significant difference in average size or area along the X direction in samples without plants, but in these control samples, there was a significant difference in the average size of aggregates along the Y direction (Figure 5.11). The aggregate size was significantly smaller at position 1 (closer to the root tip) than at position 3 (closer to the root base) and the aggregate size at position 2

was not significantly different from that at position 1 or 3. This was not the case in samples with a plant, where there was no significant difference in aggregate size along the Y direction.

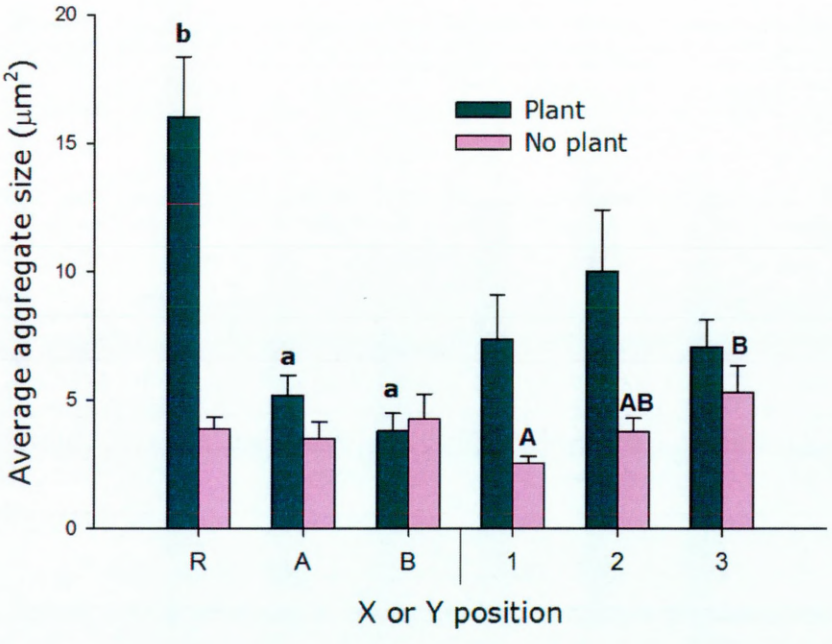

Figure 5.10. Overall mean average size of aggregates at X positions (R, A and B) and Y positions (1, 2 and 3) where there were plants or no plants. Letters above the error bars show the results of a Fisher's protected LSD test on the data where there was a significant difference in the means. Lower and upper case letters signify different tests. Error bars signify standard error.

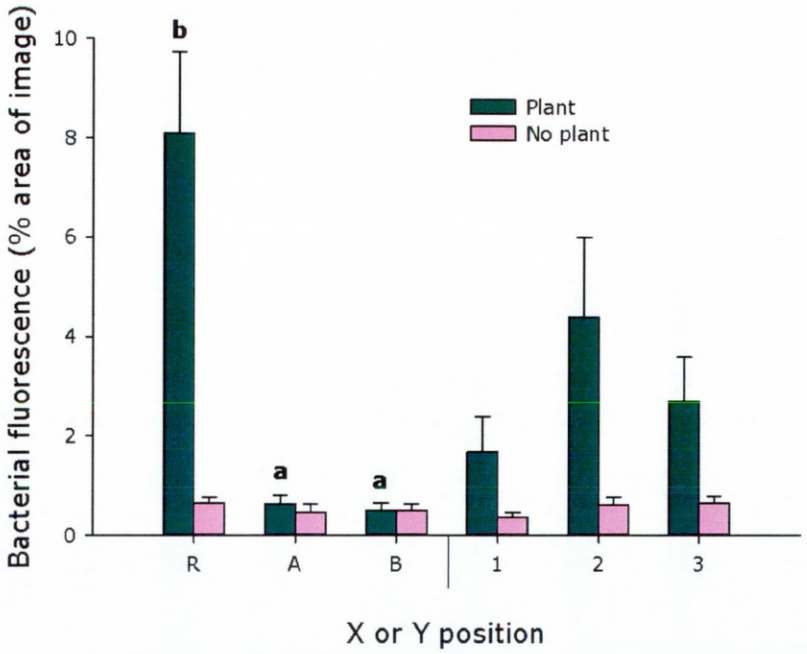

Figure 5.11. Overall mean area of bacterial fluorescence at X positions (R, A and B) and Y positions (1, 2 and 3) where there are plants or no plants. Letters above the error bars show the results of a Fisher's protected LSD test on the data where there was a significant difference in the means. Error bars signify standard error.

5.3.3 Relationship between particle perimeter length and bacterial abundance

On the micro scale, it seemed that there were a high number of bacterial aggregates closely associated with surfaces of Nafion particles compared with the pore spaces and in the images analysed, there was variation in the amount of particle surface that was included. To examine whether the amount of particle surface in the image could affect the measurements of bacterial abundance, the total perimeter of the particles was measured in each image at the A and B positions (page 132) and the results were

plotted. There was a positive correlation between the particle perimeter length and the number of bacterial aggregates ($r^2 = 0.270$, $p < 0.001$, Figure 5.12). There were no strong correlations for the other bacterial measures (i.e. aggregate size and area of image occupied).

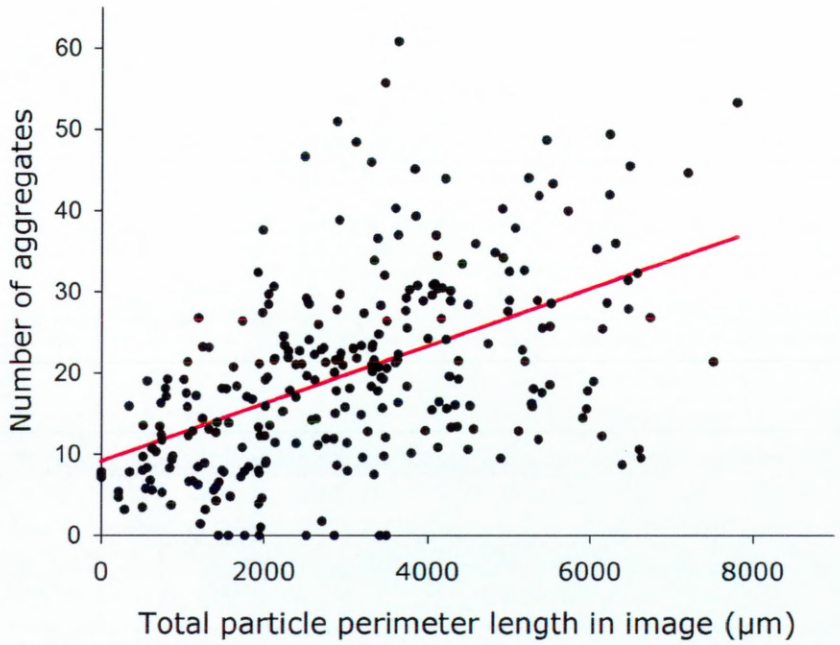

Figure 5.12. Scatter plot showing relationship between the number of bacterial aggregates recorded in an image and the total length of the perimeter of the Nafion particles in that image. The red line shows the result of a linear regression where $r^2 = 0.270$. The data on aggregate number have been square root transformed.

5.3.4 **Root colonisation pattern**

There was no significant difference in the area occupied by bacterial fluorescence at the 3 positions imaged along the root in small particles ($F_{2,32}$=1.55, p=0.3) or in large particles ($F_{2,29}$=1.64, p=0.3), (Figure 5.13). 3D images of the root surfaces with bacterial colonisation were captured at high resolution (Figure 5.14). In some cases, it was clear that the density of bacteria was higher in the junctions between epidermal cells than on the rest of the root surface (Figure 5.14, A). In other cases the distribution was more diffuse and it was more difficult to observe a relation between the root anatomy and the distribution of *P. fluorescens* on the root epidermis (Figure 5.14, B-C). In one other case, the epidermis appeared to be damaged because the root cells were not aligned in a uniform pattern as usual and some cells were not visible (Figure 5.14, D). Some of the cells appeared to be occupied by bacteria.

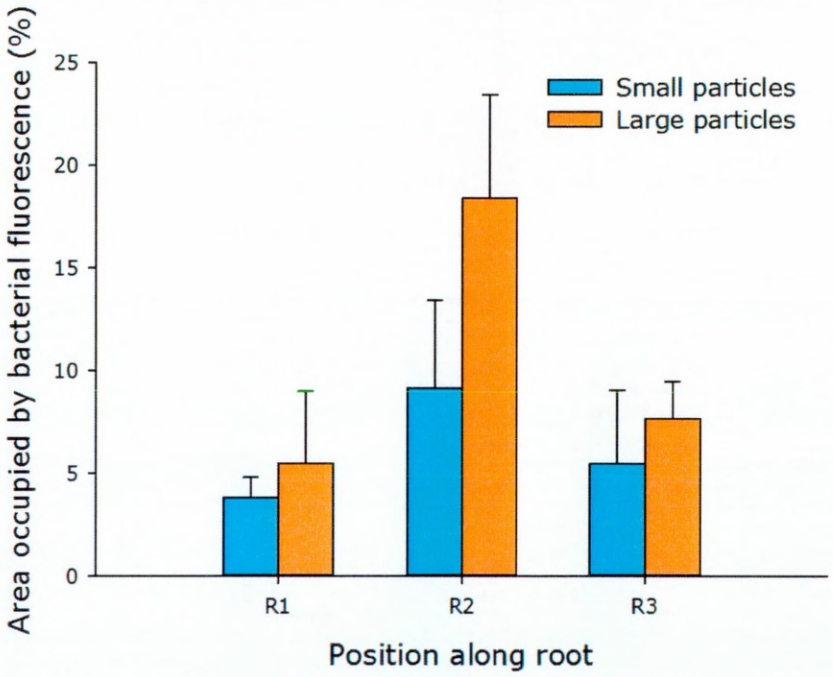

Figure 5.13. Mean area occupied by bacterial fluorescence at positions along the root.

Only images that included a root were considered. Error bars signify standard error.

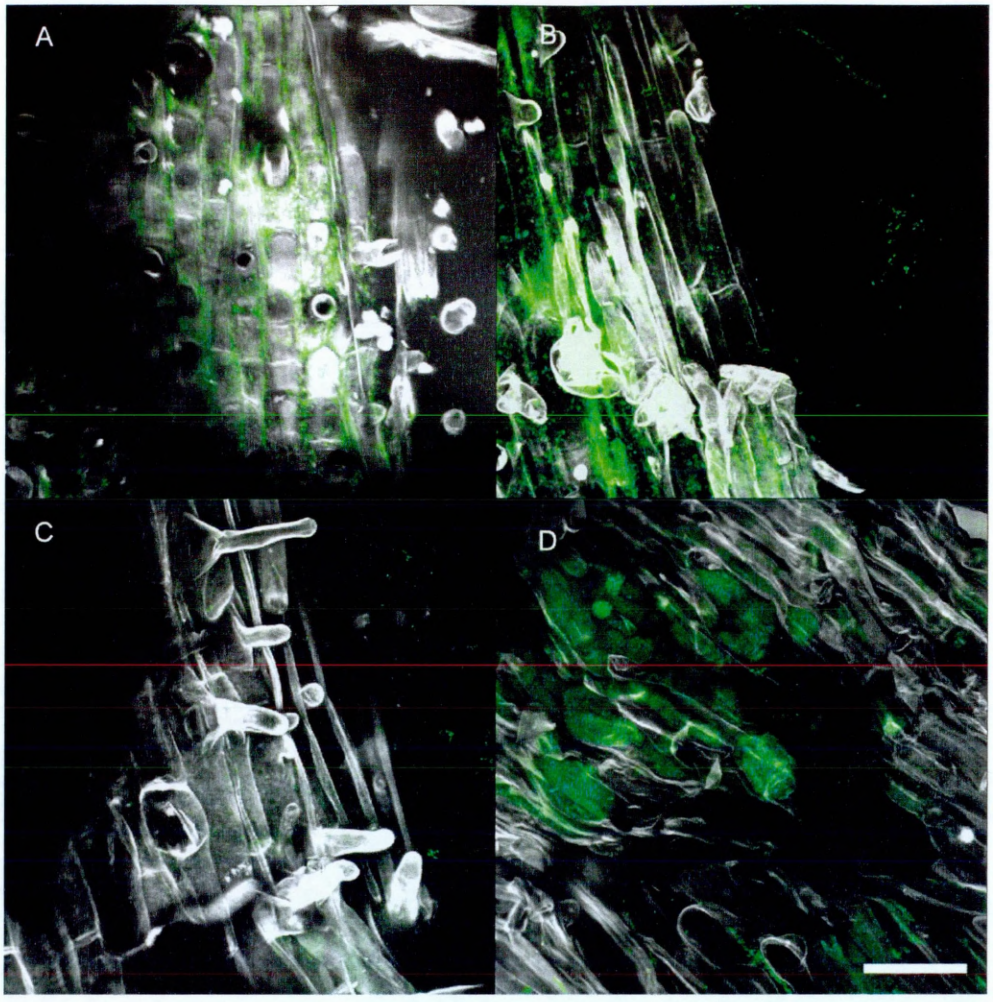

Figure 5.14. Maximum projection images of high resolution scans of lettuce roots (grey) with GFP expressing P. fluorescens *(green). A–B) The bacterial density is highest in the junctions between the epidermal cells of the root. C) Bacterial flocks are visible in the liquid surrounding the root. D) The root epidermal cells appear to be damaged, and there are bacteria occupying spaces below the surface of the root, perhaps where the epidermal cells have ruptured. Scale bar represents 50 µm.*

5.4 Discussion

5.4.1 A new system for imaging the interaction between *P. fluorescens* and lettuce roots

The transparent soil system has allowed the quantification of bacterial abundance on and around lettuce roots by image sampling a volume of the complex substrate. This has allowed analysis of the bacterial distribution along the roots, and at varying distances from the roots. It has also been possible to image the boundaries of the Nafion particles in the substrate in order to quantify the volumes where bacterial colonisation was not possible. It was difficult to incorporate an absolute measurement of bacterial cell count because individual cells could not be resolved using the microscope setup used. However, by using a higher power objective lens this would be possible or by using a microscopy technique other than confocal microscopy where very high resolution is also achievable.

It is also possible that the saturation of the substrate on the day before imaging for staining the root tissue, followed by the replacement of the liquid immediately before imaging for RI matching would disturb the bacteria, particularly those which are not attached to roots or other surfaces. The saturation procedure for the transparent soil could be improved to minimise this effect, however it is noteworthy that this disturbance is mild in comparison to the treatment of roots and bacteria in preparation for other imaging methods, such as the fluorescence in situ hybridisation (FISH) technique where the roots are extracted, washed several times and fixed before imaging (Buddrus-Schiemann et al., 2010).

5.4.2 Influence of particle size on bacterial distribution along the roots

There were consistently a higher mean number of aggregates, a greater mean area occupied by bacterial fluorescence and a larger mean bacterial aggregates size found on the roots of plants grown in transparent soil with large particle sizes (850–1200 μm) than with smaller particle sizes (500–850 μm), although the difference was not statistically significant (Figures 5.6, 5.7 & 5.8). Motility in *P. fluorescens* has been shown to play an important role in movement towards and along roots (Toyota & Ikeda, 1997) and it has been found that substrate pore size has an effect on the motility of *P. fluorescens*, where larger continuous pores allowed faster swimming speeds (Singh et al., 2002). This effect could have occurred in the transparent soil samples studied here, where effectively the chemoattractant from the roots may have diffused through the substrate with large particles (and therefore large pore spaces) more quickly than in the samples with small particles (and therefore small pore spaces), initiating the movement of the bacteria from the substrate to the roots more quickly, resulting in a higher level of colonisation along the roots in samples with large particles than in small particle samples. It is also possible that, rather than bacteria moving towards the roots, the bacteria adjacent to the root surface had a faster growth rate and divided more than the bacteria in the other sample points. These hypotheses would require further experimental testing with a greater number of samples in order to be conclusive.

5.4.3 Spatial distribution of bacteria

The clearest result from this experiment was that there were always more bacteria in images that included root sections than in the remaining images where no root was

present. This was not surprising as *Pseudomonas fluorescens* is well known to be a plant growth promoting rhizobacterium (PGPR) (e.g. Urashima & Hori, 2003, Dey et al., 2004, Jaleel et al., 2007, Abbas-Zadeh et al., 2010) and bacteria from the genus *Pseudomonas* are generally more abundant in the rhizosphere than in the bulk soil (Sørensen & Sessitsch, 2007). This was reflected in the results from all of the measurements of bacterial abundance, where the only significant differences between samples with or without plants were in the root sections and there was no significant difference at any of the sampling positions adjacent to the root. This showed that the presence of a plant in the sample did not have an effect on the abundance of *P. fluorescens* over the entire spatial range measured, but only if there was greater bacterial abundance in the immediate vicinity of the root. Qualitative assessments of the images captured of the roots (Figure 5.4) indicated that there was a high gradient of bacterial fluorescence adjacent to the roots which lessened with distance from the root. It seems that the distances between the image points was too large to capture this gradient and at the sampling positions in samples with a plant, there was an equivalent level of bacterial abundance to when no plant was present.

The spatial distribution of *P. fluorescens* outside the rhizosphere and in the bulk soil has not been well described. In this experiment, it was found that the position along the Y axis (i.e. distance from the surface) affected the average bacterial aggregate size measured (Figure 5.10), where the position furthest from the surface of the substrate had the smallest aggregate sizes, the position closest to the substrate surface had the largest aggregate sizes and in the position between these two, the aggregate size was

intermediate in samples where no plant was present. These differences could reflect a difference in oxygen availability where it is likely that more oxygen was available closer to the surface of the substrate, and therefore further from the surface the availability of oxygen could have been limiting the size of the aggregates.

In the soil, bacteria inhabit niches on the surface of soil particles (Standing & Killham, 2007) and the *P. fluorescens* bacteria in transparent soil were most often found on or adjacent to the surface of the particles which could explain the fairly weak correlation between the number of bacterial aggregates and the length of particle perimeter in the image (Figure 5.12). There was no notable correlation between Nafion perimeter and the average colony size or the total area occupied by bacterial fluorescence. This means that most of the variation in the data cannot be explained by the differences in particle surface area between the images but rather most of the variation is likely to be stochastic.

5.4.4 Bacterial distribution along the roots

Previous studies have reported scarce or no *Pseudomonas* colonisation on the root tips of inoculated plants (Kragelund & Nybroe, 1996, Simons et al., 1996, Gamalero et al., 2005, Humphris et al., 2005). On the contrary, Darwent et al. (2003) and Paterson et al. (2006) showed that the bioluminescent activity of *Pseudomonas fluorescens* was highest around root tips and in the experiment presented in this Chapter, there is clearly bacterial fluorescence present at the root tips and there was no difference in abundance across the root sections (Figures 5.4 & 5.13). There are two potential ways in which this

discrepancy could have occurred. Firstly, in the studies where no colonisation at the root tips was recorded, the inoculation was carried out on the seed (Kragelund & Nybroe, 1996), the germinated seed (Simons et al., 1996) or the seedling (Gamalero et al., 2005), whereas in the cases where bacteria were found at the root tip, the soil or substrate was inoculated. Another factor that can explain these differences is the procedure to prepare the root sample for quantification of bacteria. In some cases this involved washing steps (Kragelund & Nybroe, 1996, Gamalero et al., 2005) but in the studies where bacteria were found on the root tip, the imaging was carried out in situ. It is likely, therefore, that inoculation of the seed reduced colonisation of the root tip because the bacteria were moving down from the older parts of the root, rather than when the bacteria were colonising the root from the bulk soil. Washing steps for preparing the root for imaging may also have changed the quantity of bacteria that could be measured.

Peaks in bacterial colonisation have been observed along wheat roots between the root tip and base (Van Vuurde & Schippers, 1980) and van Bruggen et al. (2008) found a wave-like distribution of *Pseudomonas fluorescens* which may oscillate over time (van Bruggen et al., 2000) along the roots of wheat plants grown in soil inoculated with the bacteria where areas of high and low colonisation were observed at regular intervals. They used modelling techniques to show that this wave-like distribution could occur, and hypothesised that the distribution could theoretically be explained by predator–prey relations (van Bruggen et al., 2000). Although larger and older roots were used in the studies of van Bruggen et al. than the week-old plants observed here, the pattern in

colonisation that was observed along the roots could represent the beginning of a wave-like distribution (Figure 5.13). The transparent soil system could provide a useful tool for imaging the development of bacterial distribution along roots over time and in situ.

At the surface of the root, electron microscopy has been used to show that *Pseudomonas fluorescens* micro colonies inhabited the junctions in between epidermal cells, particularly near the base of the roots (Chin-A-Woeng et al., 1997). A similar distribution of bacteria between the epidermal cells has been observed in two cases here (Figure 5.14, A-B).

5.4.5 **Conclusion**

This Chapter presents the first scientific study where the 3D distribution of a live soil bacterium was quantified. It was found that there was a higher level of bacterial abundance along the roots than in volumes of the substrate surrounding the roots. There were also some interesting directional gradients revealed such as the size of bacterial aggregates along the Y direction (Figure 5.10) and the distribution of bacteria along the roots (Figure 5.13). These new insights were made possible by the development of a transparent soil that supports the growth and development of plants and soil organisms (Chapters 2 & 3). For future studies, it would be possible to conduct more detailed studies with improved replication to allow more robust statistical analyses.

Overall, this study represents an example of the kinds of analyses that are possible using transparent soil as a substrate in combination with 3D imaging techniques.

Increased understanding of plant–microbe interactions is of utmost importance in finding strategies to address the pressing issue of global food security and the application of transparent soil for 3D in situ imaging of these interactions represents a timely innovation that has the potential to uncover some of these opaque soil processes.

Chapter 6. Summary and Conclusions

6.1 Summary

To our knowledge, the method development (Chapter 2) and validation (Chapter 3) described in this thesis allowed the production of the first refractive index matched, transparent, heterogeneous substrate for imaging roots and soil microorganisms. The structural and chemical complexity of the transparent soil allowed replication of soil properties such as the triphasic structure and ion exchange, whilst allowing optical access to living organisms within the substrate. This enabled the application of optical imaging techniques such as OPT and CLSM. Fluorescent dyes were used to detect the surfaces of roots and of Nafion particles and facilitated distinction between them (Chapters 2 & 3, Downie et al., 2012). Lettuce plants were grown in transparent soil and the roots were imaged using OPT in order to quantify the root trajectories and how they varied under different substrate physical conditions (Chapter 4). The results showed that the roots displayed a wider range of curvatures when grown in substrates with larger particle sizes. Verticality varied with distance along the roots and the variation depended on the substrate, although there was an overall positive correlation showing that the roots were less vertical with distance from the root base. When the plants were grown in transparent soil with different levels of compaction, the curvature and verticality varied with distance along the roots. Transparent soil provided a complex structure which allowed movement of bacteria through aqueous networks, a process which occurs in soils (Camper et al., 1993, Singh et al., 2002, Spormann, 1999). It was

unsaturated for the growth period, promoting the survival of aerobic microorganisms. There was a higher density of *Pseudomonas fluorescens* bacteria present on roots than in the surrounding substrate, and there was a high density of bacteria in the root epidermal cell junctions.

6.2 A new approach for soil microscopy

Understanding of soil microbiology is extremely limited because of the paucity of dynamic data that describe interactions between microorganisms, soil particles and roots. Past studies have focused on cataloguing the complexity of microbial communities, and it is thought that new techniques for imaging will help to enable a systems approach for helping to relate microbial dynamics to soil function (O'Donnell et al., 2007). Further research could build on experimental systems developed in this thesis (e.g. Chapter 5) to better understand the dynamics of root bacteria interactions. For example, time lapse imaging could reveal the dynamics of the growth of bacterial microcolonies in relation to the root growth rate and cell expansion. New microscopy techniques such as selective plane illumination microscopy, would improve acquisition rate and lower the propensity for photo-damaging the sample (Huisken et al., 2004). For example, this could be used to allow tracking of bacterial cells, which would help to analyse the stages of root colonisation by bacteria with biocontrol properties.

Roots interact with many groups of microorganisms, including pathogenic bacteria and fungi, and also beneficial microorganisms which help provide nutrients to the plant or convey protection against pathogens. There is much to understand about these

interactions, and imaging in transparent soil could help with measuring, for example, the abundance of microorganisms associated with different plants, the exchange of proteins between plants and microorganisms (De-la-Pena & Vivanco, 2010), competition between groups of microorganisms (de Boer et al., 2005) and symbiotic root–bacteria associations such as nodule formation for N fixation by bacteria which can then be taken up by the plant (Garg & Geetanjali, 2007). Arbuscular mycorrhizal fungi associate with plant roots and can help plants to take up nutrients from the soil by exploring a larger volume of soil than the root system itself (Koide, 1991). Not much is known about the geometry of the fungal hyphae in situ and how their prevalence is affected by soil physical factors (Piotrowski & Rillig, 2008). Transparent soil could be combined with new techniques such as imaging of nanoparticle quantum dots to track organic nitrogen uptake and transport by fungi (Whiteside et al., 2009, Whiteside et al., 2012).

Soil physical conditions also have a strong effect on biological activity in soil, and transparent soil offers new opportunities to understand how roots respond to the soil physical conditions (Kozlowski, 1999, Moran et al., 2000, Lipiec & Hatano, 2003, Bengough et al., 2006, Pierret et al., 2007). In this thesis, work has focused on the study of root trajectories but future work using transparent soil would benefit from combining this type of data with information on the high-resolution interactions between the roots and the soil particles. For example, imaging roots over a series of time points would allow root growth rate to be quantified along with the associated movement of Nafion particles, which could be tracked using particle image velocimetry (PIV, Bengough et al., 2010). Among other things, this would be useful for analysing how different plant

genotypes respond to substrates with different levels of compaction. Imaging of the Nafion particles which make up the substrate along with the roots could also be used for measuring the contact area between the roots and the particles, which has important implications in water and nutrient uptake (Schmidt, 2011, Schmidt et al., 2012).

Plant breeding could greatly benefit from the development of cheap transparent soils. In particular, breeding crops with improved root system architecture is currently very limited because of the difficulties in observing beneficial root traits. One area of interest where data on root systems is required is high throughput root phenotyping. This requires researchers to screen multiple plant genotypes in order to select plants with desirable root traits as a part of breeding programmes, and therefore large numbers of samples are required (White et al., 2012, Gregory et al., 2009). Past studies have not considered soil conditions and therefore translation to field conditions is impossible (Pacheco-Villalobos & Hardtke, 2012). Sample size is also a consideration as applicability of results from very small, young plants to full grown plants in the field is desirable.

Transparent soil has the potential to be a competitive option in the field of 3D root system architecture phenotyping (Fang et al., 2009, Fang et al., 2011, Clark et al., 2011), but an up scaling of the production of Nafion for transparent soil would be required to meet the demand for its use in this situation. This could perhaps be carried out in collaboration with an industrial scale polymer processing company where particle size manipulation and chemical processing could be carried out efficiently. If this were pursued, the cost of Nafion as a raw material would be a limiting factor (Nafion in this

study was obtained from Ion Power Inc., Delaware USA, for $4 – 5.70 per gram). This problem could perhaps be circumvented by collaborating directly with the producers of Nafion or, alternatively, by further developing transparent soil using alternative, lower cost polymers, building on the work described here (Chapter 2). It would also be important to consider a greater level of automation in preparation for the imaging stage. As described, the substrate has to be saturated with the RI matched liquid before imaging. This process could be automated by creating sample holders with in built mechanisms for adding liquid from the base of the sample that could also be used for draining the substrate to allow imaging at multiple time points without having a permanently saturated substrate.

Data provided by transparent soils could impact soil biological sciences in many ways. It has the potential to deliver significant information on the functioning of soil systems, contributing to a better understanding of biological mechanisms and their dynamics. For example, plants and microorganisms that produce fluorescent proteins could be used to locate a specific tissue type, cell organelle, gene expression or hormone production by imaging to study plant growth processes in relation to substrate heterogeneity (Kurup et al., 2005, Faget et al., 2010, Faget et al., 2012, Federici et al., 2012). Also, fluorescent bacteria can be used to give information on other factors in the soil such as bacterial luminescence in regions with high soil carbon from root exudation (Paterson et al., 2006). Further work to combine these tools with novel light imaging techniques and transparent soil, providing an environmentally relevant substrate, to generate image data describing root and soil processes would be advantageous. This could include the

acquisition of time series data of living soil systems, made possible by non-destructive imaging in transparent soil.

The information on roots that can be obtained using transparent soil could be used to parameterise root models to describe and predict root growth direction and rate in substrates with a range of characteristics. Such models could allow valuable predictions of plant responses to soil heterogeneity (Garcia-Palacios et al., 2012). This thesis showed that transparent soil was used to obtain data at a range of scales, from plant cell nuclei and bacterial microcolonies to root systems, and therefore a would be relevant for parameterising multiscale models, from cell divisions to root system architecture (Band et al., 2012). The transparent soil presented in this thesis is the first substrate of its kind for 3D imaging of soil biota. Its application in studying root systems architecture has been validated and imaging of plant roots could be achieved to a cellular level in relation to the substrate particles.

Overall, transparent soil presents new opportunities to unravel the complex processes of plant–soil interactions in situ and in vivo and holds promise for a wide range of applications to aid the understanding of biological, chemical and physical mechanisms that underpin the sustainability of our ecosystems.

Chapter 7. References

Abbas-Zadeh, P., Saleh-Rastin, N., Asadi-Rahmani, H., Khavazi, K., Soltani, A., Shoary-Nejati, A. R. & Miransari, M. 2010. Plant growth-promoting activities of fluorescent pseudomonads, isolated from the Iranian soils. *Acta Physiologiae Plantarum,* 32, 281-288.

Acton Technologies, I. 2000 - 2008. *FluoroEtch* [Online]. Adare: Acton Technologies. Available: http://www.actontech.com/fluor1.htm [Accessed 20th August 2012].

Ahmed, M., Stal, L. J. & Hasnain, S. 2010. Association of non-heterocystous cyanobacteria with crop plants. *Plant and Soil,* 336, 363-375.

Alloush, G. A. 2003. Responses of hydroponically-grown chickpea to low phosphorus: pH changes, nutrient uptake rates, and root morphological changes. *Agronomie,* 23, 123-133.

Amos, B., Reid, E. & Reichelt, S. 2010. *Improving the magnifying glass: a new giant lens* [Online]. Available: http://www2.mrc-lmb.cam.ac.uk/va/newgiantlens/ [Accessed 31 May 2012].

Anon. 2010. *Population division, population estimates and projections section* [Online]. United Nations: Department for Economic and Social Affairs. Available: http://esa.un.org/wpp/unpp/panel_population.htm [Accessed 4/9/12.

Antonsen, F., Johnsson, A., Futsaether, C. & Krane, J. 1999. Nuclear magnetic resonance imaging in studies of gravitropism in soil mixtures. *New Phytologist,* 142, 59-66.

Aravena, J. E., Berli, M., Ghezzehei, T. A. & Tyler, S. W. 2011. Effects of root-induced compaction on rhizosphere hydraulic properties - x-ray microtomography imaging and numerical simulations. *Environmental Science & Technology,* 45, 425-431.

Badri, D. V. & Vivanco, J. M. 2009. Regulation and function of root exudates. *Plant Cell and Environment,* 32, 666-681.

Bahmani, R., Karami, O. & Gholami, M. 2009. Influence of carbon sources and their concentrations on rooting and hyperhydricity of apple rootstock MM.106. *World Applied Sciences Journal,* 6, 1513-1517.

Band, L. R., Fozard, J. A., Godin, C., Jensen, O. E., Pridmore, T., Bennett, M. J. & King, J. R. 2012. Multiscale systems analysis of root growth and development: Modeling beyond the network and cellular scales. *Plant Cell,* 24, 3892-3906.

Barlow, P. W. 2002. The root cap: Cell dynamics, cell differentiation and cap function. *Journal of Plant Growth Regulation,* 21, 261-286.

Basu, P., Pal, A., Lynch, J. P. & Brown, K. M. 2007. A novel image-analysis technique for kinematic study of growth and curvature. *Plant Physiology,* 145, 305-316.

Beck, P. S. A., Atzberger, C., Hogda, K. A., Johansen, B. & Skidmore, A. K. 2006. Improved monitoring of vegetation dynamics at very high latitudes: A new method using MODIS NDVI. *Remote Sensing of Environment,* 100, 321-334.

Beeckman, T., Burssens, S. & Inze, D. 2001. The peri-cell-cycle in *Arabidopsis*. *Journal of Experimental Botany,* 52, 403-411.

Beemster, G. T. S. & Baskin, T. I. 1998. Analysis of cell division and elongation underlying the developmental acceleration of root growth in *Arabidopsis thaliana*. *Plant Physiology,* 116, 1515-1526.

Bengough, A. G., Bransby, M. F., Hans, J., McKenna, S. J., Roberts, T. J. & Valentine, T. A. 2006. Root responses to soil physical conditions; growth dynamics from field to cell. *Journal of Experimental Botany,* 57, 437-447.

Bengough, A. G., Hans, J., Bransby, M. F. & Valentine, T. A. 2010. PIV as a method for quantifying root cell growth and particle displacement in confocal images. *Microscopy Research and Technique,* 73, 27-36.

Bengough, A. G., McKenzie, B. M., Hallett, P. D. & Valentine, T. A. 2011. Root elongation, water stress, and mechanical impedance: a review of limiting stresses and beneficial root tip traits. *Journal of Experimental Botany,* 62, 59-68.

Bengough, A. G. & Mullins, C. E. 1990. Mechanical impedance to root growth: a review of experimental techniques and root growth responses. *Journal of Soil Science,* 41, 341-358.

Bertin, C., Yang, X. H. & Weston, L. A. 2003. The role of root exudates and allelochemicals in the rhizosphere. *Plant and Soil,* 256, 67-83.

Bi, C., Zhang, H., Zhang, Y., Zhu, X., Ma, Y., Dai, H. & Xiao, S. 2008. Fabrication and investigation of SiO_2 supported sulfated zirconia/Nafion ® self-humidifying

membrane for proton exchange membrane fuel cell applications. *Journal of Power Sources,* 184, 197-203.

Bingham, I. J. & Bengough, A. G. 2003. Morphological plasticity of wheat and barley roots in response to spatial variation in soil strength. *Plant and Soil,* 250, 273-282.

Blackwell, P. S. & Wells, E. A. 1983. Limiting oxygen flux densities for oat root extension. *Plant and Soil,* 73, 129-139.

Blossfeld, S. & Gansert, D. 2007. A novel non-invasive optical method for quantitative visualization of pH dynamics in the rhizosphere of plants. *Plant, Cell & Environment,* 30, 176-186.

Blossfeld, S., Gansert, D., Thiele, B., Kuhn, A. J. & Losch, R. 2011. The dynamics of oxygen concentration, pH value, and organic acids in the rhizosphere of *Juncus* spp. *Soil Biology & Biochemistry,* 43, 1186-1197.

Blossfeld, S., Perriguey, J., Sterckeman, T., Morel, J. L. & Losch, R. 2010. Rhizosphere pH dynamics in trace-metal-contaminated soils, monitored with planar pH optodes. *Plant and Soil,* 330, 173-184.

Boonsirichai, K., Guan, C., Chen, R. & Masson, P. H. 2002. Root gravitropism: An experimental tool to investigate basic cellular and molecular processes underlying mechanosensing and signal transmission in plants. *Annual Review of Plant Biology,* 53, 421-447.

Bottomley, P. A., Rogers, H. H. & Foster, T. H. 1986. NMR imaging shows water distribution and transport in plant-root systems *in situ*. *Proceedings of the National Academy of Sciences of the United States of America,* 83, 87-89.

Bottomley, P. A., Rogers, H. H. & Prior, S. A. 1993. NMR imaging of root water distribution in intact *Vicia faba* L. plants in elevated atmospheric CO_2. *Plant Cell and Environment,* 16, 335-338.

Boyer, J. S., Silk, W. K. & Watt, M. 2010. Path of water for root growth. *Functional Plant Biology,* 37, 1105-1116.

Brady, S. M., Orlando, D. A., Lee, J. Y., Wang, J. Y., Koch, J., Dinneny, J. R., Mace, D., Ohler, U. & Benfey, P. N. 2007. A high-resolution root spatiotemporal map reveals dominant expression patterns. *Science,* 318, 801-806.

Brooks, T. L. D., Miller, N. D. & Spalding, E. P. 2010. Plasticity of *Arabidopsis* root gravitropism throughout a multidimensional condition space quantified by automated image analysis. *Plant Physiology,* 152, 206-216.

Buczko, U., Kuchenbuch, R. O. & Gerke, H. H. 2009. Evaluation of a core sampling scheme to characterize root length density of maize. *Plant and Soil,* 316, 205-215.

Buddrus-Schiemann, K., Schmid, M., Schreiner, K., Welzl, G. & Hartmann, A. 2010. Root colonization by *Pseudomonas* sp DSMZ 13134 and impact on the indigenous rhizosphere bacterial community of barley. *Microbial Ecology,* 60, 381-393.

Budwig, R. 1994. Refractive index matching methods for liquid flow investigations. *Experiments in Fluids,* 17, 350-355.

Bustos, D., Lascano, R., Villasuso, A. L., Machado, E., Senn, M. E., Cordoba, A. & Taleisnik, E. 2008. Reductions in maize root-tip elongation by salt and osmotic stress do not correlate with apoplastic $O_2^{\bullet-}$ levels. *Annals of Botany,* 102, 551-559.

Caldwell, M. M. & Richards, J. H. 1989. Hydraulic lift: water efflux from upper roots improves effectiveness of water uptake by deep roots. *Oecologia,* 79, 1-5.

Camper, A. K., Hayes, J. T., Sturman, P. J., Jones, W. L. & Cunningham, A. B. 1993. Effects of motility and adsorption rate coefficient on transport of bacteria through saturated porous media. *Applied and Environmental Microbiology,* 59, 3455-3462.

Ceynowa, J. 1984. Pore model parameters of cation-exchange membranes. *Die Angewandte Makromolekulare Chemie,* 121, 97-107.

Chin-A-Woeng, T. F. C., de Priester, W., van der Bij, A. J. & Lugtenberg, B. J. J. 1997. Description of the colonization of a gnotobiotic tomato rhizosphere by *Pseudomonas fluorescens* biocontrol strain WCS365, using scanning electron microscopy. *Molecular Plant-Microbe Interactions,* 10, 79-86.

Clark, L. J., Whalley, W. R. & Barraclough, P. B. 2001. Partial mechanical impedance can increase the turgor of seedling pea roots. *Journal of Experimental Botany,* 52, 167-171.

Clark, L. J., Whalley, W. R. & Barraclough, P. B. 2003. How do roots penetrate strong soil? *Plant and Soil,* 255, 93-104.

Clark, L. J., Whalley, W. R., Leigh, R. A., Dexter, A. R. & Barraclough, P. B. 1999. Evaluation of agar and agarose gels for studying mechanical impedance in rice roots. *Plant and Soil,* 207, 37-43.

Clark, R. T., MacCurdy, R. B., Jung, J. K., Shaff, J. E., McCouch, S. R., Aneshansley, D. J. & Kochian, L. V. 2011. Three-dimensional root phenotyping with a novel imaging and software platform. *Plant Physiology,* 156, 455-465.

Coleman, D. C., Reid, C. P. P. & Cole, C. V. 1983. Biological strategies of nutrient cycling in soil systems. *In:* MacFadyen, A. & Ford, E. D. (eds.) *Advances in Ecological Research.* London: Academic Press.

Corkidi, G., Taboada, B., Wood, C. D., Guerrero, A. & Darszon, A. 2008. Tracking sperm in three-dimensions. *Biochemical and Biophysical Research Communications,* 373, 125-129.

Crenshaw, H. C., Ciampaglio, C. N. & McHenry, M. 2000. Analysis of the three-dimensional trajectories of organisms: Estimates of velocity, curvature and torsion from positional information. *Journal of Experimental Biology,* 203, 961-982.

Daintith, J. & Martin, E. (eds.) 2005. *Oxford dictionary of science,* New York: Oxford University Press.

Dandurand, L. M., Schotzko, D. J. & Knudsen, G. R. 1997. Spatial patterns of rhizoplane populations of *Pseudomonas fluorescens*. *Applied and Environmental Microbiology,* 63, 3211-3217.

Danhorn, T. & Fuqua, C. 2007. Biofilm formation by plant-associated bacteria. *Annual Review of Microbiology.* Palo Alto: Annual Reviews.

Darwent, M. J., Paterson, E., McDonald, A. J. S. & Tomos, A. D. 2003. Biosensor reporting of root exudation from Hordeum vulgare in relation to shoot nitrate concentration. *Journal of Experimental Botany,* 54, 325-334.

Darwin, C. 1880. *The Power of Movement in Plants,* London, John Murray.

Datta, S., Kim, C. M., Pernas, M., Pires, N. D., Proust, H., Tam, T., Vijayakumar, P. & Dolan, L. 2011. Root hairs: development, growth and evolution at the plant-soil interface. *Plant and Soil,* 346, 1-14.

Day, R. N. & Davidson, M. W. 2009. The fluorescent protein palette: tools for cellular imaging. *Chemical Society Reviews,* 38, 2887-2921.

De-la-Pena, C. & Vivanco, J. M. 2010. Root-microbe interactions: the importance of protein secretion. *Current Proteomics,* 7, 265-274.

de Boer, W., Folman, L. B., Summerbell, R. C. & Boddy, L. 2005. Living in a fungal world: impact of fungi on soil bacterial niche development. *Fems Microbiology Reviews,* 29, 795-811.

De Dorlodot, S., Bertin, P., Baret, P. & Draye, X. 2005. Scaling up quantitative phenotyping of root system architecture using a combination of aeroponics and image analysis. *Aspects of Applied Biology*, 41-54.

De Smet, I., Vanneste, S., Inze, D. & Beeckman, T. 2006. Lateral root initiation or the birth of a new meristem. *Plant Molecular Biology,* 60, 871-887.

de Villeneuve, V. W. A., Dullens, R. P. A., Aarts, D., Groeneveld, E., Scherff, J. H., Kegel, W. K. & Lekkerkerker, H. N. W. 2005. Colloidal hard-sphere crystal growth frustrated by large spherical impurities. *Science,* 309, 1231-1233.

Delin, S. & Strömberg, N. 2011. Imaging-optode measurements of ammonium distribution in soil after different manure amendments. *European Journal of Soil Science,* 62, 295-304.

Dey, R., Pal, K. K., Bhatt, D. M. & Chauhan, S. M. 2004. Growth promotion and yield enhancement of peanut (*Arachis hypogaea* L.) by application of plant growth-promoting rhizobacteria. *Microbiological Research,* 159, 371-394.

Dhondt, S., Vanhaeren, H., Van Loo, D., Cnudde, V. & Inze, D. 2010. Plant structure visualization by high-resolution X-ray computed tomography. *Trends in Plant Science,* 15, 419-422.

Donlan, R. M. 2002. Biofilms: Microbial life on surfaces. *Emerging Infectious Diseases,* 8, 881-890.

Dowling, D. N. & O'Gara, F. 1994. Metabolites of *Pseudomonas* involved in the biocontrol of plant disease. *Trends in Biotechnology,* 12, 133-141.

Downie, H., Holden, N., Otten, W., Spiers, A. J., Valentine, T. A. & Dupuy, L. X. 2012. Transparent Soil for Imaging the Rhizosphere. *PLoS ONE,* 7**,** e44276.

Drew, M. C. & Saker, L. R. 1975. Nutrient supply and the growth of seminal root system in barley. II. Localized, compensatory increases in lateral root growth and rates of nitrate uptake when nitrate supply is restricted to only part of the root system. *Journal of Experimental Botany,* 26**,** 79-90.

Drew, M. C. & Saker, L. R. 1978. Nutrient supply and the growth of the seminal root system in barley. III. Compensatory increases in the growth of lateral roots, and in rates of phosphate uptake, in response to a localized supply of phosphate. *Journal of Experimental Botany,* 29**,** 435-451.

Drew, M. C., Saker, L. R. & Ashley, T. W. 1973. Nutrient supply and growth of seminal root system in barley. I. Effect of nitrate concentration on growth of axes and laterals. *Journal of Experimental Botany,* 24**,** 1189-1202.

Dubrovsky, J. G., Doerner, P. W., Colon-Carmona, A. & Rost, T. L. 2000. Pericycle cell proliferation and lateral root initiation in *Arabidopsis*. *Plant Physiology,* 124**,** 1648-1657.

Dubrovsky, J. G., Guttenberger, M., Saralegui, A., Napsucialy-Mendivil, S., Voigt, B., Baluska, F. & Menzel, D. 2006. Neutral red as a probe for confocal laser scanning microscopy studies of plant roots. *Annals of Botany,* 97**,** 1127-1138.

Dumais, J. & Kwiatkowska, D. 2002. Analysis of surface growth in shoot apices. *The Plant Journal,* 31**,** 229-241.

DuPont. 1996. *DuPont FEP* [Online]. Available: http://www2.dupont.com/Teflon_Industrial/en_US/assets/downloads/h55007.pdf.

Dupuy, L., Fourcaud, T., Stokes, A. & Danjon, F. 2005. A density-based approach for the modelling of root architecture: application to Maritime pine (*Pinus pinaster Ait.*) root systems. *Journal of Theoretical Biology,* 236**,** 323-334.

Dupuy, L., Mackenzie, J. & Haseloff, J. 2010a. Coordination of plant cell division and expansion in a simple morphogenetic system. *Proceedings of the National Academy of Sciences of the United States of America,* 107**,** 2711-2716.

Dupuy, L., Vignes, M., McKenzie, B. M. & White, P. J. 2010b. The dynamics of root meristem distribution in the soil. *Plant Cell and Environment,* 33**,** 358-369.

Dupuy, L. X. & Vignes, M. 2012. An algorithm for the simulation of the growth of root systems on deformable domains. *Journal of Theoretical Biology,* 310**,** 164-74.

Elick, J. M., Driese, S. G. & Mora, C. I. 1998. Very large plant and root traces from the Early to Middle Devonian: Implications for early terrestrial ecosystems and atmospheric $p(CO_2)$. *Geology,* 26**,** 143-146.

Esmon, C. A., Pedmale, U. V. & Liscum, E. 2005. Plant tropisms: providing the power of movement to a sessile organism. *International Journal of Developmental Biology,* 49**,** 665-674.

Evans, L. T. 1998. *Feeding the ten billion: plants and population growth,* Cambridge, Cambridge University Press.

Ezzein, F. M. & Bathurst, R. J. 2011. A transparent sand for geotechnical laboratory modeling. *Geotechnical Testing Journal,* 34**,** 590-601.

Faget, M., Liedgens, M., Feil, B., Stamp, P. & Herrera, J. M. 2012. Root growth of maize in an Italian ryegrass living mulch studied with a non-destructive method. *European Journal of Agronomy,* 36**,** 1-8.

Faget, M., Liedgens, M., Stamp, P., Flutsch, P. & Herrera, J. M. 2010. A minirhizotron imaging system to identify roots expressing the green fluorescent protein. *Computers and Electronics in Agriculture,* 74**,** 163-167.

Fang, S., Yan, X. & Liao, H. 2009. 3D reconstruction and dynamic modeling of root architecture in situ and its application to crop phosphorus research. *Plant Journal,* 60**,** 1096-1108.

Fang, S. Q., Gao, X. A., Deng, Y., Chen, X. P. & Liao, H. 2011. Crop root behavior co-ordinates phosphorus status and neighbors: from field studies to three-dimensional in situ reconstruction of root system architecture. *Plant Physiology,* 155**,** 1277-1285.

Federici, F., Dupuy, L., Laplaze, L., Heisler, M. & Haseloff, J. 2012. Integrated genetic and computation methods for in planta cytometry. *Nat Meth,* 9**,** 483-485.

Fisher, M., Downie, H., Welten, M. C. M., Delgado, I., Bain, A., Planzer, T., Sherman, A., Sang, H. & Tickle, C. 2011. Comparative analysis of 3D expression patterns of transcription factor genes and digit fate maps in the developing chick wing. *PLoS ONE,* 6**,** e18661.

Fisher, M. E., Clelland, A. K., Bain, A., Baldock, R. A., Murphy, P., Downie, H., Tickle, C., Davidson, D. R. & Buckland, R. A. 2008. Integrating technologies for comparing 3D gene expression domains in the developing chick limb. *Developmental Biology,* 317, 13-23.

Fitter, A. H. & Stickland, T. R. 1992. Fractal characterization of root-system architecture. *Functional Ecology,* 6, 632-635.

Fontenot, M. M. & Vigil, R. D. 2002. Pore-scale study of nonaqueous phase liquid dissolution in porous media using laser-induced fluorescence. *Journal of Colloid and Interface Science,* 247, 481-489.

Fourcaud, T., Zhang, X., Stokes, A., Lambers, H. & Koerner, C. 2008. Plant growth modelling and applications: The increasing importance of plant architecture in growth models. *Annals of Botany,* 101, 1053-1063.

French, A., Ubeda-Tomas, S., Holman, T. J., Bennett, M. J. & Pridmore, T. 2009. High-throughput quantification of root growth using a novel image-analysis tool. *Plant Physiology,* 150, 1784-1795.

Friend, A. L., Eide, M. R. & Hinckley, T. M. 1990. Nitrogen stress alters root proliferation in Douglas-Fir seedlings. *Canadian Journal of Forest Research-Revue Canadienne De Recherche Forestiere,* 20, 1524-1529.

Friman, O., Hindennach, M. & Peitgen, H. O. 2008. Template-based multiple hypotheses tracking of small vessels. *2008 IEEE International Symposium on Biomedical Imaging: From Nano to Macro, Vols 1-4.*

Furbank, R. T. 2009. Plant phenomics: from gene to form and function. *Functional Plant Biology,* 36, V-VI.

Gamalero, E., Lingua, G., Berta, G. & Lemanceau, P. 2003. Methods for studying root colonization by introduced beneficial bacteria. *Agronomie,* 23, 407-418.

Gamalero, E., Lingua, G., Tombolini, R., Avidano, L., Pivato, B. & Berta, G. 2005. Colonization of tomato root seedling by *Pseudomonas fluorescens* 92rkG5: Spatio-temporal dynamics, localization, organization, viability, and culturability. *Microbial Ecology,* 50, 289-297.

Garcia-Palacios, P., Maestre, F. T., Bardgett, R. D. & de Kroon, H. 2012. Plant responses to soil heterogeneity and global environmental change. *Journal of Ecology,* 100, 1303-1314.

Garg, N. & Geetanjali 2007. Symbiotic nitrogen fixation in legume nodules: process and signaling. A review. *Agronomy for Sustainable Development,* 27, 59-68.

Giuliani, S., Sanguineti, M. C., Tuberosa, R., Bellotti, M., Salvi, S. & Landi, P. 2005. Root-ABA1, a major constitutive QTL, affects maize root architecture and leaf ABA concentration at different water regimes. *Journal of Experimental Botany,* 56, 3061-3070.

Gordon, D. C., Hettiaratchi, D. R. P., Bengough, A. G. & Young, I. M. 1992. Nondestructive analysis of root growth in porous media. *Plant Cell and Environment,* 15, 123-128.

Goss, M. J. & Russell, R. S. 1980. Effects of mechanical response on root-growth in barley (*Hordeum vulgare*). 3. Observations on the mechanism of response. *Journal of Experimental Botany,* 31**,** 577-588.

Gregory, P. J., Bengough, A. G., Grinev, D., Schmidt, S., Thomas, W. T. B., Wojciechowski, T. & Young, I. M. 2009. Root phenomics of crops: opportunities and challenges. *Functional Plant Biology,* 36**,** 922-929.

Gregory, P. J., Hutchison, D. J., Read, D. B., Jenneson, P. M., Gilboy, W. B. & Morton, E. J. 2003. Non-invasive imaging of roots with high resolution X-ray micro-tomography. *Plant and Soil,* 255**,** 351-359.

Grierson, C. & Schiefelbein, J. 2002. Root hairs. *The Arabidopsis Book,* 1:e0060.

Grift, T. E., Novais, J. & Bohn, M. 2011. High-throughput phenotyping technology for maize roots. *Biosystems Engineering,* 110**,** 40-48.

Gurr, E. 1971. *Synthetic dyes in biology, medicine and chemistry,* London, Academic Press.

Gustafsson, M. G. L. 2005. Nonlinear structured-illumination microscopy: Wide-field fluorescence imaging with theoretically unlimited resolution. *Proceedings of the National Academy of Sciences of the United States of America,* 102**,** 13081-13086.

Halperin, S. J. & Lynch, J. P. 2003. Effects of salinity on cytosolic Na^+ and K^+ in root hairs of *Arabidopsis thaliana*: in vivo measurements using the fluorescent dyes SBFI and PBFI. *Journal of Experimental Botany,* 54**,** 2035-2043.

Hamza, O., Bengough, A. G., Bransby, M. F., Davies, M. C. R. & Hallett, P. D. 2006. Biomechanics of plant roots: estimating localised deformation with particle image velocimetry. *Biosystems Engineering,* 94**,** 119-132.

Hart, M. R., Quin, B. F. & Nguyen, M. L. 2004. Phosphorus runoff from agricultural land and direct fertilizer effects: A review. *Journal of Environmental Quality,* 33**,** 1954-1972.

Haseloff, J. 2003. Old botanical techniques for new microscopes. *Biotechniques,* 34**,** 1174-1182.

Haynes, J. G., Czymmek, K. J., Carlson, C. A., Veereshlingam, H., Dickstein, R. & Sherrier, D. J. 2004. Rapid analysis of legume root nodule development using confocal microscopy. *New Phytologist,* 163**,** 661-668.

Heeraman, D. A., Hopmans, J. W. & Clausnitzer, V. 1997. Three dimensional imaging of plant roots in situ with x-ray computed tomography. *Plant and Soil,* 189**,** 167-179.

Hepler, P. K. & Gunning, B. E. S. 1998. Confocal fluorescence microscopy of plant cells. *Protoplasma,* 201**,** 121-157.

Hernando Posada, R., Heredia-Abarca, G., Sieverding, E. & Sanchez de Prager, M. 2013. Solubilization of iron and calcium phosphates by soil fungi isolated from coffee plantations. *Archives of Agronomy and Soil Science,* 59**,** 185-196.

Hodge, A. 2004. The plastic plant: root responses to heterogeneous supplies of nutrients. *New Phytologist,* 162**,** 9-24.

Hodge, A. 2006. Plastic plants and patchy soils. *Journal of Experimental Botany,* 57, 401-411.

Hodge, A., Berta, G., Doussan, C., Merchan, F. & Crespi, M. 2009. Plant root growth, architecture and function. *Plant and Soil,* 321, 153-187.

Huisken, J. 2012. Slicing embryos gently with laser light sheets. *Bioessays,* 34, 406-411.

Huisken, J., Swoger, J., Del Bene, F., Wittbrodt, J. & Stelzer, E. H. K. 2004. Optical sectioning deep inside live embryos by selective plane illumination microscopy. *Science,* 305, 1007-1009.

Humphris, S. N., Bengough, A. G., Griffiths, B. S., Kilham, K., Rodger, S., Stubbs, V., Valentine, T. A. & Young, I. M. 2005. Root cap influences root colonisation by *Pseudomonas fluorescens* SBW25 on maize. *FEMS Microbiology Ecology,* 54, 123-130.

Hund, A., Trachsel, S. & Stamp, P. 2009. Growth of axile and lateral roots of maize: I development of a phenotyping platform. *Plant and Soil,* 325, 335-349.

Hutchings, M. J. & de Kroon, H. 1994. Foraging in plants – the role of morphological plasticity in resource acquisition. *Advances in Ecological Research, Vol 25.* London: Academic Press Ltd.

Iijima, M., Griffiths, B. & Bengough, A. G. 2000. Sloughing of cap cells and carbon exudation from maize seedling roots in compacted sand. *New Phytologist,* 145, 477-482.

Iskander, M. & Liu, J. Y. 2010. Spatial Deformation Measurement Using Transparent Soil. *Geotechnical Testing Journal,* 33, 314-321.

Iskander, M. G., Liu, J. Y. & Sadek, S. 2002. Transparent amorphous silica to model clay. *Journal of Geotechnical and Geoenvironmental Engineering,* 128, 262-273.

Jackson, R. B., Manwaring, J. H. & Caldwell, M. M. 1990. Rapid physiological adjustment of roots to localised soil enrichment. *Nature,* 344, 58-60.

Jahn, R., Blume, H.-P., Asio, V. B., Spaargaren, O., Schad, P., Langohr, R., Brinkman, R., Nachtergaele, F. O. & Krasilnikov, R. P. 1990. Guidelines for soil description. 4 ed. Rome: Food and agriculture organization of the United Nations.

Jakubauskas, M. E., Legates, D. R. & Kastens, J. H. 2001. Harmonic analysis of time-series AVHRR NDVI data. *Photogrammetric Engineering and Remote Sensing,* 67, 461-470.

Jaleel, C. A., Manivannan, P., Sankar, B., Kishorekumar, A., Gopi, R., Somasundaram, R. & Panneerselvam, R. 2007. *Pseudomonas fluorescens* enhances biomass yield and ajmalicine production in Catharanthus roseus under water deficit stress. *Colloids and Surfaces B-Biointerfaces,* 60, 7-11.

Josephson, R. K. & Flessa, K. W. 1972. Cryolite - medium for study of burrowing aquatic organisms. *Limnology and Oceanography,* 17, 134-135.

Kato, Y., Abe, J., Kamoshita, A. & Yamagishi, J. 2006. Genotypic variation in root growth angle in Rice (*Oryza sativa L.*) and its association with deep root development in upland fields with different water regimes. *Plant and Soil,* 287, 117-129.

Kern, V. D., Schwuchow, J. M., Reed, D. W., Nadeau, J. A., Lucas, J., Skripnikov, A. & Sack, F. D. 2005. Gravitropic moss cells default to spiral growth on the clinostat and in microgravity during spaceflight. *Planta,* 221, 149-157.

Kiss, J. Z., Wright, J. B. & Caspar, T. 1996. Gravitropism in roots of intermediate-starch mutants of Arabidopsis. *Physiologia Plantarum,* 97, 237-244.

Kockenberger, W. 2001. Nuclear magnetic resonance micro-imaging in the investigation of plant cell metabolism. *Journal of Experimental Botany,* 52, 641-652.

Koenig, M., Spindler, W., Rexilius, J., Jomier, J., Link, F. & Peitgen, H.-O. Embedding VTK and ITK into a visual programming and rapid prototyping platform. *In:* Cleary, K. R. & Galloway, R. L., eds. Medical Imaging 2006: Visualization, Image-Guided Procedures, and Display, 2006 San Diego, Ca.

Koide, R. T. 1991. Nutrient supply, nutrient demans and plant response to mycorrhizal infection. *New Phytologist,* 117, 365-386.

Kosegarten, H., Grolig, F., Esch, A., Glusenkamp, K. H. & Mengel, K. 1999. Effects of NH_4^+, NO_3^- and HCO_3^- on apoplast pH in the outer cortex of root zones of maize, as measured by the fluorescence ratio of fluorescein boronic acid. *Planta,* 209, 444-452.

Koza, A., Hallett, P. D., Moon, C. D. & Spiers, A. J. 2009. Characterization of a novel air-liquid interface biofilm of Pseudomonas fluorescens SBW25. *Microbiology-Sgm,* 155, 1397-1406.

Kozlowski, T. T. 1999. Soil compaction and growth of woody plants. *Scandinavian Journal of Forest Research,* 14, 596-619.

Kragelund, L. & Nybroe, O. 1996. Competition between *Pseudomonas fluorescens* Ag1 and Alcaligenes eutrophus JMP134 (pJP4) during colonization of barley roots. *Fems Microbiology Ecology,* 20, 41-51.

Kubo, H. & Hayashi, K. 2011. Characterization of root cells of anl2 mutant in *Arabidopsis thaliana*. *Plant Science,* 180, 679-685.

Kurup, S., Runions, J., Kohler, U., Laplaze, L., Hodge, S. & Haseloff, J. 2005. Marking cell lineages in living tissues. *Plant Journal,* 42, 444-453.

Lai, J. R., Oswald, C. J. & Mannheimer, R. J. 1994. Development of a transparent material to model the geotechnical properties of soils. *Geotechnical Testing Journal,* 17, 425-433.

Lakshmanan, V., Kumar, A. S. & Bais, H. P. 2012. *The Ecological Significance of plant-associated Biofilms,* Wymondham, Caister Academic Press.

Lal, R. (ed.) 2002. *Encyclopedia of soil science,* New York & Basel: Marcel Dekker.

Lambertsen, L., Sternberg, C. & Molin, S. 2004. Mini-Tn7 transposons for site-specific tagging of bacteria with fluorescent proteins. *Environmental Microbiology,* 6, 726-732.

Lee, K., Avondo, J., Morrison, H., Blot, L., Stark, M., Sharpe, J., Bangham, A. & Coen, E. 2006. Visualizing plant development and gene expression in three dimensions using optical projection tomography. *Plant Cell,* 18, 2145-2156.

Leis, A. P., Schlicher, S., Franke, H. & Strathmann, M. 2005. Optically transparent porous medium for nondestructive studies of microbial biofilm architecture and transport dynamics. *Applied and Environmental Microbiology,* 71, 4801-4808.

Liao, H., Rubio, G., Yan, X. L., Cao, A. Q., Brown, K. M. & Lynch, J. P. 2001. Effect of phosphorus availability on basal root shallowness in common bean. *Plant and Soil,* 232, 69-79.

Lipiec, J. & Hatano, R. 2003. Quantification of compaction effects on soil physical properties and crop growth. *Geoderma,* 116, 107-136.

Liu, J. & Iskander, M. G. 2010. Modelling capacity of transparent soil. *Canadian Geotechnical Journal,* 47, 451-460.

Lobet, G. 2012. *Root image analysis* [Online]. Available: http://www.root-image-analysis.org/ [Accessed 30 October 2012].

Lu, J., Tang, H., Xu, C. & Jiang, S. P. 2012. Nafion membranes with ordered mesoporous structure and high water retention properties for fuel cell applications. *Journal of Materials Chemistry,* 22, 5810-5819.

Lugtenberg, B. J. J., Dekkers, L. & Bloemberg, G. V. 2001. Molecular determinants of rhizosphere colonization by *Pseudomonas*. *Annual Review of Phytopathology,* 39, 461-490.

Lynch, J. P. 2007. Roots of the second green revolution. *Australian Journal of Botany,* 55, 493-512.

Mairhofer, S., Zappala, S., Tracy, S. R., Sturrock, C., Bennett, M., Mooney, S. J. & Pridmore, T. 2012. RooTrak: automated recovery of three-dimensional plant root architecture in soil from X-ray microcomputed tomography images using visual tracking. *Plant Physiology,* 158, 561-569.

Maizel, A., von Wangenheim, D., Federici, F., Haseloff, J. & Stelzer, E. H. K. 2011. High-resolution live imaging of plant growth in near physiological bright conditions using light sheet fluorescence microscopy. *The Plant journal,* 68, 377-85.

Malamy, J. E. 2005. Intrinsic and environmental response pathways that regulate root system architecture. *Plant, Cell and Environment,* 28, 67-77.

Malamy, J. E. & Benfey, P. N. 1997. Organization and cell differentiation in lateral roots of *Arabidopsis thaliana*. *Development,* 124, 33-44.

Mannheimer, R. J. & Oswald, C. J. 1993. Development of transparent porous-media with permeabilities and porosities comparable to soils, aquifers, and petroleum reservoirs. *Ground Water,* 31, 781-788.

Manton, M. J. 2010. Trends in climate extremes affecting human settlements. *Current Opinion in Environmental Sustainability,* 2, 151-155.

Marulanda, C., Culligan, P. J. & Germaine, J. T. 2000. Centrifuge modeling of air sparging - a study of air flow through saturated porous media. *Journal of Hazardous Materials,* 72, 179-215.

Massa, G. D. & Gilroy, S. 2003. Touch modulates gravity sensing to regulate the growth of primary roots of *Arabidopsis thaliana*. *Plant Journal,* 33, 435-445.

Matsubara, Y. & Harada, T. 1996. Effect of arbuscular mycorrhizal fungus infection on growth and mineral nutrient content of *Asparagus officinalis* L. seedlings. *Journal of the Japanese Society for Horticultural Science,* 65, 303-309.

McCully, M. E. 1975. The development of lateral roots. *In:* Torrey, J. G. & Clarkson, D. T. (eds.) *The Development and Function of Roots.* London: Academic Press.

Melhuish, F. M. 1968. A precise technique for measurement of roots and root distribution in soils. *Annals of Botany,* 32, 15-&.

Millar, K. D. L., Johnson, C. M., Edelmann, R. E. & Kiss, J. Z. 2011. An endogenous growth pattern of roots is revealed in seedlings grown in microgravity. *Astrobiology,* 11, 787-797.

Mohr, G. J. 2006. Polymers for optical sensors. *In:* Baldini, F., Chester, A. N., Homola, J. & Martellucci, S. (eds.) *Optical chemical sensors.* Dordrecht, The Netherlands: Springer.

Monshausen, G. B., Bibikova, T. N., Messerli, M. A., Shi, C. & Gilroy, S. 2007. Oscillations in extracellular pH and reactive oxygen species modulate tip growth of *Arabidopsis* root hairs. *Proceedings of the National Academy of Sciences of the United States of America,* 104, 20996-1001.

Monshausen, G. B., Messerli, M. A. & Gilroy, S. 2008. Imaging of the Yellow Cameleon 3.6 indicator reveals that elevations in cytosolic Ca^{2+} follow oscillating increases in growth in root hairs of *Arabidopsis*. *Plant Physiology,* 147, 1690-1698.

Mooney, S. J., Tams, A. R. & Berry, P. M. 2006. A reliable method for preserving soil structure in the field for subsequent morphological examinations. *Geoderma,* 133, 338-344.

Moore, R., Clark, W. D. & Vodopich, D. S. 1998a. How plants respond to environmental stimuli. *Botany.* 2 ed. Columbus: McGraw-Hill.

Moore, R., Clark, W. D. & Vodopich, D. S. 1998b. Primary growth: roots. *Botany.* 2 ed. Columbus: McGraw-Hill.

Moran, C. J., Pierret, A. & Stevenson, A. W. 2000. X-ray absorption and phase contrast imaging to study the interplay between plant roots and soil structure. *Plant and Soil,* 223, 99-115.

Mullen, J. L., Wolverton, C., Ishikawa, H. & Evans, M. L. 2000. Kinetics of constant gravitropic stimulus responses in *Arabidopsis* roots using a feedback system. *Plant Physiology,* 123, 665-670.

Nielsen, L., Li, X. H. & Halverson, L. J. 2011. Cell-cell and cell-surface interactions mediated by cellulose and a novel exopolysaccharide contribute to Pseudomonas putida biofilm formation and fitness under water-limiting conditions. *Environmental Microbiology,* 13, 1342-1356.

Nobbe, F. 1862. Uber die feinere Verästelung der Pflanzenwurzeln. *Landwirtschaftliche Versuchs,* 4, 212-224.

O'Donnell, A. G., Young, I. M., Rushton, S. P., Shirley, M. D. & Crawford, J. W. 2007. Visualization, modelling and prediction in soil microbiology. *Nature Reviews Microbiology,* 5, 689-699.

Oliva, M. & Dunand, C. 2007. Waving and skewing: how gravity and the surface of growth media affect root development in *Arabidopsis*. *New Phytologist,* 176, 37-43.

Oliveira, E. M. M., Ruiz, H. A., Alvarez, V. H., Ferreira, P. A., Costa, F. O. & Almeida, I. C. C. 2010. Nutrient supply by mass flow and diffusion to maize plants in response to soil aggregate size and water potential. *Revista Brasileira De Ciencia Do Solo,* 34, 317-327.

Otreba, P. 2009. The impact of light and gravity on growth directions in a root system of *Cucumis sativus*. *Acta Societatis Botanicorum Poloniae,* 78, 7-12.

Pacheco-Villalobos, D. & Hardtke, C. S. 2012. Natural genetic variation of root system architecture from *Arabidopsis* to *Brachypodium*: towards adaptive value. *Philosophical Transactions of the Royal Society B-Biological Sciences,* 367, 1552-1558.

Pansu, M. & Gautheyrou, J. 2006. Anion exchange capcity. *In:* Pansu, M. & Gautheyrou, J. (eds.) *Handbook of soil analysis.* Heidelberg: Springer.

Park, C. 2001. *The environment, principles and applications,* New York, Routledge.

Paterson, E., Sim, A., Standing, D., Dorward, M. & McDonald, A. J. S. 2006. Root exudation from Hordeum vulgare in response to localized nitrate supply. *Journal of Experimental Botany,* 57, 2413-2420.

Pawley, J. B. 2006. *Handbook of biological confocal microscopy,* New York, Springer science and business media.

Perret, J. S., Al-Belushi, M. E. & Deadman, M. 2007. Non-destructive visualization and quantification of roots using computed tomography. *Soil Biology & Biochemistry,* 39, 391-399.

Pierret, A., Doussan, C., Capowiez, Y., Bastardie, F. & Pages, L. 2007. Root functional architecture: A framework for modeling the interplay between roots and soil. *Vadose Zone Journal,* 6, 269-281.

Pierret, A., Doussan, C., Garrigues, E. & Mc Kirby, J. 2003. Observing plant roots in their environment: current imaging options and specific contribution of two-dimensional approaches. *Agronomie,* 23, 471-479.

Piotrowski, J. S. & Rillig, M. C. 2008. Succession of arbuscular mycorrhizal fungi: Patterns, causes, and considerations for organic agriculture. *In:* Sparks, D. L. (ed.) *Advances in Agronomy, Vol 97.* San Diego: Elsevier Academic Press Inc.

Polomski, J. & Kuhn, N. 2002. Root Research Methods. *In:* Waisel, Y., Eshel, A. & Kafkafi, U. (eds.) *Plant roots: the hidden half.* Boca Raton, FL: CRC Press.

Polyanskiy, M. 2008-2012. *Refractive index database* [Online]. Available: http://refractiveindex.info [Accessed 26 March 2012].

Preibisch, S., Saalfeld, S., Schindelin, J. & Tomancak, P. 2010. Software for bead-based registration of selective plane illumination microscopy data. *Nature methods,* 7, 418-419.

Preston, G. M. 2004. Plant perceptions of plant growth-promoting *Pseudomonas*. *Philosophical Transactions of the Royal Society B-Biological Sciences,* 359, 907-918.

Prieto, P., Schiliro, E., Maldonado-Gonzalez, M. M., Valderrama, R., Barroso-Albarracin, J. B. & Mercado-Blanco, J. 2011. Root hairs play a key role in the endophytic colonization of olive roots by *Pseudomonas* spp. with biocontrol activity. *Microbial Ecology,* 62, 435-445.

Raaijmakers, J. M., Vandersluis, I., Koster, M., Bakker, P., Weisbeek, P. J. & Schippers, B. 1995. Utilization of heterogeneous siderophores and rhizosphere competence of fluorescent *Pseudomonas* spp. *Canadian Journal of Microbiology,* 41, 126-135.

Ralph, J. & Chau, I. 1993-2012. *Mindat.org* [Online]. Available: http://www.mindat.org/min-1161.html [Accessed 17/8/12.

Redjala, T., Zelko, I., Sterckeman, T., Legue, V. & Lux, A. 2011. Relationship between root structure and root cadmium uptake in maize. *Environmental and Experimental Botany,* 71, 241-248.

Rengel, Z. & Marschner, P. 2005. Nutrient availability and management in the rhizosphere: exploiting genotypic differences. *New Phytologist,* 168, 305-312.

Rieberer, S. & Norian, K. H. 1992. Analytical electron-microscopy of nafion ion-exchange membranes. *Ultramicroscopy,* 41, 225-233.

Robinson, D. 1994. The responses of plants to non-uniform supplies of nutrients. *New Phytologist,* 127, 635-674.

Rogers, H. H. & Bottomley, P. A. 1987. In situ nuclear magnetic resonance imaging of roots - influence of soil type, ferromagnetic particle content and soil water. *Agronomy Journal,* 79, 957-965.

Rogers, W. S. 1933. East malling research station. *Annual Report (21st year)*, 86-91.

Rook, F. & Bevan, M. W. 2003. Genetic approaches to understanding sugar-response pathways. *Journal of Experimental Botany,* 54, 495-501.

Rosenbruch, K. J., Bretschneider, R., Charles, D. F., Emmerich, A., Hill, S., Martin, J. L., Oldfield, J. F. T. & Watts, R. S. 1974. Refractive index. International commission for uniform methods of sugar analysis, 1974 Ankara. Peterborough, England.: The International Commission for Uniform Methods of Sugar Analysis, 144-156.

Rouse, J. D., Bishop, C. A. & Struger, J. 1999. Nitrogen pollution: An assessment of its threat to amphibian survival. *Environmental Health Perspectives,* 107, 799-803.

Rovira, A. D. 1956. A study of the development of the root surface microflora during the initial stages of plant growth. *Journal of Applied Microbiology,* 19, 72-79.

Rroco, E., Kosegarten, H., Harizaj, F., Imani, J. & Mengel, K. 2003. The importance of soil microbial activity for the supply of iron to sorghum and rape. *European Journal of Agronomy,* 19, 487-493.

Russell, R. S. 1977. *Plant root systems: their function and interaction with the soil,* London, McGraw-Hill Book Company.

Saini, A. 2012. Microscopy: New lens offers scientist a brighter outlook. *Science,* 335, 1562-1563.

Salerno, H. L. S., Beyer, F. L. & Elabd, Y. A. 2012. Anion exchange membranes derived from nafion precursor for the alkaline fuel cell. *Journal of Polymer Science Part B-Polymer Physics,* 50, 552-562.

Sambrook, J., Fritsch, E. F. & Maniatis, T. 1989. *Molecular cloning: a laboratory manual,* Cold Spring Harbor, Cold Spring Harbor Laboratory Press.

Santi, P. A., Johnson, S. B., Hillenbrand, M., GrandPre, P. Z., Glass, T. J. & Leger, J. R. 2009. Thin-sheet laser imaging microscopy for optical sectioning of thick tissues. *Biotechniques,* 46, 287-294.

Scheenen, T. W. J., van Dusschoten, D., de Jager, P. A. & Van As, H. 2000. Quantification of water transport in plants with NMR imaging. *Journal of Experimental Botany,* 51, 1751-1759.

Schermelleh, L., Carlton, P. M., Haase, S., Shao, L., Winoto, L., Kner, P., Burke, B., Cardoso, M. C., Agard, D. A., Gustafsson, M. G. L., Leonhardt, H. & Sedat, J. W.

2008. Subdiffraction multicolor imaging of the nuclear periphery with 3D structured illumination microscopy. *Science,* 320**,** 1332-1336.

Schindelin, J., Arganda-Carreras, I., Frise, E., Kaynig, V., Longair, M., Pietzsch, T., Preibisch, S., Rueden, C., Saalfeld, S., Schmid, B., Tinevez, J.-Y., White, D. J., Hartenstein, V., Eliceiri, K., Tomancak, P. & Cardona, A. 2012. Fiji: an open-source platform for biological-image analysis. *Nature methods,* 9**,** 676-682.

Schmidt, S. 2011. *Root responses to soil physical conditions and the role of root-particle contact.* PhD, University of Abertay Dundee.

Schmidt, S., Bengough, A. G., Gregory, P. J., Grinev, D. V. & Otten, W. 2012. Estimating root–soil contact from 3D X-ray microtomographs. *European Journal of Soil Science,* 63**,** 776-786.

Schroth, M. H., Ahearn, S. J., Selker, J. S. & Istok, J. D. 1996. Characterization of miller-similar silica sands for laboratory hydrologic studies. *Soil Science Society of America Journal,* 60**,** 1331-1339.

Schuurman, J. J. & Goedewaagen, M. A. J. 1971. *Methods for the Examination of Root Systems and Roots,* Wageningen, Pudoc.

Sena, G., Frentz, Z., Birnbaum, K. D. & Leibler, S. 2011. Quantitation of cellular dynamics in growing *Arabidopsis* roots with light sheet microscopy. *PLoS ONE,* 6**,** e21303.

Sharpe, J., Ahlgren, U., Perry, P., Hill, B., Ross, A., Hecksher-Sorensen, J., Baldock, R. & Davidson, D. 2002. Optical projection tomography as a tool for 3D microscopy and gene expression studies. *Science,* 296**,** 541-545.

Sheldrick, W. F., Syers, J. K. & Lingard, J. 2002. A conceptual model for conducting nutrient audits at national, regional, and global scales. *Nutrient Cycling in Agroecosystems,* 62, 61-72.

Simmons, C., Soll, D. & Migliaccio, F. 1995. Circumnutation and gravitropism cause root waving in *Arabidopsis thaliana*. *Journal of Experimental Botany,* 46, 143-150.

Simons, M., vanderBij, A. J., Brand, I., deWeger, L. A., Wijffelman, C. A. & Lugtenberg, B. J. J. 1996. Gnotobiotic system for studying rhizosphere colonization by plant growth-promoting *Pseudomonas* bacteria. *Molecular Plant-Microbe Interactions,* 9, 600-607.

Singh, T., Srivastava, A. K. & Arora, D. K. 2002. Horizontal and vertical movement of *Pseudomonas fluorescens* toward exudate of *Macrophomina phaseolina* in soil: influence of motility and soil properties. *Microbiological Research,* 157, 139-148.

Smith, G. W., Hayasaka, S. S. & Thayer, G. W. 1979. Root surface area measurements of *Zostera marina* and *Halodule wrightii*. *Botanica Marina,* 22, 347-358.

Sonmez, H. 2003. Modification of the liquefaction potential index and liquefaction susceptibility mapping for a liquefaction-prone area (Inegol,Turkey). *Environmental Geology,* 44, 862-871.

Sørensen, J. & Sessitsch, A. 2007. Plant-associated bacteria - lifestyle and molecular interactions. *In:* Elsas, J. D. v., Jansson, J. K. & Trevors, J. T. (eds.) *Modern soil microbiology.* 2 ed. Boca Raton: CRC Press.

Spormann, A. M. 1999. Gliding motility in bacteria: Insights from studies of *Myxococcus xanthus*. *Microbiology and Molecular Biology Reviews,* 63**,** 621-641.

Standing, D. & Killham, K. 2007. The soil environment. *In:* Elsas, J. D. v., Jansson, J. K. & Trevors, J. T. (eds.) *Modern soil microbiology.* 2nd ed. Boca Raton: CRC Press.

Stokes, A., Atger, C., Bengough, A. G., Fourcaud, T. & Sidle, R. C. 2009. Desirable plant root traits for protecting natural and engineered slopes against landslides. *Plant and Soil,* 324**,** 1-30.

Stow, D. A., Hope, A., McGuire, D., Verbyla, D., Gamon, J., Huemmrich, F., Houston, S., Racine, C., Sturm, M., Tape, K., Hinzman, L., Yoshikawa, K., Tweedie, C., Noyle, B., Silapaswan, C., Douglas, D., Griffith, B., Jia, G., Epstein, H., Walker, D., Daeschner, S., Petersen, A., Zhou, L. M. & Myneni, R. 2004. Remote sensing of vegetation and land-cover change in Arctic Tundra Ecosystems. *Remote Sensing of Environment,* 89**,** 281-308.

Strömberg, N. 2008. Determination of ammonium turnover and flow patterns close to roots using imaging optodes. *Environmental Science & Technology,* 42**,** 1630-1637.

Strullu, D. G. & Romand, C. 1986. Méthode d'obtention d'endomycorhizes à vésicules et arbuscules en conditions axéniques. *Les Comptes Rendus de l'Académie des Sciences,* 303**,** 245-250.

Su, T. W., Xue, L. & Ozcan, A. 2012. High-throughput lensfree 3D tracking of human sperms reveals rare statistics of helical trajectories. *Proceedings of the National Academy of Sciences of the United States of America,* 109, 16018-16022.

Tan, Z. X., Lal, R. & Wiebe, K. D. 2005. Global soil nutrient depletion and yield reduction. *Journal of Sustainable Agriculture,* 26, 123-146.

Taylor, D. P., Slattery, J. & Leopold, A. C. 1996. Apoplastic pH in corn root gravitropism: A laser scanning confocal microscopy measurement. *Physiologia Plantarum,* 97, 35-38.

Taylor, H. M. & Ratliff, L. F. 1969. Root elongation rates of cotton and peanuts as a function of soil strength and soil water content. *Soil Science,* 108, 113-119.

Thomas, G. W. 1982. Exchangeable cations. *In:* Page, A. L., Miller, R. H. & Keeney, D. R. (eds.) *Methods of soil analysis.* 2nd ed. Madison, WI: American Society of Agronomy, Inc.

Thompson, M. V. & Holbrook, N. M. 2004. Root-gel interactions and the root waving behavior of *Arabidopsis*. *Plant Physiology,* 135, 1822-1837.

Tian, J.-Q., Zhou, Z.-Y., Bao, B. & Sun, J.-X. 2008. Variations of soil particle size distribution with land-use types and influences on soil organic carbon and nitrogen. *Zhiwu Shengtai Xuebao,* 32, 601-610.

Toyota, K. & Ikeda, K. 1997. Relative importance of motility and antibiosis in the rhizoplane competence of a biocontrol agent *Pseudomonas fluorescens* MelRC2Rif. *Biology and Fertility of Soils,* 25, 416-420.

Trachsel, S., Kaeppler, S. M., Brown, K. M. & Lynch, J. P. 2011. Shovelomics: high throughput phenotyping of maize (*Zea mays* L.) root architecture in the field. *Plant and Soil,* 341, 75-87.

Tracy, S. R., Black, C. R., Roberts, J. A. & Mooney, S. J. 2011. Soil compaction: a review of past and present techniques for investigating effects on root growth. *Journal of the Science of Food and Agriculture,* 91, 1528-1537.

Tracy, S. R., Black, C. R., Roberts, J. A., Sturrock, C., Mairhofer, S., Craigon, J. & Mooney, S. J. 2012. Quantifying the impact of soil compaction on root system architecture in tomato (*Solanum lycopersicum*) by X-ray micro-computed tomography. *Annals of Botany,* 110, 511-9.

Tracy, S. R., Roberts, J. A., Black, C. R., McNeill, A., Davidson, R. & Mooney, S. J. 2010. The X-factor: visualizing undisturbed root architecture in soils using X-ray computed tomography. *Journal of Experimental Botany,* 61, 311-313.

Unge, A. & Jansson, J. 2001. Monitoring population size, activity, and distribution of GFP-luxAB-tagged *Pseudomonas fluorescens* SBW25 during colonization of wheat. *Microbial Ecology,* 41, 290-300.

Urashima, Y. & Hori, K. 2003. Selection of PGPR which promotes the growth of spinach. *Japanese Journal of Soil Science and Plant Nutrition,* 74, 157-162.

Valentine, T., Shaw, J., Blok, V. C., Phillips, M. S., Oparka, K. J. & Lacomme, C. 2004. Efficient virus-induced gene silencing in roots using a modified tobacco rattle virus vector. *Plant Physiology,* 136, 3999-4009.

Valentine, T. A., Hallett, P. D., Binnie, K., Young, M. W., Squire, G. R., Hawes, C. & Bengough, A. G. 2012. Soil strength and macropore volume limit root elongation rates in many UK agricultural soils. *Annals of Botany,* 110, 259-270.

van Bruggen, A. H., Semenov, A. M. & Zelenev, V. V. 2000. Wavelike distributions of microbial populations along an artificial root moving through soil. *Microbial Ecology,* 40, 250-259.

van Bruggen, A. H. C., Semenov, A. M., Zelenev, V. V., Semenov, A. V., Raaijmakers, J. M., Sayler, R. J. & de Vos, O. 2008. Wave-like distribution patterns of GFP-marked *Pseudomonas fluorescens* along roots of wheat plants grown in two soils. *Microbial Ecology,* 55, 466-475.

van Elsas, J. D., Jansson, J. K. & Trevors, J. T. 2007. *Modern soil microbiology,* Boca Raton, Florida, CRC Press.

Van Nguyen, T., Vu Nguyen, M., Nordheden, K. J. & He, W. 2007. Effect of bulk and surface treatments on the surface ionic activity of nafion membranes. *Journal of the Electrochemical Society,* 154, 4.

Van Vuurde, J. W. L. & Schippers, B. 1980. Bacterial colonization of seminal wheat roots. *Soil Biology and Biochemistry,* 12, 559-565.

Waisel, Y., Eshel, A. & Kafkafi, U. 2002. *Plant roots: the hidden half,* Boca Raton, CRC Press.

Wang, H., Jin, J. & Yamauchi, A. 2008. Fractal analysis of root system architecture by box-counting method and its relationship with Zn accumulation in rice (*Oryza sativa* L.). *Acta Agronomica Sinica,* 34, 1637-1643.

Wang, Z., Mo, Y. W., Qian, S. Q. & Gu, Y. J. 2002. Negative phototropism of rice root and its influencing factors. *Science in China Series C-Life Sciences,* 45, 485-496.

Warrick, A. W. 2003. *Soil Water Dynamics,* USA, Oxford University Press.

Watanabe, K., Mandang, T., Tojo, S., Ai, F. & Huang, B. K. Nondestructive root-zone analysis with x-ray CT scanner. American Society of Agricultural Engineers, 1992 Charlotte, North Carolina, USA. 14.

Watt, M., Hugenholtz, P., White, R. & Vinall, K. 2006. Numbers and locations of native bacteria on field-grown wheat roots quantified by fluorescence in situ hybridization (FISH). *Environmental Microbiology,* 8, 871-884.

Weaver, J. E. 1926. *Root Development of Field Crops,* New York, McGraw-Hill.

Weller, D. M. 1988. Biological control of soilborne plant pathogens in the rhizosphere with bacteria. *Annual Review of Phytopathology,* 26, 379-407.

Whalley, W. R., Clark, L. J., Gowing, D. J. G., Cope, R. E., Lodge, R. J. & Leeds-Harrison, P. B. 2006. Does soil strength play a role in wheat yield losses caused by soil drying? *Plant and Soil,* 280, 279-290.

Whipps, J. W. & Gerhardson, B. 2007. Biological pesticides for control of seed- and soil-borne plant pathogens. *In:* Van Elsas, J. D., Jansson, J. K. & Trevors, J. T. (eds.) *Modern soil microbiology.* 2 ed. Boca Raton, Florida: CRC Press.

White, J. W., Andrade-Sanchez, P., Gore, M. A., Bronson, K. F., Coffelt, T. A., Conley, M. M., Feldmann, K. A., French, A. N., Heun, J. T., Hunsaker, D. J., Jenks, M. A., Kimball, B. A., Roth, R. L., Strand, R. J., Thorp, K. R., Wall, G. W. & Wang, G. Y. 2012. Field-based phenomics for plant genetics research. *Field Crops Research,* 133**,** 101-112.

Whiteside, M. D., Digman, M. A., Gratton, E. & Treseder, K. K. 2012. Organic nitrogen uptake by arbuscular mycorrhizal fungi in a boreal forest. *Soil Biology & Biochemistry,* 55**,** 7-13.

Whiteside, M. D., Treseder, K. K. & Atsatt, P. R. 2009. The brighter side of soils: Quantum dots track organic nitrogen through fungi and plants. *Ecology,* 90**,** 100-108.

Woolley, D. M. & Vernon, G. G. 2001. A study of helical and planar waves on sea urchin sperm flagella, with a theory of how they are generated. *Journal of Experimental Biology,* 204**,** 1333-1345.

Wuyts, N., Bengough, A. G., Roberts, T. J., Du, C. J., Bransby, M. F., McKenna, S. J. & Valentine, T. A. 2011. Automated motion estimation of root responses to sucrose in two *Arabidopsis thaliana* genotypes using confocal microscopy. *Planta,* 234**,** 769-784.

Xue, T., Trent, J. S. & Osseo-Asare, K. 1989. Characterization of nafion® membranes by transmission electron microscopy. *Journal of Membrane Science,* 45, 261-271.

Yang, J. C., Zhang, H. & Zhang, J. H. 2012. Root morphology and physiology in relation to the yield formation of rice. *Journal of Integrative Agriculture,* 11, 920-926.

Yazdanbakhsh, N. & Fisahn, J. 2009. High throughput phenotyping of root growth dynamics, lateral root formation, root architecture and root hair development enabled by PlaRoM. *Functional Plant Biology,* 36, 938-946.

Young, I. M., Crawford, J. W. & Rappoldt, C. 2001. New methods and models for characterising structural heterogeneity of soil. *Soil & Tillage Research,* 61, 33-45.

Young, I. M., Montagu, K., Conroy, J. & Bengough, A. G. 1997. Mechanical impedance of root growth directly reduces leaf elongation rates of cereals. *New Phytologist,* 135, 613-619.

Zeier, J., Goll, A., Yokoyama, M., Karahara, I. & Schreiber, L. 1999. Structure and chemical composition of endodermal and rhizodermal hypodermal walls of several species. *Plant, Cell and Environment,* 22, 271-279.

Zhou, Z., Zhou, X., Luo, X. & Li, Q. 2006. Study on Matlab-based segmentation algorithms for X-ray CT image of plant root. *Nongye Jixie Xuebao = Transactions of the Chinese Society for Agricultural Machinery,* 37, 118-121.

Zhu, J. M., Ingram, P. A., Benfey, P. N. & Elich, T. 2011. From lab to field, new approaches to phenotyping root system architecture. *Current Opinion in Plant Biology,* 14, 310-317.

Zhu, J. M., Zhang, C. C. & Lynch, J. P. 2010. The utility of phenotypic plasticity of root hair length for phosphorus acquisition. *Functional Plant Biology,* 37**,** 313-322.

Appendix 1

Research article: Transparent soil for imaging the rhizosphere

Authors: Helen Downie[1,2], Nicola Holden[1], Wilfred Otten[2], Andrew J. Spiers[2], Tracy A. Valentine[1], Lionel X. Dupuy[1*]

Affiliations:

[1]The James Hutton Institute, Invergowrie, Dundee DD2 5DA, UK.

[2] The SIMBIOS Centre, University of Abertay Dundee, Bell Street, Dundee DD1 1HG, UK.

*Correspondence to: Lionel.Dupuy@Hutton.ac.uk, Tel: +44 1382 568521

PLoS ONE, 7, e44276, 2012.

http://www.plosone.org/article/info:doi/10.1371/journal.pone.0044276

Abstract

Understanding of soil processes is essential for addressing the global issues of food security, disease transmission and climate change. However, techniques for observing soil biology are lacking. We present a heterogeneous, porous, transparent substrate for in situ 3D imaging of living plants and root-associated microorganisms using particles of the transparent polymer, Nafion, and a solution with matching optical properties. Minerals and fluorescent dyes were adsorbed onto the Nafion particles for nutrient supply and imaging of pore size and geometry. Plant growth in transparent soil was similar to that in soil. We imaged colonization of lettuce roots by the human bacterial pathogen *Escherichia coli* O157:H7 showing micro-colony development. Micro-colonies may contribute to bacterial survival in soil. Transparent soil has applications in root biology, crop genetics and soil microbiology.

Introduction

The ability of plants and microorganisms to successfully exploit soil resources underpins the survival of all terrestrial life. Soil is a complex assemblage of mineral and organic particles that can host a very diverse range of biological organisms [1]. It comprises a solid phase, consisting of minerals and organic matter particles, and an aqueous phase with dissolved minerals and gasses essential for plant nutrition and microbial activity. In non-saturated soil, air is also available in large pores supplying gasses required for metabolic processes of plants and microbes. Imaging technologies are required to study and quantify soil biological processes [2], but this is difficult because of the inherent opacity of soil. Non-optical imaging techniques have been used to image plant roots in

soil, for example, x-ray microtomography and MRI [3,4], but these methods are not adapted for imaging biological activity, mostly because of the inability to use them to detect common fluorescent markers.

Biological studies are benefiting immensely from emerging optical imaging technologies. For example, Optical Projection Tomography (OPT), which uses a collection of 2D projections to reconstruct 3D volumes, has allowed the distribution of fluorescent markers to be mapped across intact whole embryos [5]. Recent advances in Selective Plane Illumination microscopy (SPIM) have allowed the light doses received by samples to be drastically reduced during live imaging. Using this technique, it was possible for the first time to track individual cell growth and cell division events across entire embryos during 24 hours [6]. It is now also possible to overcome diffraction limitations and increase resolution with techniques such as 3D structured illumination microscopy. This is now a common technique to observe sub-cellular processes [7].

Unfortunately, the study of soil biota is not benefiting much from technological advances in optical imaging because most soil organisms, such as many types of fungi, cannot be cultured in current artificial substrates, whilst others have their functions strongly affected by the medium they are grown in [8]. We have developed a substrate called transparent soil, with a matrix of solid particles and a pore network containing liquid and air. The physical structure was manipulated with the aim of generating 3D optical images of soil biota in a physically complex yet controllable environment.

Results and Discussion

Making soils transparent using Refractive Index matching

At the boundary of two transparent materials with different refractive indices, the path of light is distorted through refraction. By matching the refractive index (RI) of a solid and a liquid, this effect is negated so that the boundaries between the materials become invisible. RI matching has proved a powerful approach in many areas of physical sciences, such as fluid dynamics [9] and colloid sciences [10]. In soil mechanics, amorphous silica particles have been used with oil-based RI matching solutions [11] and have similar mechanical properties to clay [12]. This system has been used for investigating particle displacement in response to the application of mechanical forces. Recently, the technique of RI matching has been adapted for growing and imaging aquatic biofilms [13] where limited RI matching was achieved using water. In the present study, we have used particles of Nafion, which has a low refractive index (1.34), close to that of water (1.33), and therefore allows RI matching with an aqueous solution (Fig. 1A,B). During the period of plant and microbial growth, pores were partially saturated with a plant nutrient solution [14] and air spaces were maintained for aerobic respiration. Roots can grow freely in 3D trajectories whilst responding to heterogeneous, complex touch stimuli, replicating the mechanical processes that would occur in soil [15]. Immediately before imaging, the substrate was saturated using a RI matched liquid plant nutrient solution so that imaging of roots and microorganisms could be carried out in situ (Fig. 1A).

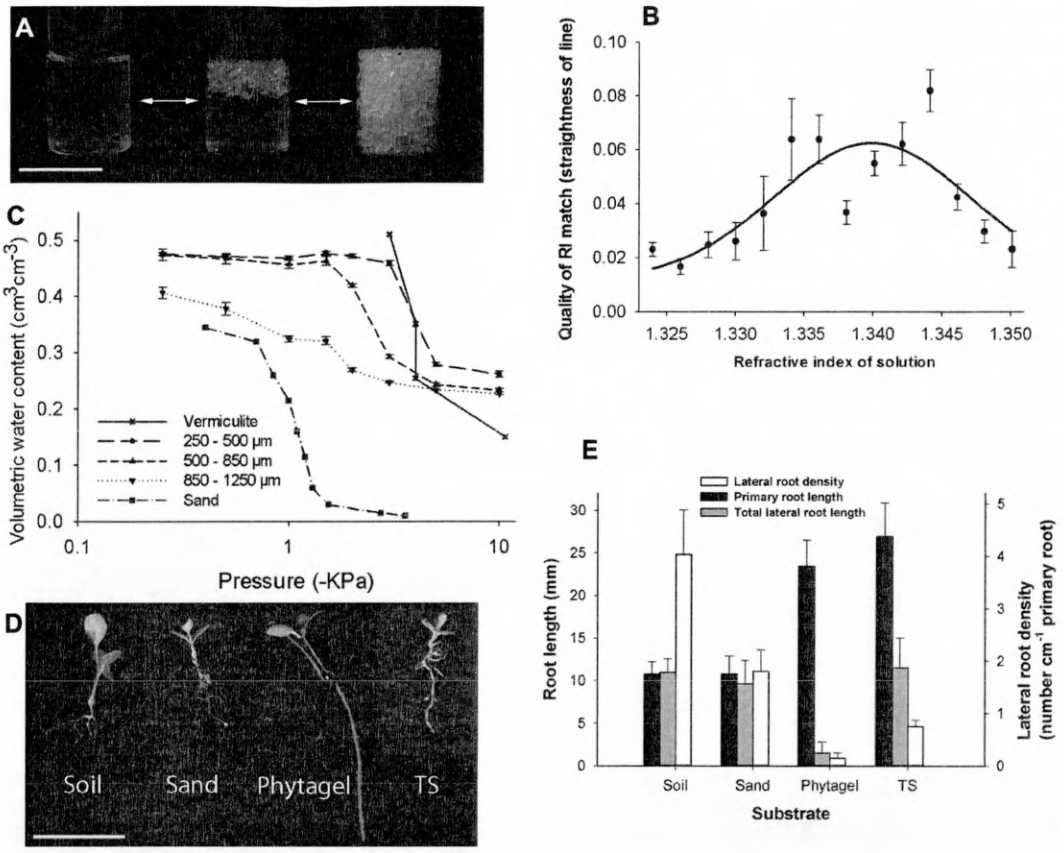

Figure 1. A) Transparent soil is prepared for imaging by saturation with RI-matched solution to achieve transparency (left, fully saturated; right, larger pores are drained). Scale bar = 2.5 cm. B) Optimal RI of nutrient solution for RI matching with Nafion using projected straight line images deformed by the substrate. Curve shows Gaussian non-linear regression (R2 = 0.38). C) Water retention in transparent soil with 3 different Nafion particle sizes compared to vermiculite [37] and sand [16]. Error bars show standard error. D–E) Comparison of plant growth in transparent soil and other substrates. D) Excavated plants with representative root systems from each substrate type after 2 weeks of growth. Scale bar represents 1 cm. E) Quantification of root system parameters in different substrates. Plants grown in transparent soil had lateral root lengths and densities more similar to plants grown in soil than plants grown in phytagel.

Mimicking physical and chemical properties of soil

We have also sought to mimic physical and chemical properties important for supporting plant and microbial growth in soils in the transparent soil system. Nafion, the building block of transparent soil, is a transparent ionomer (synthetic polymer with ionic properties) that is physically and chemically adaptable. Nafion particle size distribution has been manipulated by freezer milling (250 – 1600 μm). We have also altered the surface chemistry of the particles in order to control water retention and nutrient availability through changes in ion exchange capacity. We analysed the water retention of transparent soil with 3 particle size categories and compared this to vermiculite and sand (Fig. 1C). In the 2 smallest size categories, and in vermiculite, the sharpest release of water occurred between -1.5 and -5 kPa. The water release in the largest sized particles was more gradual but in all sizes, a levelling off of water release occurred towards -10 kPa and the residual water content measured in transparent soil ranged from 0.23 to 0.26 cm^3cm^{-3}. This value was higher than is usual in sand [16], despite the similarity in particle size. Nafion has a complex structure incorporating networks of hydrophilic channels that allow transport of water and other polar solvents [17]. Although the exact nature of these networks is still unclear, it is estimated that the diameter of these channels varies between 1 and 6 nm [18,19,20]. At this range of scales, the hydrogen bonds holding the water molecules are extremely strong and the water sorbed in the Nafion particles cannot be accessed by most biological organisms.

Cation exchange is an important characteristic of natural soils, particularly in those containing clay, which acts as a buffer for minerals in the soil solution. The cation exchange capacity (CEC) of transparent soil was quantified as 81 meq 100 g^{-1}. This is within the range that could be expected for vermiculite (80 – 150 meq 100 g^{-1} [21]). Additionally, anion exchange in soils involves some essential plant nutrients such as nitrate and phosphate, which are of strong interest in plant nutrition. The anion exchange capacity (AEC) of cationic Nafion [22] was 47 meq 100 g^{-1}.

Root growth in transparent soil

Transparent soil can be used for a large range of other applications. At the macroscopic level, quantifying the growth of root systems is essential in understanding how plants obtain resources. To analyse root growth in transparent soil, we have measured primary root length, total root length and root diameter of root systems of plants grown on phytagel, sandy loam soil, sand, and transparent soil. The Analysis of Variance showed the type of substrate had a significant effect on root length ($p \leq 0.003$) (Fig 1E) and root diameter ($p=0.026$). The mean root diameter was 0.24 ± 0.01 mm in soil, 0.24 ± 0.03 mm in sand, 0.18 ± 0.02 mm in phytagel and 0.28 ± 0.03 mm in transparent soil. The least significant difference test showed that plants grown on transparent soil, soil, or sand had more lateral roots and a higher biomass than plants grown on phytagel (a common substrate used for growing plants and imaging roots). Root systems from soil and sand had shorter primary roots than plants grown on gel and transparent soil, but plants grown in phytagel had long primary roots and almost no laterals (Fig. 1D,E). Our results

indicate that root growth in transparent soil is similar to that observed in soil and sand and demonstrate the importance of physical heterogeneity in the growth substrate for producing soil-like root systems.

Transparent soil is suitable for growing and imaging the roots of various plant species, including alfalfa, barley, maize (data not shown), tobacco, lettuce and thale cress (*Arabidopsis*), and imaging at the whole root level can be achieved using OPT (Fig. 2A). Transparent soil provides images with low levels of noise and opens avenues for automated analyses of genetic screens [23]. In addition, the availability of fluorescent signals eases the discrimination of biological structures where separation of the different wavelengths provides much of the segmentation of the biological structures (Fig. 2B,C). Transparent soil can also be used to capture cellular events using plants with plasma membrane and nucleus-localized reporter gene-encoded proteins (Fig. 2C, S1, Videos S1-S3, Appendix 2 & enclosed CD), which could be used for automated analysis of multicellular development [24,25]. For example, we have imaged the 3D distribution of auxin in Arabidopsis thaliana root tips (Fig. 2F) using auxin reporter lines [26].

Application of transparent soil to the study of root bacteria interactions

We have applied transparent soil to study the mechanisms of transmission of food-borne human pathogens on fresh produce plants using GFP-labelled Escherichia coli O157:H7. Although this strain is an enteric animal pathogen, it is able to use plants as alternative hosts. The contamination route can be from crop irrigation or manure, via the rhizosphere before entering the human food chain [27]. In order to study the

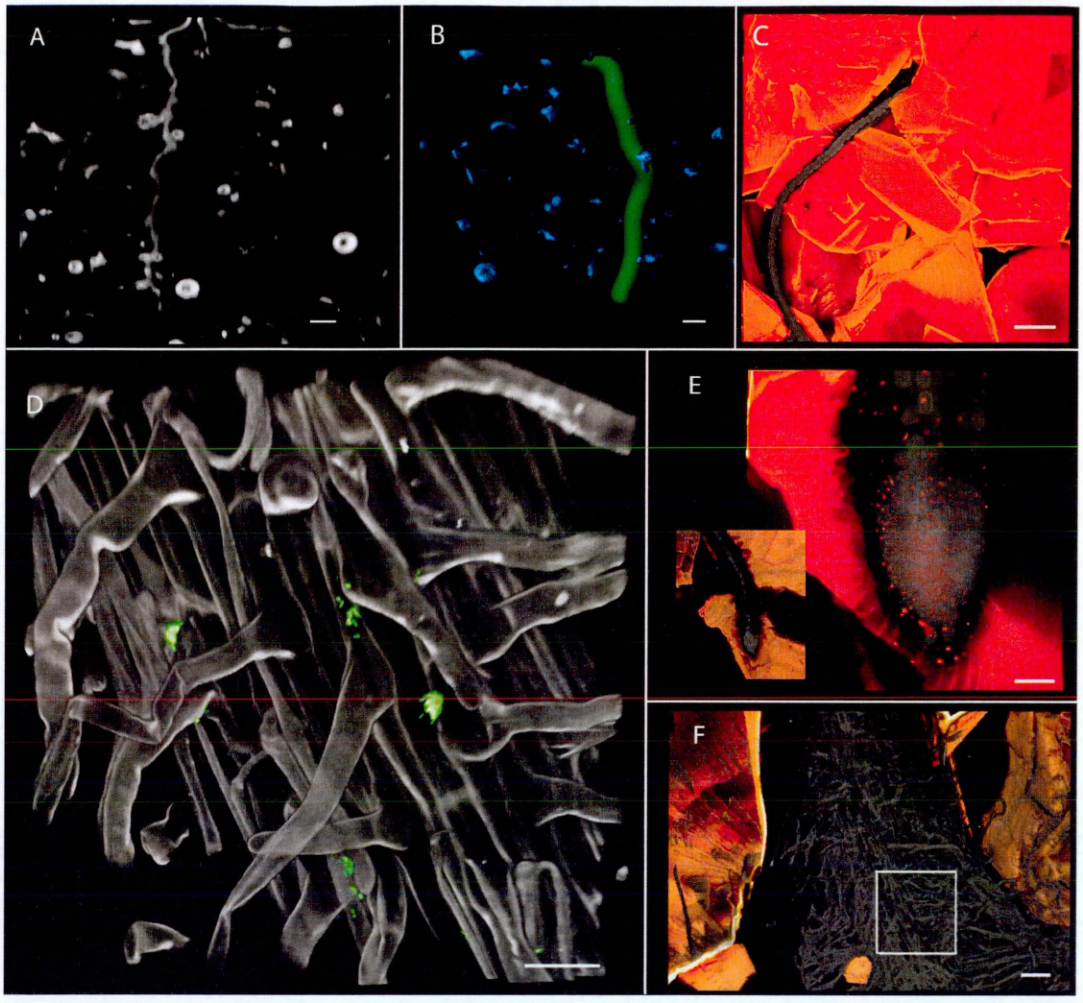

Figure 2. Imaging roots and microorganisms in transparent soil using OPT and confocal microscopy. A) Projection image from OPT scan of Nicotiana benthamiana *roots. Scale bar represents 1 mm. B) Root tracking algorithm is applied to the reconstructed data to segment and dilate (to improve visibility) the root (green) from the small air bubbles (blue). Scale bar represents 1 mm. C–F) Snapshots of volume renderings of confocal scans. C)* Arabidopsis thaliana *roots expressing GFP in plasma membranes (grey) in transparent soil with sulphorhodamine-B-dyed particles (orange) where scale bars represents 300 µm. Inset shows root skeletonisation and edge detection applied to scan (C) to detect roots and particles. D) GFP labelled* Escherichia coli *O157:H7 cells and colonies on surface of* Lactuca sativa *(lettuce) root with prominent root hairs. Scale bar represents 30 µm. E) Box shows enlarged region of lettuce root in (D) with Nafion particles visible in orange. Scale bar represents 100 µm. F)* Arabidopsis thaliana *root tip with nuclear RFP expression linked to auxin reporter [41]. Inset with box shows enlarged region. Scale bar represents 54 µm.*

mechanisms of survival of E. coli O157:H7 in a soil-like environment, lettuce seeds were germinated and inoculated with E. coli O157:H7 before transferring them to the transparent soil. Our results showed that after 7 days of growth, E. coli O157:H7 had survived in a soil like environment in the form of micro-colonies of various sizes. Micro-colonies developed in the rhizosphere [28]. Since E. coli O157:H7 is not solely a rhizosphere bacteria, the formation of micro-colonies shows an adaptation to the plant host, which will increase survival in the root zone (Fig. 2D). As a pathogenic bacteria, E. coli O157:H7 survives by colonizing host organisms and in the initial stages of colonization, adheres to the host [29]. When using transparent soil, there is a potential problem of moving the bacteria during saturation of the substrate in preparation for imaging but this should not affect attached bacteria such as E. coli O157:H7 in the preliminary stages of colonization. Saturation is, however, a potential limitation of the method if studying microbes that are not attached to surfaces because it is likely that these would be moved during saturation. In summary, our results show that transparent soil is ideal for imaging studies of certain plant-microbe interactions in situ at the microscopic level.

New opportunities for plant sciences

Soil microbes provide numerous important services [30] and their interactions with plants enhance the supply of nutrients, for example by nodulation [31] or by biological fertilization [32]. The transfer of human pathogens in the food chain [27] and spread of crop diseases [33] also involve complex plant-microbe interactions. The use of

transparent soil will facilitate quantitative imaging of the dynamics of in situ root-microbe interactions using high resolution imaging with fluorescence for detecting microorganisms expressing fluorescent proteins (Fig. 2D). For plant genetics and crop breeding, transparent soil could be integrated with high-throughput screening systems for root traits [34] that may improve nutrient acquisition and reduce the need for fertilizers [35]. Overall, this approach presents new opportunities to unravel the complex processes of plant-soil interactions in situ and in vivo and holds promise for a wide range of applications to aid the understanding of important underlying relationships that underpin the sustainability of our ecosystems.

Materials and methods

Construction of transparent soil

Nafion was from Ion Power Inc., USA, in the form of 4 mm × 3 mm pellets. Acid (NR50 1100) and precursor (R1 100) forms were used. Size reduction of Nafion particles was performed using a freezer mill (6850, SPEX SamplePrep, UK). The final particle size range was 350 - 1600 μm. Cation exchanging Nafion particles were made by ensuring full conversion to the acid form by washing in a solution of 15% v/v KOH, 35% v/v DMSO and 50% dH_2O at 80 °C for 5 hours, then with dH_2O (milliQ) at room temperature for 30 minutes followed by several dH_2O rinses. This was followed by 2 washes in 15% v/v nitric acid at room temperature for 1 hour and then overnight. The particles were treated with 1M sulphuric acid for 1 hour at 65 °C, and the acid was removed and replaced with dH2O at 65 °C for 1 hour. After cooling, the particles were washed several

times with dH2O. They were washed in 3 wt % H_2O_2 solution at 65 °C for 1 hour and allowed to cool. The particles were rinsed again multiple times with fresh dH2O [36]. To titrate the particles with mineral ions, stock solutions of MSR medium were used to immerse the particles. These were shaken at 30 °C for 30 minutes before replacing the nutrient solution. This was repeated until the pH was neutral and stable. The particles were rinsed with dH_2O to remove excess MSR. Before use, the particles were autoclaved in dH_2O for sterilisation.

Refractive index matching

To determine the best refractive index match between the particles and liquid, plastic cuvettes were filled with acid Nafion particles and saturated with a range of concentrations of sorbitol solutions from 0-13% (w/v) to achieve a range of refractive indices. On one side of each cuvette, a straight line was drawn from top to bottom and a projection image was taken through solid / liquid mix. There were 5 replicate images taken at each sorbitol concentration at 20 °C. The straightness of the line for each image was used as an indicator of the light path distortion by refraction. The thresholded image was skeletonized and a bounding box around the line was created. The straightness was calculated as straightness = height of bounding box / area of bounding box. Nutrient-titrated Nafion particles were also tested in this way, but with a larger range of sorbitol concentrations.

Characterising properties of transparent soil

Water retention was measured in transparent soil with 3 size categories of Nafion particles (200 – 500 μm, 500 – 850 μm and 850 -1250 μm, n=3), with a dry mass of 10.3 ± 0.1 g. Saturated samples were placed on ceramic plates in glass funnels, which were connected to hanging water columns. Different suctions were achieved by moving the water level in the water column to a specific height. At each pressure, the water content of the sample was allowed to equilibrate and the mass was recorded to allow calculation of volumetric water content. Data on water retention in vermiculite and sand from other studies were used for comparison with our data on water retention in transparent soil [16,37]. Exchangeable cations were extracted using the ammonium acetate method [38] and cation exchange capacity was quantified by subsequent ICP-MS analysis. To measure anion exchange capacity, sorbed chloride ions were exchanged with nitrate ions and exchange capacity was determined by measuring the extracted chloride ions [39]. Chemical analyses were carried out by Macaulay Analytical at The James Hutton Institute.

Plant culture

Arabidopsis thaliana expressing 35S:LTI6b- EGFP (constitutively expressed enhanced green fluorescent protein targeted to the plasma membrane), in the C24 background (originally obtained from Dr. J. Haseloff, University of Cambridge, UK) [40] and auxin reporter lines [41] were used for confocal microscopy. *Nicotiana benthamiana* (tobacco) and *Lactuca sativa* (lettuce, var. capitata, Seed Parade, UK) seeds were surface sterilized

by washing in 10% bleach for 20 minutes followed by several sterile dH_2O washes. *Arabidopsis thaliana* seeds were sterilized on filter paper by adding 70% ethanol, allowed to dry slightly and addition of 90% ethanol before allowing to air dry. MSR nutrient media [14] was used for culturing tobacco seeds and half-strength Murashige and Skoog (M&S) basal media (Sigma) was used for lettuce and Arabidopsis seeds. Seedlings were germinated before use in experiments by sowing seeds in petri dishes with 5 g L^{-1} phytagel (Sigma) with MSR or M&S nutrient media. Plants were incubated at 20 °C with 16 hours light: 8 hours darkness.

Analysis of plant growth in different substrates

The substrates used for analysing plant growth were 1. sandy-loam soil from Lower Pilmore field, The James Hutton Institute, Dundee, UK. The soil was sieved to 3 mm and packed to a density of 1.2 g cm^{-3} with a gravimetric moisture content of 20% (n=9). 2. Horticultural grit sand (Gem, UK), with a dry bulk density of 1.5 g cm^{-3} and MSR to achieve a gravimetric moisture content of 15.2% (n=9). 3. 4 g L^{-1} phytagel (Sigma) with MSR (n=9). 4. Transparent soil, prepared as described below and packed to a density of 1.03 g cm^{-3} (n=6). Growth period was 2 weeks after transferring the seedlings to the media in cylindrical glass sample holders, diameter = 2.5 cm, height 7.5 cm. All plants were excavated, the roots were washed and they were mounted onto acetate sheets for scanning using a flatbed scanner (Epson expression 1640 XL, Hemel Hempstead, UK). Primary and lateral roots were measured using the segmented line function from ImageJ software (National Institute of Health, USA).

Bacterial culture and experimental setup

Escherichia coli O157 : H7 was transformed with a fluorescent reporter plasmid (loc8-egfp) [42] and grown in MOPS glucose media with amino acids and chloramphenicol (25 $\mu g\ \mu l^{-1}$) at 18 °C with aeration for 20 hours. One day after sowing the lettuce seeds, germination occurred and 15 ml of bacteria suspended in half-strength M&S media at a cell density of 2 × 107 cfu/ml was used to inoculate the seedlings in a Petri dish, at room temperature, for 30 minutes, before transferring the seedlings into growth chambers with transparent soil, as described above. Imaging was carried out after 5 days after sowing. The method used for bacteria–plant interactions allowed colonization of the roots to develop from infected seedlings, rather than from the addition of the inoculum directly to the substrate or the more mature roots.

3D optical imaging of soil biological processes

For OPT imaging the samples were prepared in glass cylindrical specimen tubes (2.5 cm in diameter, 7.5 cm in height) with a substrate volume of 15 cm3. Duration of growth was dependent on plant species but in general, imaging was performed before the roots reached the base of the tube. Tobacco plants used for OPT were imaged 10 days after sowing. Arabidopsis plants used for confocal imaging were imaged 10-14 days after sowing. The OPT setup was built in-house and consists of a light box, stage for sample with rotating stepper motor, stereo microscope (Leica MZ 16 FA) and camera (Leica DFC 350 FX). The stage and camera were controlled by software also built in-house, allowing control of the number of images acquired for each sample. The projection images were

reconstructed to produce 3D data using a filtered backprojection algorithm with the Iradon function in Matlab (The MathWorks, Inc.).

For CLSM, plants were grown in purpose-built chambers, constructed using a microscope slide and long cover glass with a 4 mm spacer between them on 3 sides and an opening at the top. The spacer was glued to the slide and cover glass using Araldite glass and ceramic adhesive (Huntsman International). The chambers were covered with aluminium foil on the outside during growth to exclude light from the roots. Foil was removed immediately before imaging. Before imaging, transparent soil was saturated with MSR containing 13% (w/v) sorbitol or 98% Percoll (Sigma). The refractive index of the solution matches the refractive index of the Nafion particles used here to provide complete transparency in the substrate. Sulphorhodamine B (Sigma) at 1 μg ml-1 was used to dye the particles in situ before imaging. A Leica TCS SP2 confocal laser scanning microscope and objective lenses 2.5× / 0.07, 10× / 0.30, 20× / 0.50, 40× / 0.80 and 63× / 0.90 were used to obtain the confocal scans.

Data analysis

Analysis of variance and multiple comparisons were carried out using Genstat 13th Edition (VSN International Ltd.). Sigmaplot 12 (Syststat Software, Inc.) was used for non-linear regression. Avizo software (VSG) was used for visualisation of CLSM images. Image analysis was carried out using Mevislab [43] and Fiji Software [44]. Root tracking used an algorithm by Friman et al [45]. Skeletonization and edge detection was carried out using

the standard Mevislab algorithms developed respectively by Milo Hindennach and Olaf Konrad and Wolf Spindler.

Acknowledgements

We thank Prof. Yossef A. Elabd for the cationic Nafion protocol, Ian McNaugton and Jim Anderson for the OPT construction, Carol Kyle, Vicky Helbig, Jason Owen, Audrey Derumier and Kath Wright for their general assistance and Jim Haseloff and Fernan Federici for *Arabidopsis* seeds.

References

1. Young IM, Crawford JW (2004) Interactions and self-organization in the soil-microbe complex. Science 304: 1634-1637.

2. Eickhorst T, Tippkötter R (2008) Detection of microorganisms in undisturbed soil by combining fluorescence in situ hybridization (FISH) and micropedological methods. Soil Biology and Biochemistry 40: 1284-1293.

3. Gregory PJ, Hutchison DJ, Read DB, Jenneson PM, Gilboy WB, et al. (2003) Non-invasive imaging of roots with high resolution X-ray micro-tomography. Plant and Soil 255: 351-359.

4. Bottomley PA, Rogers HH, Foster TH (1986) NMR imaging shows water distribution and transport in plant-root systems in situ. Proceedings of the National Academy of Sciences of the United States of America 83: 87-89.

5. Sharpe J, Ahlgren U, Perry P, Hill B, Ross A, et al. (2002) Optical projection tomography as a tool for 3D microscopy and gene expression studies. Science 296: 541-545.

6. Huisken J, Swoger J, Del Bene F, Wittbrodt J, Stelzer EHK (2004) Optical sectioning deep inside live embryos by selective plane illumination microscopy. Science 305: 1007-1009.

7. Schermelleh L, Carlton PM, Haase S, Shao L, Winoto L, et al. (2008) Subdiffraction multicolor imaging of the nuclear periphery with 3D structured illumination microscopy. Science 320: 1332-1336.

8. Malamy JE (2005) Intrinsic and environmental response pathways that regulate root system architecture. Plant Cell and Environment 28: 67-77.

9. Budwig R (1994) Refractive index matching methods for liquid flow investigations. Experiments in Fluids 17: 350-355.

10. de Villeneuve VWA, Dullens RPA, Aarts D, Groeneveld E, Scherff JH, et al. (2005) Colloidal hard-sphere crystal growth frustrated by large spherical impurities. Science 309: 1231-1233.

11. Mannheimer RJ, Oswald CJ (1993) Development of transparent porous-media with permeabilities and porosities comparable to soils, aquifers, and petroleum reservoirs. Ground Water 31: 781-788.

12. Iskander MG, Liu JY, Sadek S (2002) Transparent amorphous silica to model clay. Journal of Geotechnical and Geoenvironmental Engineering 128: 262-273.

13. Leis AP, Schlicher S, Franke H, Strathmann M (2005) Optically transparent porous medium for nondestructive studies of microbial biofilm architecture and transport dynamics. Applied and Environmental Microbiology 71: 4801-4808.

14. Declerck S, Strullu DG, Plenchette C (1998) Monoxenic culture of the intraradical forms of *Glomus* sp. isolated from a tropical ecosystem: a proposed methodology for germplasm collection. Mycologia 90: 579-585.

15. Massa GD, Gilroy S (2003) Touch modulates gravity sensing to regulate the growth of primary roots of *Arabidopsis thaliana*. Plant Journal 33: 435-445.

16. Schroth MH, Ahearn SJ, Selker JS, Istok JD (1996) Characterization of miller-similar silica sands for laboratory hydrologic studies. Soil Science Society of America Journal 60: 1331-1339.

17. Mauritz KA, Moore RB (2004) State of understanding of Nafion. Chemical Reviews 104: 4535-4585.

18. Ceynowa J (1984) Pore model parameters of cation-exchange membranes. Die Angewandte Makromolekulare Chemie 121: 97-107.

19. Xue T, Trent JS, Osseo-Asare K (1989) Characterization of nafion® membranes by transmission electron microscopy. Journal of Membrane Science 45: 261-271.

20. Rieberer S, Norian KH (1992) Analytical electron-microscopy of nafion ion-exchange membranes. Ultramicroscopy 41: 225-233.

21. Lal R, editor (2002) Encyclopedia of soil science. New York & Basel: Marcel Dekker.

22. Salerno HLS, Beyer FL, Elabd YA (2011) Anion exchange membranes derived from nafion precursor for the alkaline fuel cell. Journal of Polymer Science Part B: Polymer Physics: online.

23. French A, Ubeda-Tomas S, Holman TJ, Bennett MJ, Pridmore T (2009) High-throughput quantification of root growth using a novel image-analysis tool. Plant Physiology 150: 1784-1795.

24. Dumais J, Kwiatkowska D (2002) Analysis of surface growth in shoot apices. The Plant Journal 31: 229-241.

25. Dupuy L, Mackenzie J, Haseloff J (2010) Coordination of plant cell division and expansion in a simple morphogenetic system. Proceedings of the National Academy of Sciences of the United States of America 107: 2711-2716.

26. Federici F, Dupuy L, Laplaze L, Heisler M, Haseloff J (2012) Integrated genetic and computation methods for in planta cytometry. Nat Meth 9: 483-485.

27. Holden NJ (2010) Plants as reservoirs for human enteric pathogens. CAB Reviews: Perspectives in Agriculture, Veterinary Science, Nutrition and Natural Resources 5: 1-11.

28. Habteselassie MY, Bischoff M, Applegate B, Reuhs B, Turco RF (2010) Understanding the role of agricultural practices in the potential colonization and contamination by *Escherichia coli* in the rhizospheres of fresh produce. Journal of Food Protection 73: 2001-2009.

29. Holden N, Pritchard L, Toth I (2009) Colonization outwith the colon: plants as an alternative environmental reservoir for human pathogenic enterobacteria. Fems Microbiology Reviews 33: 689-703.

30. Costanza R, dArge R, deGroot R, Farber S, Grasso M, et al. (1997) The value of the world's ecosystem services and natural capital. Nature 387: 253-260.

31. Haynes JG, Czymmek KJ, Carlson CA, Veereshlingam H, Dickstein R, et al. (2004) Rapid analysis of legume root nodule development using confocal microscopy. New Phytologist 163: 661-668.

32. Miransari M (2011) Soil microbes and plant fertilization. Applied microbiology and biotechnology 92: 875-885.

33. Mendes R, Kruijt M, de Bruijn I, Dekkers E, van der Voort M, et al. (2011) Deciphering the rhizosphere microbiome for disease-suppressive bacteria. Science 332: 1097-1100.

34. de Dorlodot S, Forster B, Pagès L, Price A, Tuberosa R, et al. (2007) Root system architecture: opportunities and constraints for genetic improvement of crops. Trends in Plant Science 12: 474-481.

35. Boyes DC, Zayed AM, Ascenzi R, McCaskill AJ, Hoffman NE, et al. (2001) Growth stage-based phenotypic analysis of *Arabidopsis*: A model for high throughput functional genomics in plants. Plant Cell 13: 1499-1510.

36. Van Nguyen T, Vu Nguyen M, Nordheden KJ, He W (2007) Effect of bulk and surface treatments on the surface ionic activity of nafion membranes. Journal of the Electrochemical Society 154: 4.

37. Schmidt S (2011) Root responses to soil physical conditions and the role of root-particle contact. Dundee: University of Abertay Dundee.

38. Thomas GW (1982) Exchangeable cations. In: Page AL, Miller RH, Keeney DR, editors. Methods of soil analysis. 2nd ed: American Society of Agronomy, Inc.

39. Pansu M, Gautheyrou J (2006) Anion exchange capcity. In: Pansu M, Gautheyrou J, editors. Handbook of soil analysis: Springer. pp. 755-766.

40. Kurup S, Runions J, Kohler U, Laplaze L, Hodge S, et al. (2005) Marking cell lineages in living tissues. Plant Journal 42: 444-453.

41. Federici F, Dupuy L, Laplaze L, Heilsler M, Haseloff J (2012) Integration of genetic and computation techniques for in planta cytometry. Nature methods in press.

42. Low AS, Holden N, Rosser T, Roe AJ, Constantinidou C, et al. (2006) Analysis of firnbrial gene clusters and their expression in enterohaernorrhagic *Escherichia coli* O157 : H7. Environmental Microbiology 8: 1033-1047.

43. Koenig M, Spindler W, Rexilius J, Jomier J, Link F, et al. (2006) Embedding VTK and ITK into a visual programming and rapid prototyping platform. In: Cleary KRGRL, editor. Medical Imaging 2006: Visualization, Image-Guided Procedures, and Display.

44. Preibisch S, Saalfeld S, Schindelin J, Tomancak P (2010) Software for bead-based registration of selective plane illumination microscopy data. Nature methods 7: 418-419.

45. Friman O, Hindennach M, Peitgen HO (2008) Template-based multiple hypotheses tracking of small vessels. 2008 IEEE International Symposium on Biomedical Imaging: From Nano to Macro, Vols 1-4. pp. 1047-1050.

Appendix 2

Captions for videos on CD

Video S1. In situ 3D image of branched *Arabidopsis thaliana* roots expressing GFP in plasma membranes (green) in transparent soil with sulphorhodamine B dyed particles (red).

Video S2. In situ 3D image of *Arabidopsis thaliana* root with emerging lateral root expressing GFP in plasma membranes (green) in transparent soil with sulphorhodamine B dyed particles (orange).

Video S3. In situ 3D image of *Arabidopsis thaliana* root with root hairs expressing GFP in plasma membranes (green) with Nafion particle of transparent soil (orange).